MATHEMATICAL MODELLING OF GRANULAR FLOWS AND ITS APPLICATIONS

WARIAM CHUAYJAN

A THESIS SUBMITTED IN PARTIAL FULFILMENT
OF THE REQUIREMENTS FOR
THE DEGREE OF DOCTOR OF PHILOSOPHY
(MATHEMATICS)
FACULTY OF GRADUATE STUDIES
MAHIDOL UNIVERSITY
2010

Thesis

entitled

MATHEMATICAL MODELLING OF GRANULAR FLOWS AND ITS APPLICATIONS

.....
Ms. Wariam Chuayjan
Candidate

.....
Assoc. Prof. Benchawan Wiwatanapataphee,
Ph.D.
Major advisor

.....
Prof. Yong Hong Wu,
Ph.D.
Co-advisor

.....
Prof. I Ming Tang,
Ph.D.
Co-advisor

.....
Prof. Banchong Mahaisavariya,
M.D., Dip Thai Board of Orthopedics
Dean
Faculty of Graduate Studies
Mahidol University

.....
Prof. Yongwimon Lenbury,
Ph.D.
Program Director
Doctor of Philosophy Program
in Mathematics
Faculty of Science
Mahidol University

Thesis

entitled

MATHEMATICAL MODELLING OF GRANULAR FLOWS AND ITS APPLICATIONS

was submitted to the Faculty of Graduate Studies, Mahidol University
for the degree of Doctor of Philosophy (Mathematics)
on
August 19, 2010

.....
Ms. Wariam Chuayjan
Candidate

.....
Assoc. Prof. Suabsagun Yooyuanyong,
Ph.D.
Chair

.....
Assoc. Prof. Benchawan Wiwatanapataphee,
Ph.D.
Member

.....
Prof. I Ming Tung,
Ph.D.
Member

.....
Prof. Yong Hong Wu,
Ph.D.
Member

.....
Prof. Banchong Mahaisavariya,
M.D., Dip Thai Board of Orthopedics
Dean
Faculty of Graduate Studies
Mahidol University

.....
Assoc. Prof. Nardtida Tumrasvin,
M.S.
Acting Dean
Faculty of Science
Mahidol University

ACKNOWLEDGEMENTS

I would like to express my sincere gratitude and deep appreciation to my advisor, Associate Professor Benchawan Wiwatanapataphee, for her guidance, enthusiasm, and encouragement throughout the entire project. Her support has been of great value to me in this research that enabled me to complete this dissertation successfully.

I would like to thank my co-advisor, Professor Yong Hong Wu for his advices and valuable comments. I am very grateful to my co-advisor. Professor I Ming Tang, for his helpful advices and suggestions. I am deeply indebted to my external examiner, Associate Professor Suabsagun Yooyuanyong, for his helpful comments.

Special appreciation is further extended to my teachers who taught me at every levels of study. I also wish to thank the Department of Mathematics, Mahidol University for providing me with necessary facilities. My thanks also go to all staff members for their great cooperation and warm friendship.

I am deeply grateful to the Staff Development Project of the Commission on Higher Education, Thailand for financial support during my study at Mahidol University and a one year period for research in Syracuse University, USA which broadened my vision in many aspects.

Finally, I am greatly to my family and my friends for their love and encouragement.

Wariam Chuayjan

MATHEMATICAL MODELLING OF GRANULAR FLOWS AND ITS APPLICATIONS.

WARIAM CHUAYJAN 4838802 SCMA/D

Ph.D. (MATHEMATICS)

THESIS ADVISORY COMMITTEE : BENCHAWAN WIWATANAPATAPHEE, Ph.D., YONG HONG WU, Ph.D., I MING TANG, Ph.D.,

ABSTRACT

In this thesis, two mathematical models have been developed to study particle flow in a vertical-sided silo with a conical hopper bottom. One mathematical model is for studying particle flow in the silo. The governing equations are the principle of conservation of linear momentum and the principle of conservation of angular momentum. The model is solved using a Discrete Element Method to investigate the behavior of granular flow in the silo, the effects of inlet flow rate, and bottom angles on the pressure distribution on the hopper wall throughout the static process of material filling into the silo. Influences of bottom angles on the discharge pattern and the pressure distribution on discharging problem in a varied mass-flow silo and a constant mass-flow silo are also discussed. Another mathematical model is for studying the air-particle flow in the silo. The governing equations for the the air flow are the continuity equation and the Navier-Stokes equations. To determine the particle movement, Newton's law is applied. The model is solved by the Finite Element Method, based on the Arbitrary Lagrangian Eulerian approach. The flow pattern in the silo and the pressure distribution along the hopper wall are investigated. The results show that the models can capture the flow pattern of particles in the silo.

KEY WORDS : MATHEMATICAL MODEL/GRANULAR FLOW
DISCRETE ELEMENT METHOD/RIGHT-CONICAL SILO

102 pages

การจำลองแบบคณิตศาสตร์ของการไหลของอนุภาคในไซโลและการประยุกต์
MATHEMATICAL MODELLING OF GRANULAR FLOWS AND ITS APPLICATIONS.

วาเรียม ช่วยจันทร์ 4838802 SCMA/D

ปร.ด. (คณิตศาสตร์)

คณะกรรมการที่ปรึกษาวิทยานิพนธ์ : เบญจวรรณ วิวัฒนปฐพี, Ph.D., Yong Hong Wu , Ph.D., I Ming Tang, Ph.D.,

บทคัดย่อ

งานวิจัยนี้พัฒนาแบบจำลองคณิตศาสตร์ 2 แบบ เพื่อศึกษาการไหลของอนุภาคในไซโลฐานกรวย แบบจำลองคณิตศาสตร์แบบแรกใช้เพื่อศึกษาการไหลของอนุภาคในไซโล สมการควบคุมใช้หลักการของโมเมนตัมเชิงเส้นและหลักการของโมเมนตัมเชิงมุม โดยใช้วิธีดิสครีทเอลิเมนต์ (Discrete Element Method) เพื่อตรวจสอบพฤติกรรมการไหลของอนุภาคในไซโลและศึกษาผลกระทบของอัตราการไหลเข้าและขนาดของมุมกรวยที่มีต่อการกระจายค่าแรงดันบนผนังของกรวยในกระบวนการบรรจุ (Filling process) นอกจากนี้ยังได้ศึกษาผลกระทบของขนาดมุมกรวยที่มีต่อรูปแบบการไหลและการกระจายค่าแรงดันในกระบวนการจำหน่าย (Discharging process) สำหรับไซโลที่มีจำนวนอนุภาคเปลี่ยนแปลง (A varied mass-flow silo) และไซโลที่มีจำนวนอนุภาคคงที่ (A constant mass-flow silo) แบบจำลองคณิตศาสตร์อีกแบบหนึ่งใช้เพื่อศึกษาการไหลของอากาศและอนุภาคในไซโลในกระบวนการบรรจุ สมการควบคุมการไหลคือสมการความต่อเนื่อง (continuity equation) และสมการเนเวียร์สโตกส์ (Navier-Stokes equations) การเคลื่อนที่ของอนุภาคใช้กฎของนิวตัน (Newton's law) การหาผลเฉลยของแบบจำลองข้างต้นนั้นใช้วิธีไฟไนต์เอลิเมนต์ (Finite Element Method) โดยอาศัยวิธีค่าเลือกแบบลากรองจ์ ออยเลอร์ (Arbitrary Lagrangian Eulerian approach) รูปแบบการไหลของอนุภาคในไซโลและการกระจายค่าแรงดันบนผนังกรวยได้ถูกตรวจสอบ ผลการศึกษาพบว่าแบบจำลองนี้สามารถอธิบายรูปแบบการไหลของอนุภาคในไซโลได้

102 หน้า

CONTENTS

CONTENTS (cont.)

CONTENTS (cont.)

LIST OF TABLES

Tables **Page**

LIST OF FIGURES

Figures **Page**

LIST OF FIGURES (cont.)

Figures **Page**

LIST OF FIGURES (cont.)

Figures **Page**

CHAPTER I

INTRODUCTION

1.1 The Filling and Discharging Processes

The filling and discharging processes, involving the flow of granular materials in silos, is used in many industries such as agriculture, mining, chemical and food processing. Although there are many different kinds of silos being used in industries, new developments are still occurring on in regards terms of silo designs and operation systems. The essential feature of the filling and discharging processes is illustrated in Figure 1.1. In the filling process, particles start to flow from the top of the silo into the silo, fall under gravity and finally the assembly particles come to rest on the base of the silo as seen in figure 1.1(a). The discharging process starts when the outlet of the silo is opened and particles flow out from the silo as seen in figure 1.1(b).

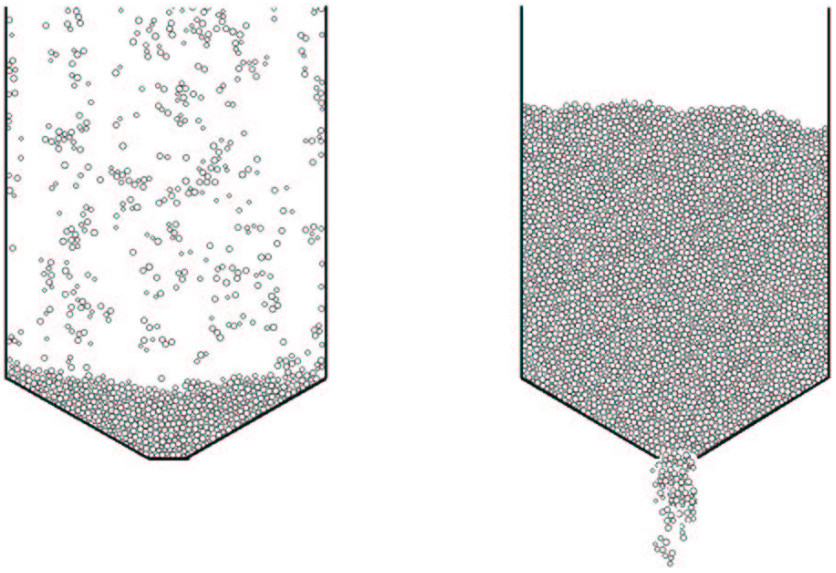

(a) Filling process (b) Discharging process

Figure 1.1: Filling and discharging processes

Many problems still encountered during the filling and discharging processes as seen in Figure 1.2. These problems are mainly

- the formation of stable arch formed above the hopper outlet. Figure 1.2(a) shows the appearance of arching. The arch shape or bridge shape is formed above the outlet of the hopper and block any further discharge, leading the flow of granular solids to be stopped.
- the piping or rotholing as seen in Figure 1.2(b) which occurs in silo if only the granular solid above the outlet is flowing out and the remaining granular solid keeps on its place without flowing.
- the segregation during filling as seen in Figure 1.2(c) are due to particle size since the large particles accumulate close to the silo walls, while the smaller particles collect in the centre. Thus, the small particles are discharged first and the large particles are discharged at the end.

In addition, silo collapse as shown in Figure 1.3 causes a lot of damage. The silo is poorly designed due to a lack of understanding of concentrated granular flow behaviors and their properties.

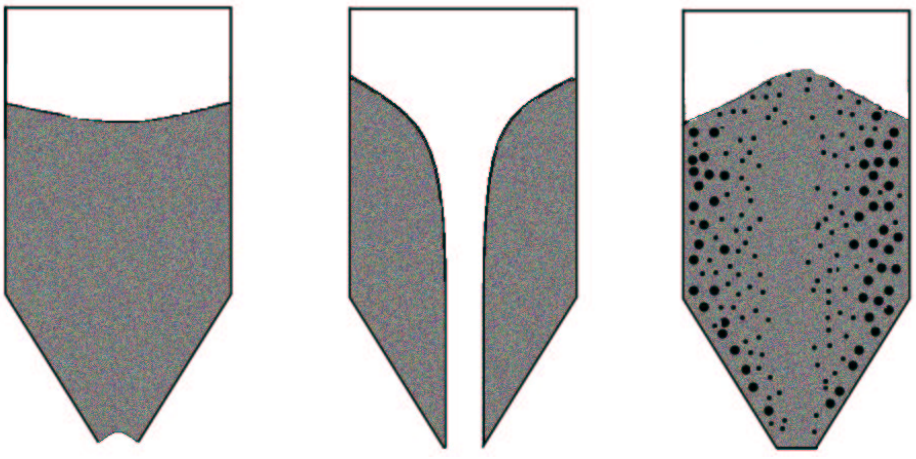

(a) Arching (b) Piping (ratholing) (c) Segregation

Figure 1.2: Flow problems

To overcome the problem, understanding fully the physics of granular flow is needed. Therefore, further study of the filling and the discharging pro-

Figure 1.3: Collapse of a silo due to a poor design [22]

cesses and development of robust mathematical models for simulating the flow of granular material become more and more important for the design of new silo systems and the optimization of these processes.

1.2 Scope and Objectives

Over the past two decades, extensive studies have been carried out to model many aspects of granular flow in silos. These studies have resulted in a basic understanding of physics of granular flow and provided some basic guideline for the design of the silo. However, many phenomena, such as the pressure distribution on the silo wall, the formation of arching and the flow behavior in the silo, have not been fully understood nor well controlled. In addition, more efficient and robust mathematical models of granular flow have to be developed. The propose of this project is to model the granular flow in silo and to develop a robust discrete element method and finite element method based computation algorithm for filling and discharging processes. More specifically, the project aims to

- develop a mathematical model for simulating the flow behavior of granular materials in a vertical-sided silo with conical hopper bottom;

- investigate the effects of inlet flow rate and bottom angles on the pressure distribution on the hopper wall through out the static process of material filling into the silo;

- investigate the effects of bottom angle on the discharge pattern and of normal pressure distribution on the discharge problem in a varied mass-flow silo and in a constant mass-flow silo.

1.3 Outline of the Thesis

This thesis is divided into six chapters. Chapter I describes the essential features of the filling and the discharging processes involving granular flow though the silo, highlights the problem arising in industries and presents the objectives and scope of the study.

Chapter II summarizes previous research works closely related to the scope of this study and particularly granular flow through silos via experimental models and mathematical models.

Chapter III presents a detailed formulation of two-dimensional discrete element model, three-dimensional discrete element model and continuum modelling of granular flows.

Chapter IV presents the development of 2-D discrete element model for the study of granular flow in the filling and discharging processes. The governing equations describing the motion of particles are the principle of conservation of linear momentum and the principle of conservation of angular momentum. Some numerical investigations on the effect of inlet flow rate and bottom angle on the pressure distribution and the flow pattern are also presented in this chapter.

Chapter V concerns the development a finite element model based on Arbitrary Lagrangian Eulerian approach to study air-particle flow in a vertical-sided silo with conical hopper bottom. Some examples of our numerical investigation of air-particle flow in the silo on the flow pattern and the pressure distributions along the hopper wall are presented in this chapter.

Chapter VI presents the conclusion gained from the present study. Discussion on future research work is given in this chapter.

CHAPTER II

PRIOR MODELLING STUDIES

2.1 General Overview

The filling and discharging processes involve many complex phenomena which occur during the processes such as pressure acting on the silo walls, the formation of arching and the flow behavior. The pressure acting inside a silo during filling and discharging processes are mainly affected by the silo configuration and the properties of the stored granular solid. Understanding these phenomena is essential for the design of silos and for minimizing problems in industrial practice. Over the past 4 decades, extensive research has been carried out to study the physics of granular material including the properties of granular materials, the silo pressure, the flow rates of granular material flowing out of silos, etc. Early research focused mainly on experimental investigation [3, 71, 86] and on deriving approximate analytical methods [34, 35, 37, 78, 79]. In general, due to the large number of particles used in the system, experiment is limited and numerical methods have been the major approach used in the study of the precess. Hence, the latest research focused mainly on developing sophisticated mathematical models and on numerical algorithms for numerically investigating various aspects of the process. Further study of the filling and discharging processes and development of robust mathematical models for simulating the flow of granular materials have become more and more important for the design of silos and optimization of these processes.

The models developed and investigations carried out previously are mainly in two areas:

- experimental models

- mathematical models.

In the following three sections, we introduce granular materials and industrial particle flows, review the experimental models and the mathematical models, and the Finite Element Method, Discrete Element Method and Hybrid method.

2.2 Granular Materials and Industrial Particle Flows

A granular material can be defined as a collection of a large number of discrete particles. Examples of such materials include sands, soil, cement, grains, chemical powders, coal, plastic pellets and mineral products. Properties of granular material are different from the collective properties of the three classical states: solid, liquid, or gas. Granular materials are neither solid nor liquid but combine properties of both solid and liquid. A granular material can behave like a solid in some cases and like a liquid in other cases depending on the stress state. Particle size of the granular material can be classified according to their mean size from small to large including ultrafine powders ($0.1-1.0\ \mu m$), superfine powders ($1.0-10\ \mu m$), granular powders ($10-100\ \mu m$), granular solids ($100\ \mu m-3.0\ mm$) and broken solids ($3.0-10\ mm$) [33]. These days, granular materials are widely used in industrial processing such as mining, cement, food, feed mill and plastics industries. To improve the quality and productivity of products, it is necessary to understand the behavior of granular flows.

Industrial application can be broadly classified according to the key physical processes such as drying, mixing, screening, storage and discharge processes.

- **Drying process**

  In an industrial drier, optimization and control of drying process have been studies [25, 59] in order to improve the management and possibly the design of industrial driers. Naon et al. (1995, [59]) proposed mathematical model to describe mass and energy transfers during convection drying of natural rubber. Hasatani et al. (1991, [25]) proposed an experimental

model to confirm the effectiveness of radiative heating on drying of wet granular materials. They examined quantitative evaluation of the radiation effect and a theoretical model.

- **Mixing process**

  Powder mixing is a key process in many industrial blending system. Prediction of powder motion is important in many systems including pharmaceutical, food and polymer manufacturing. Many researches have been carried out to study granular flows related to powder mixing [40, 58, 73]. Portillo et al. (2006, [66]) simulated a powder mixing process based on compartment modelling. The V-blender is an example system. The effects of the sample location, number of samples, particles with the sample and sampling time have investigated. The results showed that initial loading could substantially increase the required mixing time to reach a homogenous state. More detail of mixing of granular material can be seen in Hill's review paper [29].

- **Screening process**

  Industrial screening is a process used for particle separation in the food industry and the pharmaceutical industry. The study of particulate systems has been carried out to understand the complicated size distribution and composition. This physical understanding is led to a great economic impact. Li et al. [49, 50] studied screening separation of a granular mixture of two types of particles: soybeans and mustard seeds on an inclined screen. The results indicated that the effect of particle bed depth is crucial to particle segregation in material layers and hence to screening efficiency. Dong et al. (2009, [17]) simulated a three dimensional discrete element model of typical 3-deck and 5-deck banana screens. They investigated an effects of vibration conditions and geometry of the screen on the sieving processes. Their model has been to be very useful to the development of a better understanding and the control of banana screening processes.

- **Storage and Discharge Processes**

The storage of bulk solids has been studied using the discrete element method. Many researche works have studied the solid phase stresses in simple shear flow with periodic boundaries [19, 41, 46, 56]. Many devices such as silo, hopper, bin and bunker can be used to store granular materials. The silo is often used for storing and discharging the granular materials in mineral processing and manufacturing industries. There are variety of shapes of the silos as shown in Figure 2.1. The flow of granular materials from these silos are frequently studied. When a granular material is discharged from the silo, there are two different types of flow: mass flow and funnel flow. In mass flow, all particle inside the silo is in motion during discharging process as shown in Figure 2.2(a). Figure 2.2(b) presents the funnel flow, only material in the center above the hopper outlet is in motion while some of the materials near the wall remain stationary during the discharging process. There is also the special case that combines both of mass flow and funnel flow and this called mixed flow as shown in Figure 2.2(c). In mixed flow, the boundary on the flowing solid intersects the vertical walls of the silo at a point called effective transition.

2.3 Experimental Models

To fully understand the physics of granular flows in silo, the pressure distribution in silos have been measured. The pressure distribution at the bottom of a silo was firstly reported by Janssen (1895, [34]). In 1964, Jenike [35] studied the importance of characterising the flow during discharge process of a silo and noticed its effect on the wall pressure distribution. In 1969, Aoki and Tsunakawa [1] measured wall pressure in a hopper and a bin-hopper system under stationary and flowing conditions. They found that the material bed near the outlet becomes loose under gravity flow condition and the velocity of individual particles increased rapidly, resulting in a continuous increased in the dynamic pressure on the wall. In 1990, Ooi et al. [64] measured pressures on the walls of a prototype silo subject to both concentric and eccentric flow. Their experiment included filling, storage and both concentric and eccentric discharge. They investigated

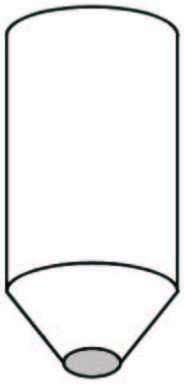

(a) Conical Hopper

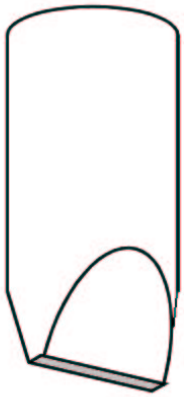

(b) Chisel

(c) Wedge

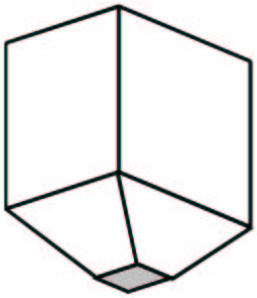

(d) Pyramid

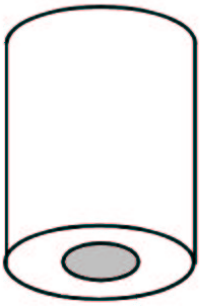

(e) Cylindrical flat-bottomed slot

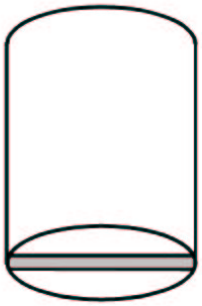

(f) Cylindrical flat-bottomed circular

Figure 2.1: Silo geometries

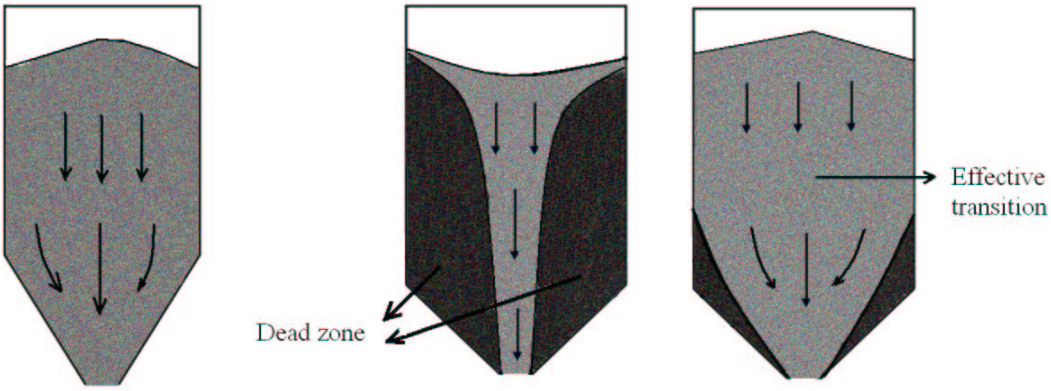

(a) Mass flow (b) Funnel flow (c) Mixed flow

Figure 2.2: Flow patterns in silos

systematic unsymmetrical pressure patterns. The results provided a region basis for the representation of pressure distributions for silo design.

In 2000, Brown et al. [3] carried out experiments on a square steel silo containing two different free-flowing granular solids, sand and pea gravel. They investigated the patterns of pressure during filling, storage and discharge processes. The results showed that the pressure across the face of each wall was non-uniform. High pressure was seen to develop near the corners and low pressure near the centre of the wall. The results showed that changes in the stiffness of the walls affected the pressure distribution around the circumference of a rectangular silo.

In 2001, Yang and Hsiau [86] carried out on experiment to investigate the flow pattern and wall normal stress of the silo during discharging process. They used two different inserts in funnel flow to improve the flow pattern to mass flow type. The effects of using differently shaped inserts on the flow pattern and wall stress were analyzed. Zhong et al. [88] carried out in a pilot scale silo storing plastic pellets and barley. The silo is thin-walled and made of aluminium and has a flat bottom. They investigated the flow pattern and wall stresses. The results showed that the filling process had a marked effect on the solids flow pattern and the wall stresses for plastic pellets, but very little effect on those for barley.

In 2002, Rotter et al. [71] performed experiments in a rectangular planform silo with flexible walls. They focused on pressures measured at the

end of the filling process. Two different solids, sand and gravel, were used in the experiment. The results showed that the pressure distribution at any level was systematically non-uniform, though most existing silo pressure theories and design codes assume uniformity in any horizontal. High pressures were found to develop in the corners of the silo.

Recently, Chen et al. (2007, [8]) carried out experiments in a full-scale silo storing approximately 250 tonnes of iron ore pellets. They measured both the flow pattern and the wall pressures. The experiments showed a strong correlation between the flow channel and the discharge pressure distribution.

2.4 Mathematical Models

In the past, many simulation tools have been used to investigate the flow behavior of granular solids and the pressure distribution in silos. These tools include Finite Element Method (FEM), Discrete Element Method (DEM), averaging method, statistical analysis and hybrid method. However in this study, we review three well known methods: FEM, DEM, and hybrid method.

2.4.1 Finite Element Method

The finite element method has been used to simulate the dynamics with continuum and discontinuum. Here, we present the use of FEM to study the granular flow in silo.

In 1991, Ooi and Rotter [65] studied the pressures on the walls of conical silo hoppers based on the assumption that the material stored within the hopper is in an elastic state. The simulation is conducted using a finite element analysis. The effects of hopper wall friction and hopper wall flexibility on the stress distribution were investigated. The results indicated that the pressure distributions were quite insensitive to assumed elastic properties of the solid. An increase in the wall friction coefficient decreases the wall pressures. In very shallow hoppers, the maximum pressure tends to occur towards the bottom. As the hopper is made steeper, the maximum pressure occurs progressively higher up the hopper.

In 1996, Ooi et al. [63] presented a finite element model to analyze the mechanical behavior of coal and its effect on silos arching and pressures acting on silo walls. The results showed that the finite element predictions lay close to the average of all the classical theory predictions. Near the top and the bottom, the finite element predictions differed significantly from classical predictions. In 1998, Karlsson et al. [39] used a fluid model to study granular flows in silos. The FE simulation gave a flow pattern representing either a mass or funnel flow simulation.

In 2003, Guaita et al. [23] proposed three dimensional model to study the influence of hopper eccentricity on pressure using FEM. Based on assumption that the stored material is an elasto-plastic behavior. The computation domain is a circular cylindrical silo with an eccentric hopper. The result indicated that the pressure increased on the side opposite to the outlet displacement, as the eccentricity of the hopper increased. Within the same eccentricity, the pressure along the wall of the cylinder as well as on the wall of the hopper increased as the internal friction angle decreased. Goodey et al. [20] developed a finite element model for the filling pressure distribution in a square planform silo with flexible walls. The results were compared with experimental study. They investigated both the state of stress in the stored solid and the pressures imposed on the silo walls. The results showed that the horizontal pressure distribution at any given depth at the end of filling was far from uniform, with larger pressures developing in the corners than against the mid-side of the silo walls.

In 2006, Goodey et al. [21] used a three dimensional finite element model for square planform thin-walled silos to predict the wall pressures in a wide range of geometries after filling with three different solids: sand, gravel and wheat. They investigated the state of stress in the stored solid, the pressures imposed on the silo walls and the non-uniform horizontal pressure distribution at any given depth at the end of filling in silo with flexible walls. The results showed that the hyperbolic function proposed for this horizontal pressure distribution gave a close representation of the new predictions.

In 2007, Wu et al. [83] developed a finite element model to study

the flow of dry granular solids through a domain involving a frictional contact boundary. The granular material is assumed as a compressible viscous-elastic-plastic continuum. The FEM in space and the finite different method in time are used to solve the problem. The results were qualitatively satisfactory in the sense of capturing the pressure concentration in the transition area of vertical and converging hopper wall.

2.4.2 Discrete Element Method

The DEM, which was introduced by Cundall and Strack in 1979 [16], has become more popular for studying the physics of granular materials. The DEM can describe granular flow at a particle scale based on the Newton's second law. The motion of each individual particle have two types: transitional and rotational motions. Equations of motion are the principle of linear momentum and the principle of angular momentum. By integrating the equations of motion for each particle with respect to time, the velocity and displacement of the particles at any instant of time are derived. Over the last few decades, a great deal of effort has been carried out in developing various different discrete element models to describe the flow behavior of granular material. These models can be classified into two categories, namely the hard particle models (Campbell and Gong (1986, [6]), Hopkins and Louge (1991, [31]) and Hopkins and Shen (1986, [32])) and the soft particle models (Cundall and Strack (1979 [16]), Walton and Braun (1986, [80])). The soft particle model originally developed by Cundall and Strack [16]. This model allows for deformation of particle which is modeled as an overlap of the particles. The hard particle model assumes that particles are rigid.

The simulations carried out in the past were either performed in two-dimensional model (Langston et al. [45–48], Banton et al. [2], Yang and Hsiau [86]) and three-dimensional model (Cleary and Sawley (1999 [13], 2002 [14])), Hirshfeld and Rapaport (2001, [30]), Li et al. (2004, [51]), Zhao et al. (2006, [87]), Cleary (2004, [9]), and Goda and Ebert (2005, [19])).

In 1979, Nguyen et al. [62] presented an approximate solution to the flow of a cohesionless granular material in a conical hopper. The material is

modelled as a perfectly plastic continuum which satisfies the Mohr-Coulomb yield condition. They derived analytical expressions of the mass flow rate and the wall stress which were compared to some experimental data and other analyzes.

In 1995, Langaton et al. [46] simulated filling and discharge in flat bottomed and conical hoppers. The granular material was modelled as an assembly of non-cohesive discs for the two dimension, and spheres for the three dimension. Numerical values for discharge rate, static average bulk density, static hopper wall stress and discharge wall stress in two and three dimension were obtained. They also observed the appearance of rupture zone within the material and associated wall stress peaks where the rupture zones intersect with the hopper wall. Rong et al. [69] simulated flow behavior of idealized particles in a bin of various shapes using the DEM. They focused on two distinct aspects: occurrence of shear bands and use of flow corrective inserts. The results showed that particle properties and outlet size influenced the formation and development of shear bands. Flow corrective insert placed at an optimum height could reduce stagnant zones, stabilize discharge rate and enhance uniform flow.

In 1999, Zhou et al. [89] studied sandpiles of glass beads using both experiments and simulations. They used a modified DEM model in which the effect of rolling resistance was considered. In their consequent study, both the rolling and sliding friction were examined, together with the influence of density and size of the particles. The result showed that the angle of repose increases significantly with the rolling friction coefficient and decreases with particle size. Cleary [9, 10, 12] and Cleary and Sawley [13, 14] presented a series of three dimensional simulations of a number of industrial applications including ball mill, Hicom nutating mill, discharge from single- and four- port cylindrical hoppers and particle size separation by a vibration screen. Numerical simulation based on DEM was carried out to investigate the effect of particle shape and interparticle cohesion on the granular flows. The results obtained indicate that DEM modelling is now sufficiently advanced that it can make useful contributions to process optimization and equipment design.

In 2000, Masson and Martinez [56] performed discrete element simula-

tions of the filling and discharge of a plane rectangular silo with a set of different values of particle mechanical parameters. They examined the influence of friction and stiffness of contacts. The results showed that these parameters played a major role in the flow kinematics and the stress field during filling and discharging processes.

In 2001, Yang and Hsiau [86] investigated the flow pattern and wall normal stress of the filling and discharging processes for two-dimensional plane silos. They used both the simualtion method of DEM and experimental methods. The effects of using differently shaped inserts on the flow pattern and wall stress were analyzed. The results showed that the wall normal stress distribution was significantly changed as the inserts were installed in silos. Hirshfeld and Rapaport [30] proposed molecular dynamics methods to study the gravity-driven flow of granular material through a horizontal aperture, a model for discharge from a storage silo. The results showed that spatial kinetic distributions reveal where the translational and rotational motion was strongest. The model with velocity-dependent damping forces could describe the dynamics of granular behavior.

In 2002, Masson and Martinez [57] investigated the effect of particle properties and silo geometry using discrete element simulations. They used a flat-bottomed silo and a cylinder-hopper silo, containing 10,000 and 8,500 particles in simulation. The results showed that both the mechanical properties of the particles, namely contact stiffness and friction play a major role on the force transmission patterns, and more specifically on arching effects.

In 2003, Markino et al. [54] developed a mathematical model using the DEM coupled with airflow analysis. This model was applied to free fall, blow and aeration filling on the behavior of sand particles during the sand molding processes. The influences of the air pressure on blow and aeration filling were investigated. Their result has provided new and valuable information on the behavior of sand particles during the sand molding processes.

In 2004, Li et al. [51] studied three-dimensional flows of granular particles in a rectangular hopper using both experiment and DEM. In experiment, they focused on the particle flow behavior, arching effects and the measurement of par-

ticle mass flow rate at different hopper opening using high-speed video recording analysis. The flow behavior of particles and their arching and discharging in the hopper were analyzed and compared with the DEM for three hopper openings. The results indicated that DEM has the potential to analyse particle packing structure and flow patterns more thoroughly than the experiment.

In 2005, Zhu and Yu [90] investigated the microscopic and macroscopic behavior of the granular materials in a cylindrical hopper with flat bottom based on DEM. The silo contained 24,000 multi-sized spherical particles. They analyzed the dependence of flow behavior on the geometric and physical parameters of the hopper and particles, such as the orifice size and wall roughness of hoppers, and frictional and damping coefficients between particles. The results indicated that there were four different zones in the hopper flow: a stagnant zone, a plug flow zone, a converging flow zone, and a transition zone from plug flow to converging flow. Goda and Ebert (2005) [19] modelled the initial fill and the subsequent discharge of a hopper using three-dimensional discrete element simulations. The different containers were filled using 40,000 mono-sized spherical particles. They investigated both the flow patterns and the distributions of the normal wall forces. They showed that the pressure distributions calculated during the discharge were in accordance with both analytical and two-dimensional simulation results. In the case of silo flow, a pressure peak has appeared at the transition from the vertical-sided section to the hopper bottom. The peak value in the hopper section was about two times greater than the one in the vertical-sided section. Since the models were not sufficiently high in vertical direction, the static wall pressures did not reach a constant, height-independent value. Instead, they showed a linear tendency. Zhu et al. [91] analyzed three popular methods simulating granular flow at different time and length scales: DEM, averaging method and viscous, elastic-plastic continuum model. They considered mathematical models of these methods and applied to hopper flows. Their results were found that discrete element simulation was an effective method to study the micro-dynamic behavior of the granular flow such as flow pattern, velocity, and force structures. The macroscopic quantities such as velocity and stress can be obtained by FEM.

In 2006, Markauskas [55] performed the DEM modelling using complex axi-symmetrical particles for the hopper filling and discharge. The influence of particle shape on discharge rate was analysed. The hopper filled with 2,000 spherical particles and 1,000 complex particles. The results showed that the spherical particles ran out from the hopper in significantly shorter time period comparing with the complex particle. Zuo et al. [92] simulated the dynamic feature of bulk granular material during sudden braking of a truck by applying DEM. The effects of inertia dynamic force with different braking speeds and inter-particle interactions were investigated. The results obtained may provide useful information for the examination of the strength of the truck frame and also for a proper design of this type of trucks.

In 2008, Kim [43] proposed mathematical model for simulating granular motion by DEM. His model was based on Voigt model in which the elastic and damping forces were involved. The results showed that the particle motions in the processes were well described by the presented model. Fraige et al. [18] developed a model for cube-shaped particles using the DEM. Their model based on multi-contact principles. Laboratory experiments and simulations in terms of static packing, flow pattern and flow rates for spherical and cubic particles were compared. The results showed that the multiple-contact model was a better solution for surface-surface contact than the single-contact version and should be used for polyhedral shapes. The simulation results were compared with experimental measurements and the results were in good agreement.

In 2009, Li et al. [52] proposed DEM model to study cylindrical pebble flow during discharge process under gravitational force with in a semi-cylindrical silo. In their model, two cases were considered. One was for tracking the trajectories of identified particles with 11,500 glass beads, and the other was for double-zone flow for estimation the mixing evolution with 10,460 glass beads. The numerical results were compared with experimental measurements and the results were in good agreement. The DEM model can predict real pebble flow. Wu et al. [81] performed a multi-scale study of the particle flow by means of DEM. They investigated the flow behaviors on the particles diameter distribu-

tion and silo geometry to establish the spatial and statistical distributions of microdynamic variables related to flow and silo structures. The results showed that the distribution of particle diameter has great effects on particle flow. The silos geometry has greater effects on granular flow than particle size distribution and inserts can improve the flow behavior of funnel flow type to mass flow. Ketterhagen [42] studied the mode of power flow in a series of three-dimensional conical hoppers and a quasi-three-dimensional wedge-shaped hoppers using the discrete element method. The effects of friction, hopper shape, and hopper wall angle on the nature of flow from a hopper were examined. The results demonstrated that the DEM predictions were generally in very good agreement with the Jenike design charts [35, 36]. Banton et al. [2] simulated well-controlled unsteady channelized granular flows using the DEM. They performed a parametrical analysis on a simple 2-D model to estimate the influence of particle shape, friction parameters, and restitution coefficients on the dynamics of the flow and on the deposit geometry. The results demonstrated the capability of the DEM technique for modeling avalanche of granular material.

More detail of an international collaborative study into the predictive capacity of current discrete element and finite element calculations for granular solids in silos can be seen in a Rotter's review paper [72], a Nielsen's review paper [61], a Campblell's review paper [7], a Ketterhagen's review paper [42], and a Sitharam's review paper [75].

2.4.3 Hybrid Method

A hybrid method is based on FEM and DEM. Very little attempts have studied the flow of granular materials using the hybrid method. In 1977, Negi et al. [38, 53, 60] proposed a hybrid numerical model based on FEM and DEM to predict the stress and velocity fields for particulate materials during discharge from silos. The FEM was used to model the granular materials as a continuum. In regions where the granular material no longer behaves as a continuum and in regions where there are large shear deformations, the DEM was used. The results indicated that the model was capable of predicting flow velocities, stresses and

wall pressure during discharging. In 1998, Rotter et al. [72] compared between FEM and DEM analysis for predicting the behavior of granular solids in silos. They focused on three problems: filling process, discharge of granular solid from a silo with a flat-bottom and a tapered hopper.

2.5 Concluding Remarks

By over-viewing the development of the filling and discharging processes and examining previous researches on the modelling of granular flows, the formation of arching above the outlet of the silo in the process, the following conclusions can be made.

(a) Although the filling and discharging processes have been used in many industrial applications for over 4 decades, many problems such as flow blockage, dead zones, segregation and silo collapse still frequently occur in practice. These problems are expected to become more and more critical to success of the process. Thus, further study of the filling and discharging processes is essential in order to have proper silo design and control of the process to minimize problems in the industrial practice.

(b) The filling and discharging processes are a many faceted big industrial problem which gives rise to many sub-problems. Although previous work has resulted in a better understanding of the granular flows occurring in the filling and discharging processes, many phenomena are still not fully understood and required further vigorous investigation. The most important problem which requires further intensive investigation is stress analysis and pressure on the wall of the silo. To date, proposed mechanisms for granular flow behavior and formation of arching above the outlet of the silo have been mainly conceptual in nature and relationships between silo parameters and the observed pressure are rationalized in a qualitative manner only. Although previous mathematical work looks very promising, no complete model and corresponding numerical technique has been developed and shown to be able to simulate the granular flows in a long time period.

(c) Mathematical models and numerical methods have been proposed to investigate complex phenomena in the filling and discharging processes. These complex phenomena include the flow behavior, the formation of arching and rathole. Although many mathematical models and numerical schemes have been developed, further work is still required.

CHAPTER III

MATHEMATICAL MODELS

3.1 General Overview

As reviewed in Chapter II, flow pattern of granular materials in silos during the filling and discharging processes plays an important role in many industries. In order to optimize the process, a proper understanding of the complex phenomena through silos is important, which can only be achieved with a simulation. The formation of arching, and flow behavior such as zig-zag flow and tunnel flow occurring during the filling and discharging of granular materials through silos have been studied by both experimental model and mathematical model over the last 4 decades. However, very little work has been done to describe these phenomena within a proper mathematical framework. Hence, development of efficient and comprehensive models to investigate the flow behavior of granular materials in silos is a worthwhile undertaking.

In the following three sections, we present the 3-D discrete element model and the continuum model of granular flows, respectively.

3.2 Dimensional Discrete Element Model

A model of particle-particle interaction in normal and tangential directions as shown in Figure 3.1 has been proposed by Cundall and Strack [16] to formulate a simple model using a spring, dash-pot and slider. In the model, based on Newton's second law, the forces acting on particles can be obtained [4].

Here, we consider an assembly of spherical particles. There are two types of particle motion: translational and rotational motions. The translation motion is caused by the contact force and gravitational force and the rotational motion is caused by the moment acting on particle. The governing equations to

describes translational and rotational motions of particle i are as follows:

$$m_i \frac{d^2}{dt^2}\mathbf{r}_i(t) + \lambda m_i \frac{d}{dt}\mathbf{r}_i(t) = \mathbf{F}_C(t) + m_i\mathbf{g}, \tag{3.1}$$

$$I_i \frac{d^2}{dt^2}\theta_i(t) + \lambda I \frac{d}{dt}\theta_i(t) = \mathbf{M}(t), \tag{3.2}$$

where $\mathbf{r}_i(t)$ is the function of time presenting the position vector of the particle at time t, $\mathbf{F}_C$ is the total contact force acting on particle, m_i is the mass, $\mathbf{g}$ is the gravity acceleration, θ is the angle of rotation, $\mathbf{M}$ is the total moment acting on particle, I_i is the inertia moment of the particle.

The contact force $\mathbf{F}_C$ in equation (3.1) consisting of spring force and damping force can be calculated by using the model of Cundall and Strack as shown in Figure 3.1. Based on those models, the force is divided into two components of the normal component and the tangential component.

Considering the normal component of the contact force $\mathbf{f}_{Cnij}$ acting on particle i, we have

$$\mathbf{f}_{Cnij} = (-k_n\delta_{nij} - c_n(\mathbf{v}_{ri} - \mathbf{v}_{rj}) \cdot \mathbf{n}_{ij})\mathbf{n}_{ij} \tag{3.3}$$

where k_n is the stiffness of spring, δ_{nij} is the overlap distance between particle i and particle j, c_n is the damping coefficient in normal direction which can be estimated by $c_n = 2\sqrt{k_n m_{ij}}$, $\mathbf{v}_r$ is the velocity of particles and $\mathbf{n}_{ij}$ is the unit vector from the center of particle i to that of particle j.

The tangential components of the contact forces are $\mathbf{f}_{Csij}$ and $\mathbf{f}_{Cpij}$ which can be calculated by the equations (3.4) and (3.5),

$$\mathbf{f}_{Csij} = -k_s\mathbf{u}_{sij} - c_s\mathbf{v}_{sij}, \tag{3.4}$$

$$\mathbf{f}_{Cpij} = -k_p\mathbf{u}_{pij} - c_p\mathbf{v}_{pij} \tag{3.5}$$

where k_s, k_p are the tangential stiffness; c_s, c_p are the damping coefficients in tangential direction which can be estimated as the damping coefficient in normal direction; $\mathbf{u}_{sij}, \mathbf{u}_{pij}$ are the relative displacements in the tangential direction and $\mathbf{v}_{sij}$, $\mathbf{v}_{pij}$ are the relative velocity vectors in the tangential direction at the contact point and they are given by

$$\mathbf{v}_{sij} = (\mathbf{v}_{ri} - \mathbf{v}_{rj}) \cdot \mathbf{s}_{ij} + \left(R_i\left(\frac{d}{dt}\theta_i \times \mathbf{n}_{ij}\right) + R_j\left(\frac{d}{dt}\theta_i \times \mathbf{n}_{ij}\right)\right) \cdot \mathbf{s}_{ij}, \tag{3.6}$$

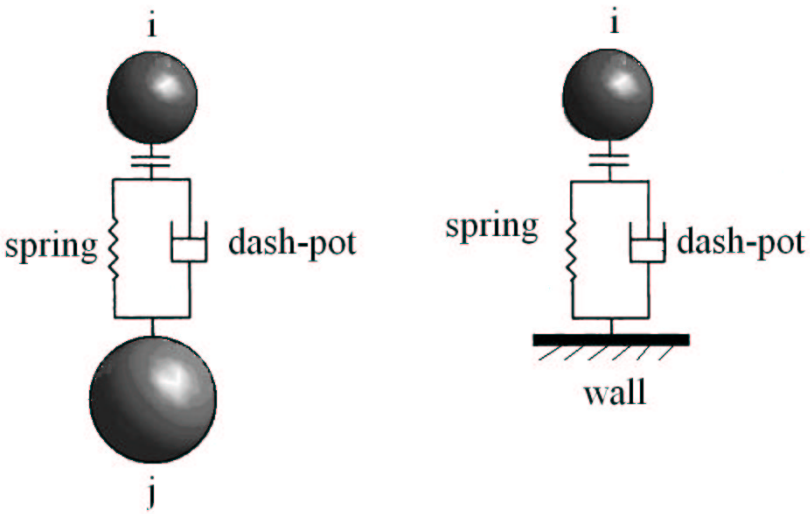

(a) Normal force

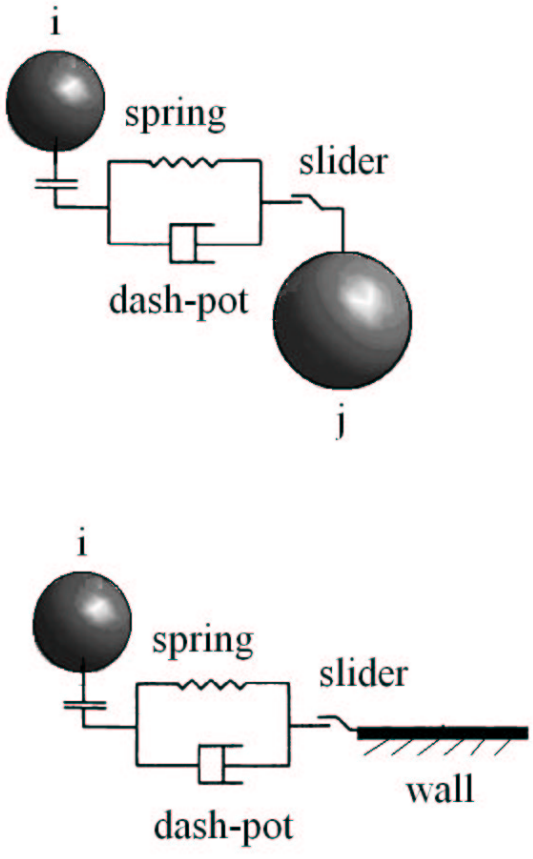

(b) Tangential force

Figure 3.1: Models of contact forces in normal and tangential directions

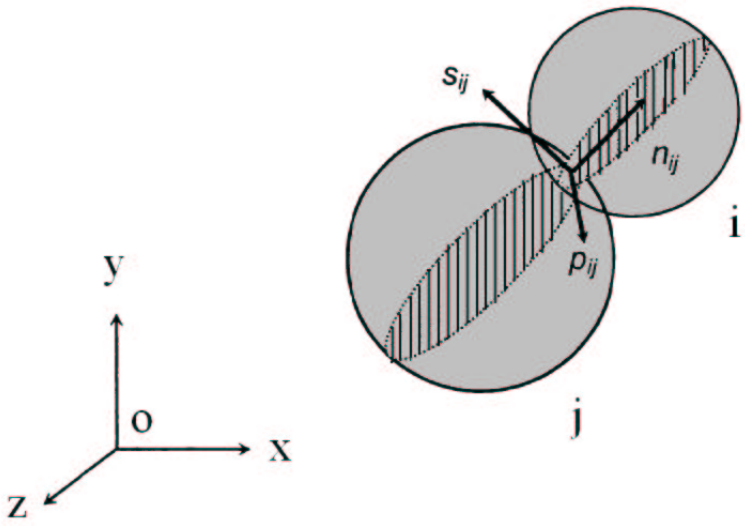

Figure 3.2: Relation between two coordinate systems (x, y, z) and $(\mathbf{n}, \mathbf{s}, \mathbf{p})$

$$\mathbf{v}_{pij} = (\mathbf{v}_{ri} - \mathbf{v}_{rj}) \cdot \mathbf{p}_{ij} + \left(R_i \left(\frac{d}{dt}\theta_i \times \mathbf{n}_{ij} \right) + R_j \left(\frac{d}{dt}\theta_i \times \mathbf{n}_{ij} \right) \right) \cdot \mathbf{p}_{ij}, \qquad (3.7)$$

where R_i and R_j are respectively the radii of the particle i and j; $\mathbf{s}_{ij}$ and $\mathbf{p}_{ij}$ are the unit vector in tangential direction as shown in Figure 3.2. In the above calculations when a particle i contacts with the wall, the index j then is replaced w which means $\mid \mathbf{v}_j \mid = \mid \frac{d}{dt}\theta_j \mid = 0$. The forces in the tangential directions must satisfy the Coulomb's friction law.

Based on the Coulomb's friction law, if the condition

$$\sqrt{\mathbf{f}_{Csij}^2 + \mathbf{f}_{Cpij}^2} > \mu |\mathbf{f}_{Cnij}| \qquad (3.8)$$

is satisfied, then the particle i slides and the tangential forces become

$$\mathbf{f}_{Csij} = -\mu \mid \mathbf{f}_{Cnij} \mid \frac{\mathbf{v}_{sij}}{\sqrt{\mathbf{v}_{sij} + \mathbf{v}_{pij}}}, \qquad (3.9)$$

$$\mathbf{f}_{Cpij} = -\mu \mid \mathbf{f}_{Cnij} \mid \frac{\mathbf{v}_{pij}}{\sqrt{\mathbf{v}_{sij} + \mathbf{v}_{pij}}}. \qquad (3.10)$$

Due to the contact forces in the tangential direction, the moment acting on particle i, is given by

$$\mathbf{M}_{ij} = R_i \mathbf{n}_{ij} \times (\mathbf{f}_{Csij} + \mathbf{f}_{Cpij}). \qquad (3.11)$$

In general, some particles may contact with a particle i at the same time, the total force and the moment acting on the particle i can be obtained by the equations

(3.12) and (3.13),

$$\mathbf{f}_{Ci} = \sum_j (\mathbf{f}_{Cnij} + \mathbf{f}_{Csij} + \mathbf{f}_{Cpij}), \tag{3.12}$$

$$\mathbf{M}_i = \sum_j (R_i \mathbf{n}_{ij} \times (\mathbf{f}_{Csij} + \mathbf{f}_{Cpij}). \tag{3.13}$$

Substituting $\mathbf{f}_{Ci}$ and $\mathbf{M}_i$ in equations (3.12) and (3.13) into equations (3.1) and (3.2) gives a equations (3.14) and (3.15),

$$m_i \frac{d^2}{dt^2}\mathbf{r}_i(t) = \sum_j (\mathbf{f}_{Cnij} + \mathbf{f}_{Csij} + \mathbf{f}_{Cpij}) + m_i \mathbf{g}, \tag{3.14}$$

$$I_i \frac{d^2}{dt^2}\theta_i(t) = \sum_j (R_i \mathbf{n}_{ij} \times (\mathbf{f}_{Csij} + \mathbf{f}_{Cpij}), \tag{3.15}$$

Solving the equations (3.14) and (3.15), by integrating step by step then the velocity and the position of a particle after each time step $\triangle t$ are given by

Translational motion:

$$\frac{d}{dt}\mathbf{r}^{t+\frac{1}{2}} = \frac{d}{dt}\mathbf{r}^{t-\frac{1}{2}} + \frac{\mathbf{F}_C^t}{m} \triangle t, \tag{3.16}$$

$$\frac{d}{dt}\mathbf{r}^{t+1} = \mathbf{r}^{t-1} + \frac{d}{dt}\mathbf{r}^{t+\frac{1}{2}} \triangle t, \tag{3.17}$$

Rotational motion:

$$\frac{d}{dt}\theta^{t+\frac{1}{2}} = \frac{d}{dt}\theta^{t-\frac{1}{2}} + \mathbf{M}^t \frac{\triangle t}{I}, \tag{3.18}$$

$$\frac{d}{dt}\theta^{t+1} = \theta^{t-1} + \frac{d}{dt}\theta^{t+\frac{1}{2}} \triangle t. \tag{3.19}$$

Choosing the time step

$$\triangle t < 2\sqrt{\frac{m}{k_n}}, \tag{3.20}$$

we can obtain the stable solution of the problem.

3.3 Continuum Model of Granular Flows

3.3.1 Viscous Elastic-Plastic Model

Based on a plastic potential g_p which is a function of stress, if the stress state satisfies the yield condition $f = 0$, plastic deformation occurs and the plastic

strain rates d_{ij}^p are proportional to the derivatives of the plastic potential with respect to the corresponding stress, i.e,

$$d_{ij}^p = \lambda \frac{\partial g_p}{\partial \sigma_{ij}}. \tag{3.21}$$

If g_p is identical to the yield function f, then the flow rule is called associated. Otherwise it is non-associated. The most widely used yield condition is the so-called Mohr-Coulomb failure criterion. It states that the material fails when the shear stress τ acting on the surface of a material element attains the critical value $\tau = c + \sigma \texttt{tan}\phi$ for the compressive normal stress σ, the cohesion c and the angle ϕ of internal friction. Based on the Mohr-coulomb criterion, various types of constitutive equations have been developed to predict the stress field. Due to unrealistically large dilation rates of the result, two other types of models have been proposed. One type abandons Coulomb's failure and replaces it by a family of yield curves depending on the current density [70]. Another type uses a plastic potential different to the yield function [44, 74].

Wu and Schmidt [84] developed a no-tension elastic-plastic model as a special case to describe the no-tension behavior of granular materials. Various researches have combined the plastic flow rule theory with the elasticity theory and the fluid mechanics theory to describe the viscous behavior of granular flow. It is called as a viscous, elastic-plastic model. In the model, the stress tensor consists of a rate dependent part $\overset{\circ}{\sigma}_v$ and a rate independent part $\overset{\circ}{\sigma}_s$, namely

$$\overset{\circ}{\sigma} = \overset{\circ}{\sigma}_v + \overset{\circ}{\sigma}_s, \tag{3.22}$$

where σ° is the co-rotational rate of stress, namely

$$\overset{\circ}{\sigma} = \frac{\partial \sigma}{\partial t} + v \cdot \bigtriangledown \sigma + \sigma w - w\sigma. \tag{3.23}$$

Due to the viscous effect, the rate dependent part σ_v is determined either by the linear viscous fluid model or a non-Newtonian fluid model. Due to the elastic-plastic deformation, the rate independent part σ_s is determined by the plastic flow rule model. Thus

$$\overset{\circ}{\sigma} = Hd + \overset{\circ}{G}d, \tag{3.24}$$

where d and w denote respectively deformation rate and spin tensors.

The governing equations of the stress and velocity fields are the stress equations of motion, the viscous elastic-plastic constitutive equations and boundary conditions. Thus, the boundary value problem is: find σ and v such that

$$\begin{aligned}
\sigma_{ji,j} + X_i - \rho\frac{Dv_i}{Dt} &= 0 \ \text{ in } \Omega, && (3.25)\\
\overset{\circ}{\sigma}_{ij} &= H_{ijrs}d_{rs} + G_{ijrs}\overset{\circ}{d}_{rs} \ \text{ in } \Omega, && (3.26)\\
v_i|_{t=0} &= \overset{\circ}{v}_i, \quad \sigma_{ij}|_{t=0} = \overset{\circ}{\sigma}_{ij}, \ \text{ in } \Omega, && (3.27)\\
v_i &= 0 \ \text{ on } \partial\Omega_a, \quad \sigma_{ij}n_j = \overline{f}_i \ \text{ on } \partial\Omega_t, && (3.28)\\
v_i n_i &= 0, \quad f_t = -sgn(v_t)\mu f_n \ \text{ on } \partial\Omega_t, && (3.29)
\end{aligned}$$

where the domain $\Omega \in R^3$ and the boundary $\partial\Omega = \partial\Omega_a = \partial\Omega_a \cup \partial\Omega_t \cup \partial\Omega_f$ of Ω, n denotes the unit outward normal vector of $\partial\Omega$. Due to the complexity of the underlying equations, various numerical techniques based on the Galerkin finite element method and the boundary element method have been proposed to solve boundary value problems of practical interest [67, 83, 84].

3.3.2 Double-Shearing Models

Based on the Mohr-coulomb yield condition, the double-shearing flow theory state that the stress reaches the yield condition, flow of granular occurs by shearing along two families of planes, namely the α- and β-characteristics. These two planes are inclined at angles $\pm\theta_\alpha(\theta_\alpha = \frac{\pi}{4} + \frac{\theta}{2})$ to the direction of the principal stress σ_1 where ϕ is the angle of material internal friction, as shown in Figure 3.3.

The most significant pioneering work on the development of the double-shearing theory is due to Spencer [76]. Based on the assumption that the complete deformation at any point of the material consists of two shearing motions on the α- and β-lines and which are superposed one on another. Many studies have been carried out to further examine the Spencer's theory and to extend the theory to axially symmetric cases and three-dimensional cases [29]. Spencer & Kingston [77] proposed a dilatant model by expanding an amount which is equal in all spatial directions based on the hypothesis that the volume of granular material

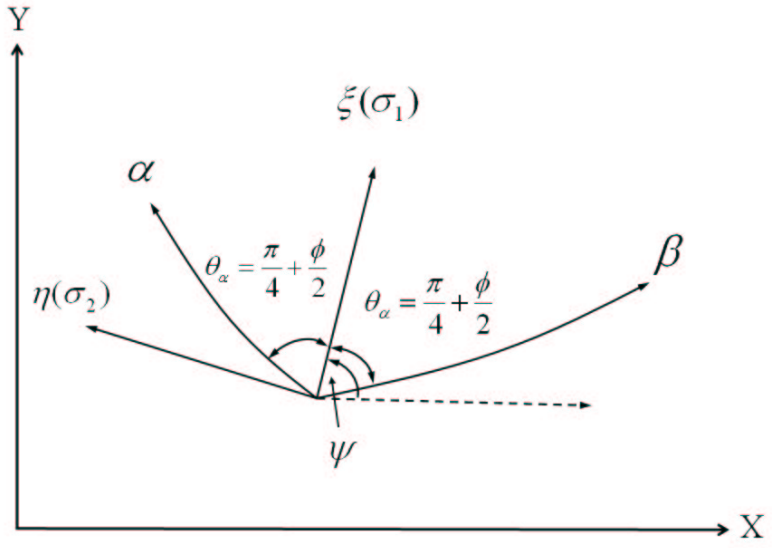

Figure 3.3: Coordinate systems, α- and β-lines

increases during flow. The density is thus a state variable which is related to the stress and deformation history. Another type of models has been proposed by Harris [24] and Hill & Wu [27]. This model based on the kinematic proposal of Butterfield & Harkness [5] states that any change in velocity relative to the slip-line field is in a direction inclined at ν to the conjugate slip-line. The constitutive equations for the dilatant double shearing model are

$$\left[\left(\frac{\partial v_x}{\partial x} - \frac{\partial v_y}{\partial y}\right) cos2\psi + \left(\frac{\partial v_x}{\partial y} + \frac{\partial v_y}{\partial x}\right) sin2\psi\right] sin\nu \qquad (3.30)$$
$$- \left(\frac{\partial v_x}{\partial x} + \frac{\partial v_y}{\partial y}\right) cos(\phi - \nu) = 0,$$
$$\left[\left(\frac{\partial v_x}{\partial x} - \frac{\partial v_y}{\partial y}\right) sin2\psi + \left(\frac{\partial v_x}{\partial y} + \frac{\partial v_y}{\partial x}\right) cos2\psi\right] cos\nu \qquad (3.31)$$
$$- \left(\frac{\partial v_x}{\partial y} - \frac{\partial v_y}{\partial x} + 2\Omega\right) sin(\phi - \nu) = 0,$$

which become the double-shearing model when $\nu = 0$ and the Coulomb associated flow rule model when $v = \phi$. The double shearing model includes the stress equations of motion, the double-shearing constitutive equations and a yield function. Many attempts have been made to solve the model analytically [26, 28]. However, for the solution of boundary value problems, sophisticated numerical techniques are needed. Various numerical schemes based on the method of char-

acteristic have been proposed to calculate the stress and velocity field [15, 82].

3.3.3 Newtonian and non-Newtonian Models

For Newtonian and non-Newtonian models, the governing equations include the continuity equation and the equations of motion as follows:

$$\nabla \cdot \mathbf{v} = 0, \tag{3.32}$$

$$\frac{\partial \mathbf{v}}{\partial t} + \mathbf{v} \cdot \nabla \mathbf{v} = \frac{1}{\rho} \nabla \cdot \sigma, \tag{3.33}$$

where ρ is density, v_i is the component of velocity vector in the i^{th} direction, σ is the stress tensor related to the pressure p and the velocity v and is determined by

$$\sigma_{ji} = -p\delta_{ji} + \mu_n \frac{d\gamma}{dt}(v_{j,i} + v_{i,j}), \tag{3.34}$$

where μ_n and $\frac{d\gamma}{dt}$ denote the viscosity of the material and the shear rate $\frac{d\gamma}{dt} = \sqrt{2tr\left(\frac{1}{2}(v_{i,j} + v_{j,i})\right)^2}$ respectively. For Newtonian model, the viscosity μ_n is a constant. But for non-Newtonian models based on power law model, the viscosity μ_n depends on the shear rate γ and is determined by

$$\mu_n = m\frac{d\gamma^{n-1}}{dt}, \tag{3.35}$$

where m and n are material constants. For Carreau's shear-thinning model

$$\mu_n = \eta_{initial} + (\mu_0 - \mu_\infty)\left[1 + (\lambda\frac{d\gamma}{dt})^2\right]^{\frac{n-1}{2}}, \tag{3.36}$$

where μ_0 and μ_∞ denote the zero shear viscosity and the infinite shear viscosity, λ and γ are constants.

3.4 Concluding Remarks

By over-viewing the details of development of discrete element model, the granular flows are described by the soft particle model and the hard particle model base on Newton 's second law and forces acting between any pair particles and particle and wall are controlled by dash-pot-shearing and slider model. For continuum model, there are three types of models including viscous elastic-plastic models, double-shearing models and newtonian and non-newtonian models. The

use of each model is based on properties of granular materials such as stress and velocity.

CHAPTER IV

DISCRETE ELEMENT MODEL FOR GRANULAR FLOW

4.1 General Overview

The 2-D discrete element model and the continuum model are used to study the effect of inlet flow rate and bottom angle on pressure distribution on the hopper wall through out the static process of material filling into the silo, and in the discharging process, the effect of bottom angle on discharge pattern and normal pressure distribution on hopper wall in a varied mass-flow and constant mass-flow silo.

In this chapter, we develop 2-D discrete element model to study the behavior of granular flow in silos. A numerical investigation has been conducted to analyze the effect of silo configuration on the flow behavior of granular materials in a vertical-sided silo with a conical hopper bottom during filling and discharging processes. The rest of this chapter is organized as follows. The mathematical model and computational domain for the filling and discharge processes of two dimensional (2-D) silo geometry are presented in section 4.2. In section 4.3, the method developed is applied to study the effect of inlet flow rate and bottom angle on pressure distribution on the hopper wall through out the static process of material filling into the silo and also study in detail the dynamic process of granular discharging from the silo. The influence of bottom angle on discharge pattern and normal pressure distribution on discharge problem in a varied mass-flow silo and a constant mass-flow silo is presented. Finally, some concluding remarks are given in section 4.4.

4.2 Mathematical Model and Computational Domain

4.2.1 Particle Interaction Model

In this section, we present an interaction of each individual particle with other particle and the system boundary. For two-dimensional discrete element model, the particles were considered as a set of circular discs.

(a) **Particle-particle Contact**

When a group of particles are moving, the contact of any two particles occurs whenever they overlap. The search of contacts of a particle i can be performed by detecting the distance between the centre of particle i and the centre of its neighboring particles. Therefore, two particles i and j as shown in Figure 4.1 are in contact if the following condition is satisfied:

$$\delta_n = (R_i + R_j) - \parallel \mathbf{r}_i - \mathbf{r}_j \parallel \geq 0, \tag{4.1}$$

where δ_n represents the amount of the overlap between particle i and j, R_i and R_j are the radii of particles i and j respectively, $\mathbf{r}_i = (x_i, y_i)$ and $\mathbf{r}_j = (x_j, y_j)$ are the position vectors of the centres of particles i and j, respectively.

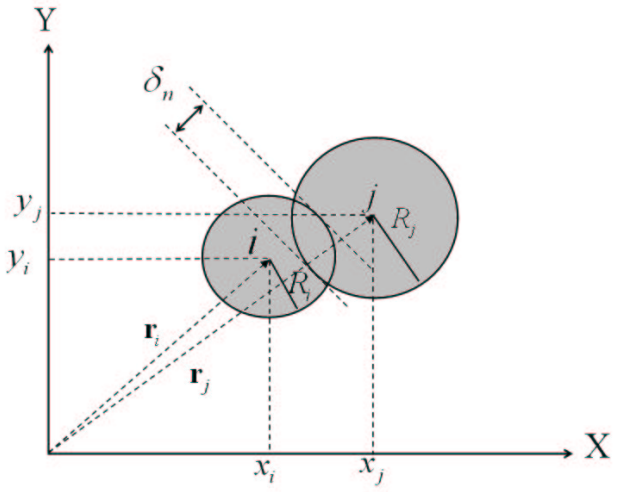

Figure 4.1: Particle-particle contact

(b) **Particle-wall Contact**

The contact between a particle i and boundary wall w is shown in Figure 4.2. The wall is defines by its reference coordinate at the end points, (x_1, y_1) and the length of wall w, L. Each boundary wall is assumed to be smooth.

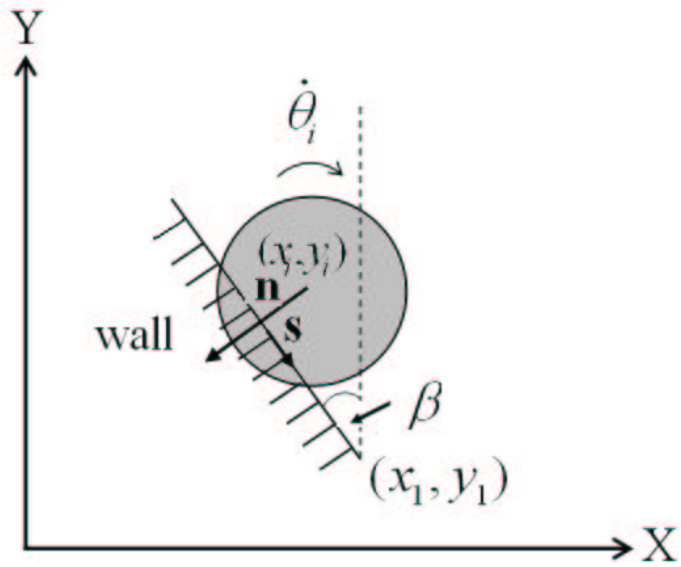

Figure 4.2: Particle-wall contact

4.2.2 Particle Flow Model

In order to construct a defining equation for moving particle, we assume that

- particle behaves as soft body
- damping force can be ignored because of the soft particle.

Under the above assumptions, the granular flow in silos is governed by the principle of linear momentum and the principle of angular momentum, namely

$$m_i \frac{d^2}{dt^2}\mathbf{r}_i(t) = \mathbf{F}_i(t) + m_i\mathbf{g}, \tag{4.2}$$

$$I_i \frac{d^2}{dt^2}\theta_i(t) = M_i(t), \tag{4.3}$$

where $\mathbf{r}_i$ and θ_i are the position vector and the rotation vector of the center of the particle; m_i and I_i denote respectively the mass and the moment of inertia

of the particle; $\mathbf{F}_i(t)$ and $M_i(t)$ represent the total force and torque acting on particle i at time t, respectively.

The total force, $\mathbf{F}_i(t)$ in equation (4.2) acting on particle i, is defined by

$$\mathbf{F}_i(t) = \sum_{j=1, j\neq i}^{q_p(t)} \mathbf{F}_{i,j} + \sum_{w=1}^{q_w(t)} \mathbf{F}_{i,w}, \tag{4.4}$$

in which the first and the second terms on the RHS of equation (4.4) are the interaction force acting on particle i by all contact particles $j = 1, ..., q_p$ and the wall contact force acting on particle i by all contact walls $w = 1, ..., q_w$, respectively.

Based on a dynamic process and a viscoelastic model as shown in Figure 4.3, the interaction force is the sum of the normal force and the tangential force:

$$\mathbf{F}_{i,j}(t) = F_{ijn}(t)\mathbf{n} + F_{ijs}(t)\mathbf{s}, \tag{4.5}$$

where $\mathbf{n}$ and $\mathbf{s}$ are unit vectors in the normal and tangential directions of the contact plane as shown in Figure 4.4.

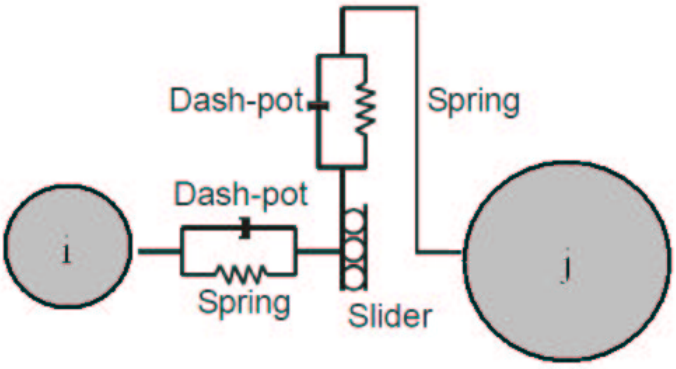

Figure 4.3: The viscoelastic contact model

Once the contact condition

$$\delta_n = R_i + R_j - \parallel \mathbf{r}_i - \mathbf{r}_j \parallel \geq 0, \tag{4.6}$$

is met, two particles i and j with radii R_i and R_j are in contact and

$$F_{ijn}(t) = -k_n\delta_n + \eta_n(\mathbf{v}_{ij} \cdot \mathbf{n}), \tag{4.7}$$

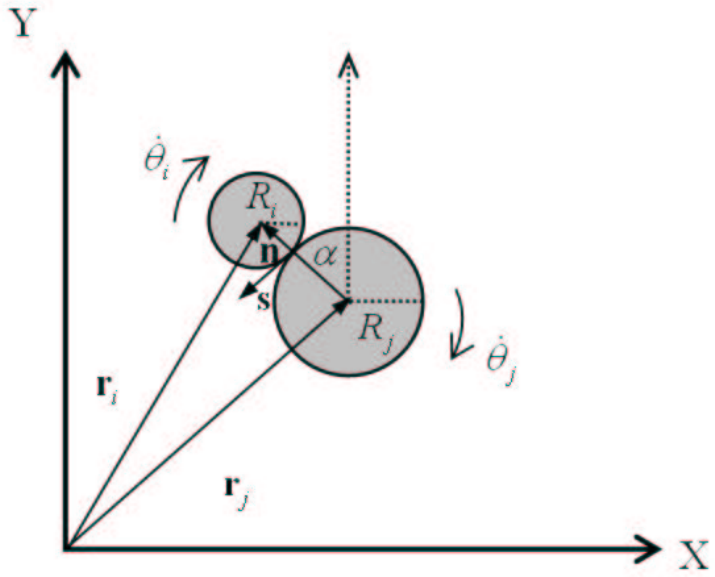

Figure 4.4: Particle pair in contact

where k_n and η_n denote respectively the stiffness of the spring and the damping coefficient in the normal directions, δ_n represents the amount of overlap as defined in equation (5), and $\mathbf{v}_{ij}$ is the relative velocity determining the interaction force via a contact force law and is defined by

$$\mathbf{v}_{ij} = \left(\frac{d}{dt}\mathbf{r}_i - \frac{d}{dt}\mathbf{r}_j\right) + \left(R_i\frac{d}{dt}\theta_i + R_j\frac{d}{dt}\theta_j\right)\mathbf{s}. \tag{4.8}$$

The tangential force in equation (4.5) can be determined if the slip condition

$$\mu|F_{ijn}| < k_s|\mathbf{v}_{ij}\cdot\mathbf{s}| \tag{4.9}$$

is met and

$$F_{ijs}(t) = [sign(\delta_s)\mu|F_{ijn}|(\mathbf{v}_{ij}\cdot\mathbf{s})]\,\mathbf{s}, \tag{4.10}$$

where μ and k_s denote respectively the friction coefficient and the stiffness of the spring in the tangential direction, and δ_s is defined by

$$\delta_s = \left[(\mathbf{v}_i - \mathbf{v}_j)\cdot\mathbf{s} - R_j\frac{d}{dt}\theta_j - R_i\frac{d}{dt}\theta_i\right]\triangle t \tag{4.11}$$

for the small time step $\triangle t$.

The wall contact force acting on particle i by the wall w can be expressed as

$$\mathbf{F}_{i,w}(t) = F_{iwn}(t)\mathbf{n} + F_{iws}(t)\mathbf{s}, \tag{4.12}$$

where $\mathbf{n}$ and $\mathbf{s}$ are unit vectors in the normal and tangential directions of the wall contact plane as shown in Figure 4.2.

To determine the above forces, we firstly convert coordinates of the particle into local wall coordinates. The new coordinates of the particle can be expressed as

$$\begin{bmatrix} x_n \\ y_n \end{bmatrix} = \begin{bmatrix} cos\beta & sin\beta \\ -sin\beta & cos\beta \end{bmatrix} \begin{bmatrix} x_i - x_1 \\ y_i - y_1 \end{bmatrix}, \tag{4.13}$$

where β is an angle between the wall w and the y-axis, x_1 and y_1 are the minimum values of relevant coordinates of the wall. The particle i and the wall with the length L are in contact if the following conditions are satisfied:

(i) the contact with the top part of the wall occurs when $y_n > L$ and $\delta_{mag} = x_n^2 + (y_n - L)^2 \leq R_i^2$;

(ii) the contact with the end part of the wall occurs when $y_n < 0$ and $\delta_{mag} = x_n^2 + y_n^2 \leq R_i^2$;

(iii) the contact with the middle part of the wall occurs when $\delta_{mag} =\mid x_n \mid< R_i^2$.

Once one of the above wall contact conditions is met, the wall contact force can be calculated by

$$F_{iwn}(t) = -k_n\gamma_n + \eta_n(\mathbf{v}_w - \mathbf{v}_i) \cdot \mathbf{n}, \tag{4.14}$$

$$F_{iws}(t) = sign(\gamma_s)\mu|F_{iwn}|, \tag{4.15}$$

where the amount of overlap γ_n can be determined by

$$\gamma_n = R_i - \sqrt{\delta_{mag}} \tag{4.16}$$

for the conditions (i) and (ii) and

$$\gamma_n = R_i - \delta_{mag} \tag{4.17}$$

for the condition (iii). The parameter γ_s in equation (4.15) is given by

$$\gamma_s = \left[(\mathbf{v}_w - \mathbf{v}_i) \cdot \mathbf{s} - R_i \frac{d}{dt}\theta_i \right] \triangle t, \tag{4.18}$$

where $\mathbf{v}_w$ and $\mathbf{v}_i$ denote velocities of the wall and particle i, respectively.

The total force acting on the wall at time t is calculated by

$$\mathbf{F}_w(t) = -\frac{1}{L} \sum_{i=1}^{Q} \mathbf{F}_{i,w}(t). \tag{4.19}$$

where L is the length of the wall and Q is the number of particles in contact with the wall at time t.

In this study, we consider only the tangential torque causing a particle to rotate. The moment $M_i(t)$ in equation (4.3) is then determined by

$$M_i(t) = R_i F_{ijs}. \tag{4.20}$$

To simulate the granular flow of N particles, we let

$$\frac{d}{dt}\mathbf{r}_i(t) = \mathbf{v}, \qquad \frac{d}{dt}\theta(t) = \omega, \tag{4.21}$$

and from equations (4.2) and (4.3), we obtain

$$m_i \frac{d}{dt}\mathbf{v}_i(t) = \mathbf{F}_i(t) + m_i\mathbf{g}, \tag{4.22}$$

$$I_i \frac{d}{dt}\omega_i(t) = M_i(t). \tag{4.23}$$

Assembling the equations of motions of all particles yields a system of $8N$ first order differential equations in 3-D cases, namely

$$\frac{d}{dt}\mathbf{z}(t) = \mathbf{w}(t), \tag{4.24}$$

$$\frac{d}{dt}\mathbf{w}(t) = \mathbf{P}(t), \tag{4.25}$$

where

$$\begin{aligned} \mathbf{z}(t) &= [\mathbf{r}_1(t), \theta_1(t), ..., \mathbf{r}_N(t), \theta_N(t)]^T, \\ \mathbf{w}(t) &= [\mathbf{v}_1(t), \omega_1(t), ..., \mathbf{v}_N(t), \theta_\omega(t)]^T, \\ \mathbf{P} &= \left[\frac{\mathbf{F}_1}{m_1} + \mathbf{g}, \frac{M_1}{I_1}, ..., \frac{\mathbf{F}_N}{m_N} + \mathbf{g}, \frac{M_N}{I_N} \right]^T. \end{aligned}$$

Using the centered difference formulation, we can calculate the unknown variables as follows

$$\mathbf{w}^{n+1} = \mathbf{w}^{n-1} + 2\triangle t\mathbf{P}^{n}, \tag{4.26}$$

$$\mathbf{z}^{n+1} = \mathbf{z}^{n-1} + 2\triangle t\mathbf{w}^{n+1}. \tag{4.27}$$

Using the 2-D DEM and numerical scheme, a numerical investigation has been conducted to analyze the effect of silo configuration on the flow behavior of granular materials in the static and dynamic processes of material filling and discharging of a silo. The computational model in our simulation is shown in Figure 4.5. The silo system under consideration include vertical-side silos with various hopper bottoms of α angles of 15°, $30^{\circ}, 45^{\circ}$ and 60° and various outlet widths of $0.04\,m$, $0.06\,m$, and $0.08\,m$ and the silo is made of a steel-sheet. The height and the width of the silo are $1.2\,m$ and $0.4\,m$, respectively. To study the pressure distribution on the bottom wall, we divide the hopper wall into ten segments of each part of the wall. Granular materials are soybean having two sizes of $0.006\,m$ and $0.0075\,m$. In each of the simulations shown here, an assembly of $7,500$ particles is considered. Figure 4.6 shows computational models for the filling and discharging processes of the two dimensional silo geometry under consideration. The investigation schemes, the model parameters listed in Table 4.1 are used.

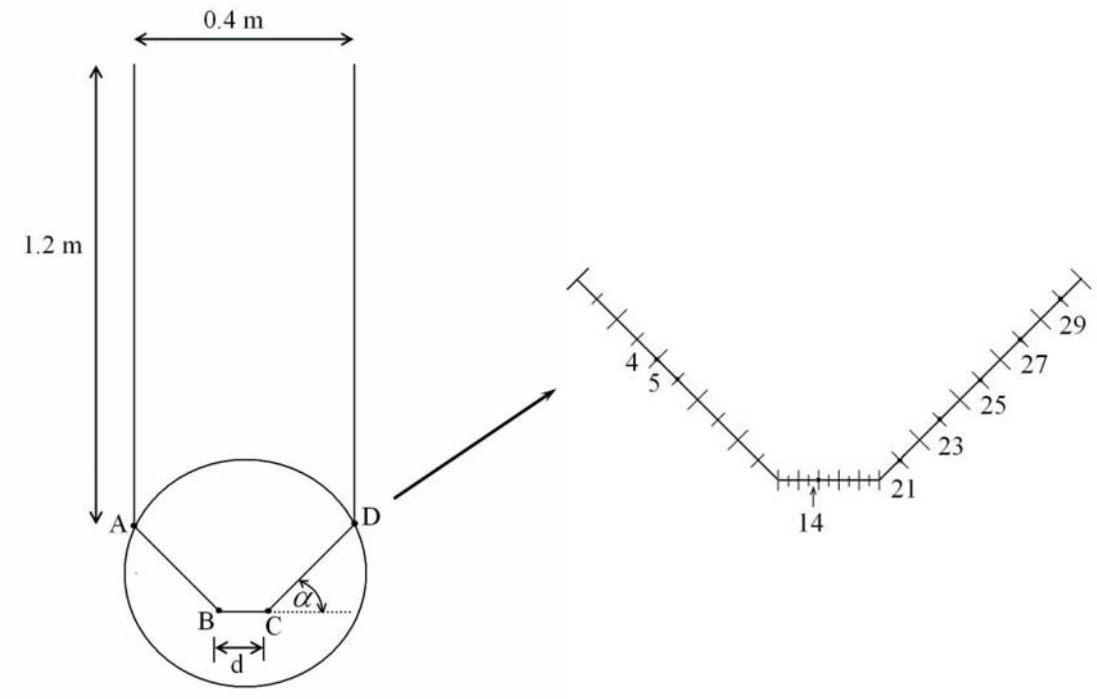

Figure 4.5: Silo geometry and hopper wall segments

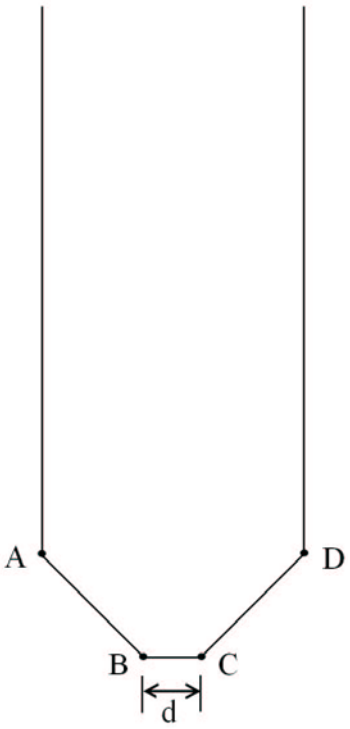

(a) Empty silo for filling process

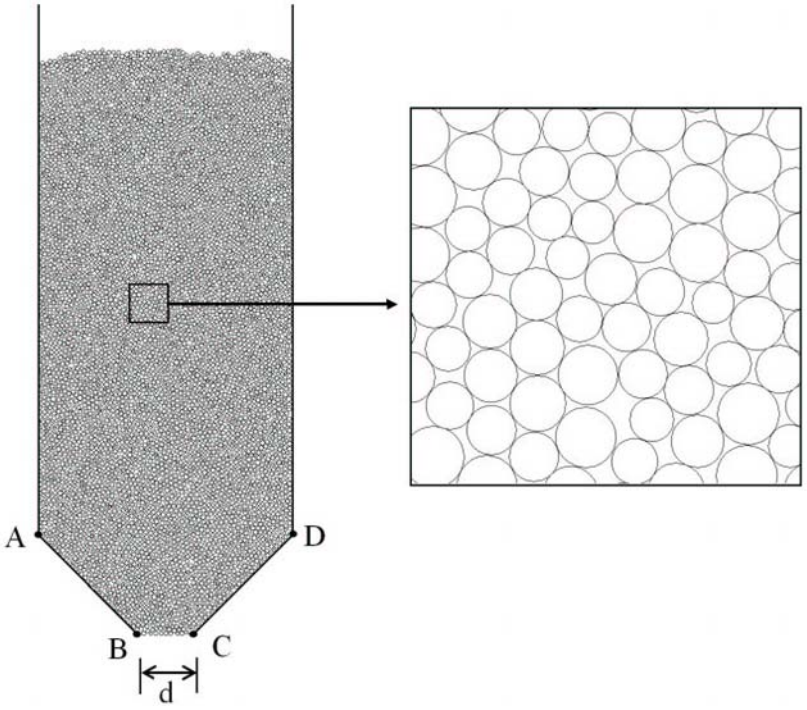

(b) Silo with $7,500$ particles for discharging process

Figure 4.6: Computational domains

Table 4.1: Values of the model parameters used in the simulation.

Parameters	**Value**	
Silo geometry		
height, (m)	1.2	
width, (m)	0.4	
Granular material	Soybean	
Particle diameter, (mm)	6 and 7.5	
Number of particles with size of $6\,mm$	$3,500$	
Number of particles with size of $7.5\,mm$	$4,000$	
Particle density, $\rho\,(kg/m^3)$	$1,033$	
Simulation time step, $\triangle t\,(s)$	5.2711×10^{-6}	
Properties	**Particle-particle**	**Particle-wall**
Normal contact stiffness, $k_n\,(N/m)$	2.8322×10^4	5.6645×10^4
Tangential contact stiffness, $k_s\,(N/m)$	2.5740×10^4	4.5314×10^4
Normal damping constant, $\eta_n\,(N/m)$	1.3048×10^2	1.3962×10^2
Frictional coefficient, μ	0.33	0.35

4.3 Numerical Studies

To simulate the static process of granular filling in the silo, we use the silo with the outlet width of $0.08\,m$ and choose two inlet flow rates of $32\,ml/s$ and $172\,ml/s$ and three bottom angles of $15°, 45°$ and $60°$. During the filling process, the outlet of the silo is closed.

At $t = 0\,s$, particles start to flow with inlet flow rate into the empty silo. All particles fall under gravity and finally the assembly particles come to rest on the base of the silo due to the frictional and damping forces. To investigate pressure distribution on the bottom walls of the hopper, we divide the hopper wall into ten segments of each wall as shown in Figure 4.5.

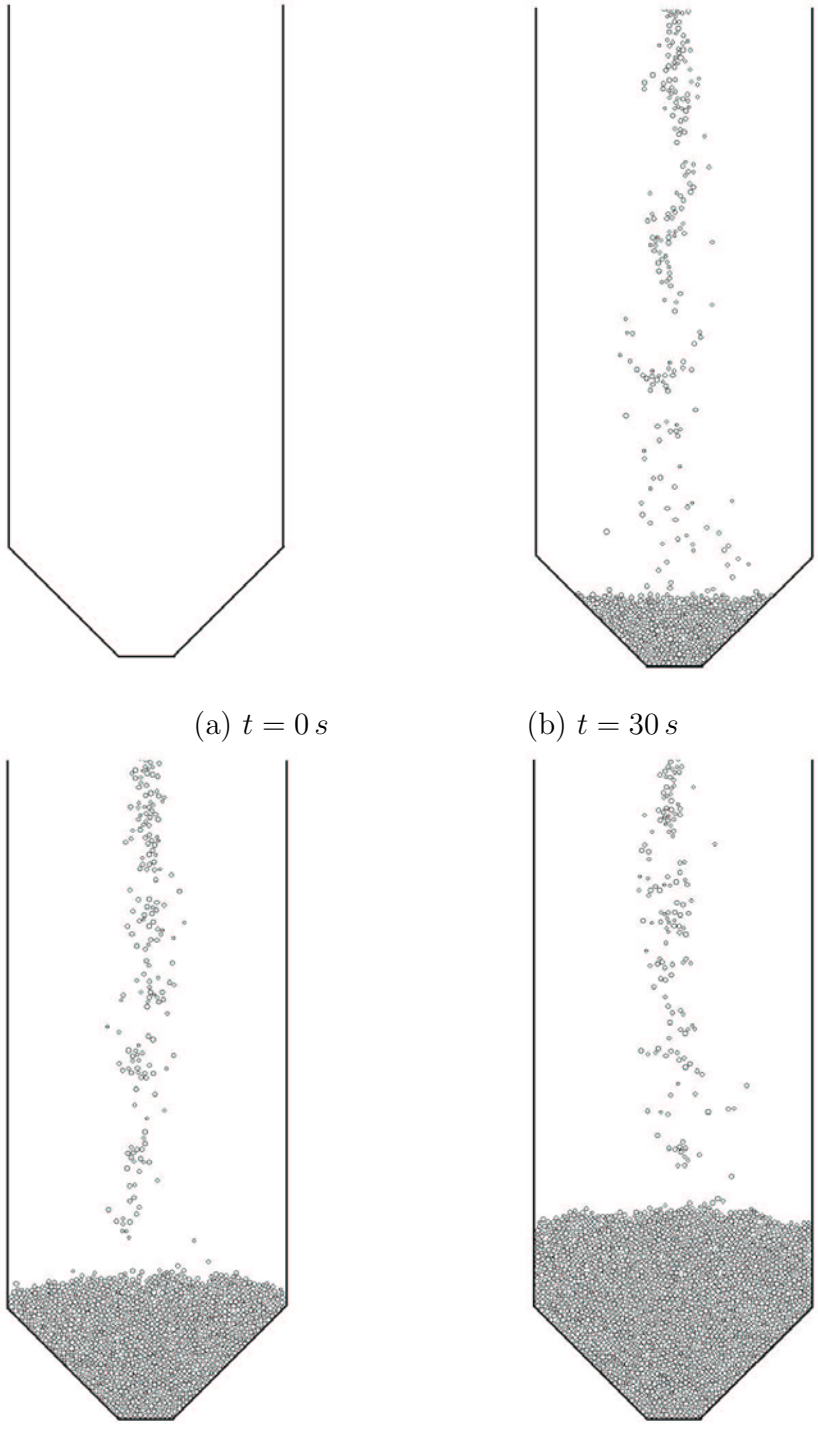

(a) $t = 0\,s$ (b) $t = 30\,s$

(c) $t = 70\,s$ (d) $t = 110\,s$

Figure 4.7: Filling pattern of particles in the silo with 45° bottom angle and $0.08\,m$ outlet width at four different times of $0\,s, 30\,s$, $70\,s$ and $110\,s$ for inlet flow rate of $32\,ml/s$.

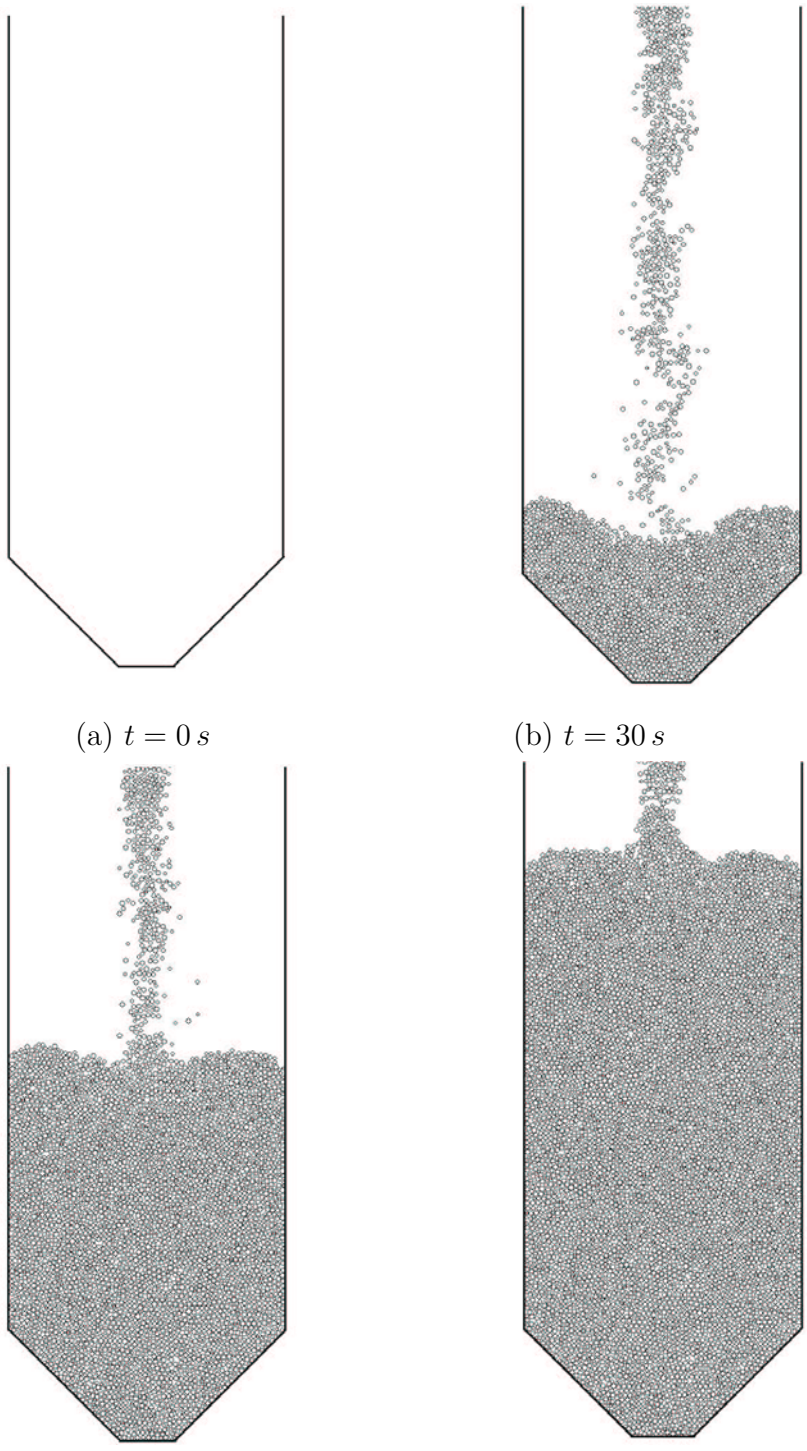

(a) $t = 0\,s$ (b) $t = 30\,s$

(c) $t = 70\,s$ (d) $t = 110\,s$

Figure 4.8: Filling pattern of particles in the silo with 45° bottom angle and $0.08\,m$ outlet width at four different times of $0\,s, 30\,s$, $70\,s$ and $110\,s$ for inlet flow rate of $172\,ml/s$.

4.3.1 Effect of Inlet Flow Rate and Bottom Angle

Two different values of inlet flow rate have been used in the computations to investigate pressure distribution on the hopper wall during material filling into the silo. The computations were conducted using the value of the model parameters shown in Table 4.1. Figure 4.7 shows filling pattern of particles in the silo with 45° bottom angle and $0.08\,m$ outlet width at four different times of $0\,s$, $30\,s$ $70\,s$ and $110\,s$ for inlet flow rate of $32\,ml/s$. Filling pattern of particles in the silo with 45° bottom angle and $0.08\,m$ outlet width for inlet flow rate of $172\,ml/s$ is shown in Figure 4.8.

To investigate the wall pressure distribution at the bottom wall, we recorded pressure distribution at 10 sections of the wall at time t from $t = 0\,s$ to $t = 130\,s$. Effect of the inlet flow rate on the wall pressure in the process of the filling the silo is shown in Figure 4.9. The comparison indicates that the model with higher inlet flow rate gives higher pressure on the base of the hopper. Figure 4.10 shows the variation of normal pressure with time on segments $4, 5, 14, 25$ and 27 of the hopper wall. The investigation shows that the pressure variation is large at the early stage of the filling process and it then becomes smaller as the height of the bulk material increases.

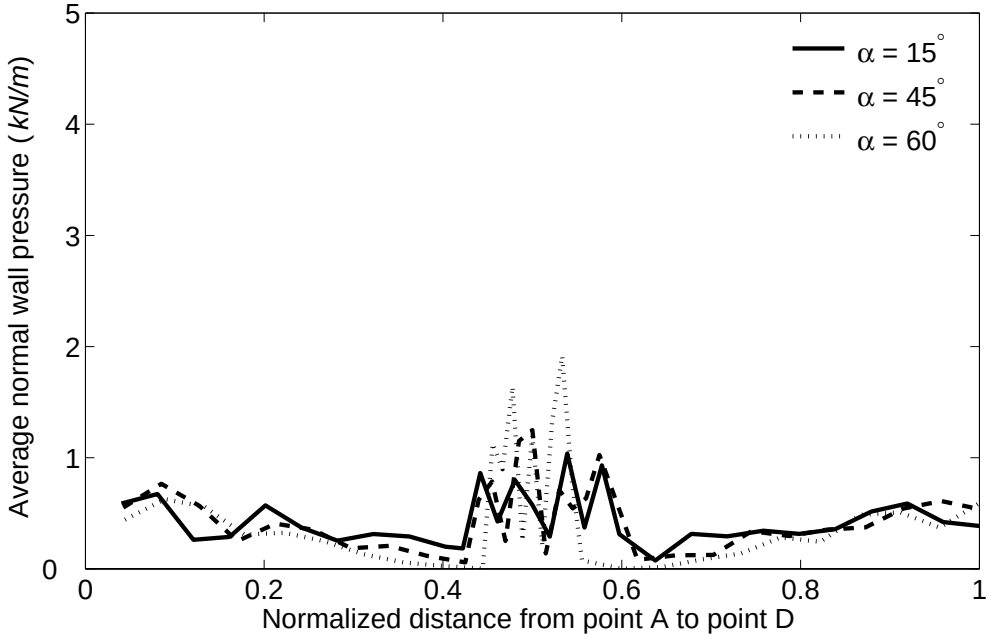

(a) $Q = 32\,ml/s$

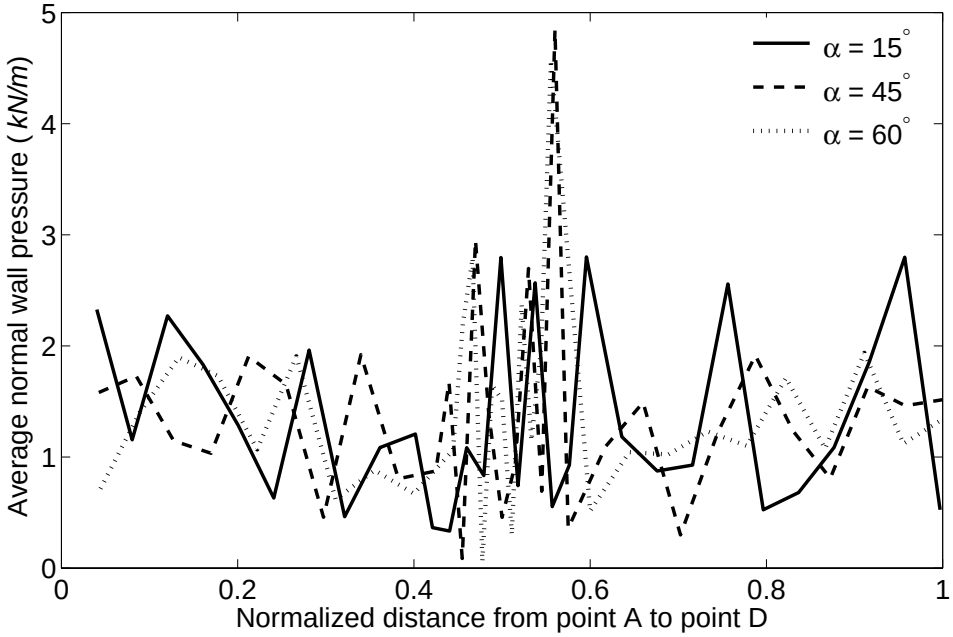

(b) $Q = 172\,ml/s$

Figure 4.9: Effect of inlet flow rate and bottom angle on the average normal pressure (a solid line for 15°, a dashed line for 45° and a dotted line for 60°) in the process of the filling the silo: (a) $Q = 32\,ml/s$; (b) $Q = 172\,ml/s$.

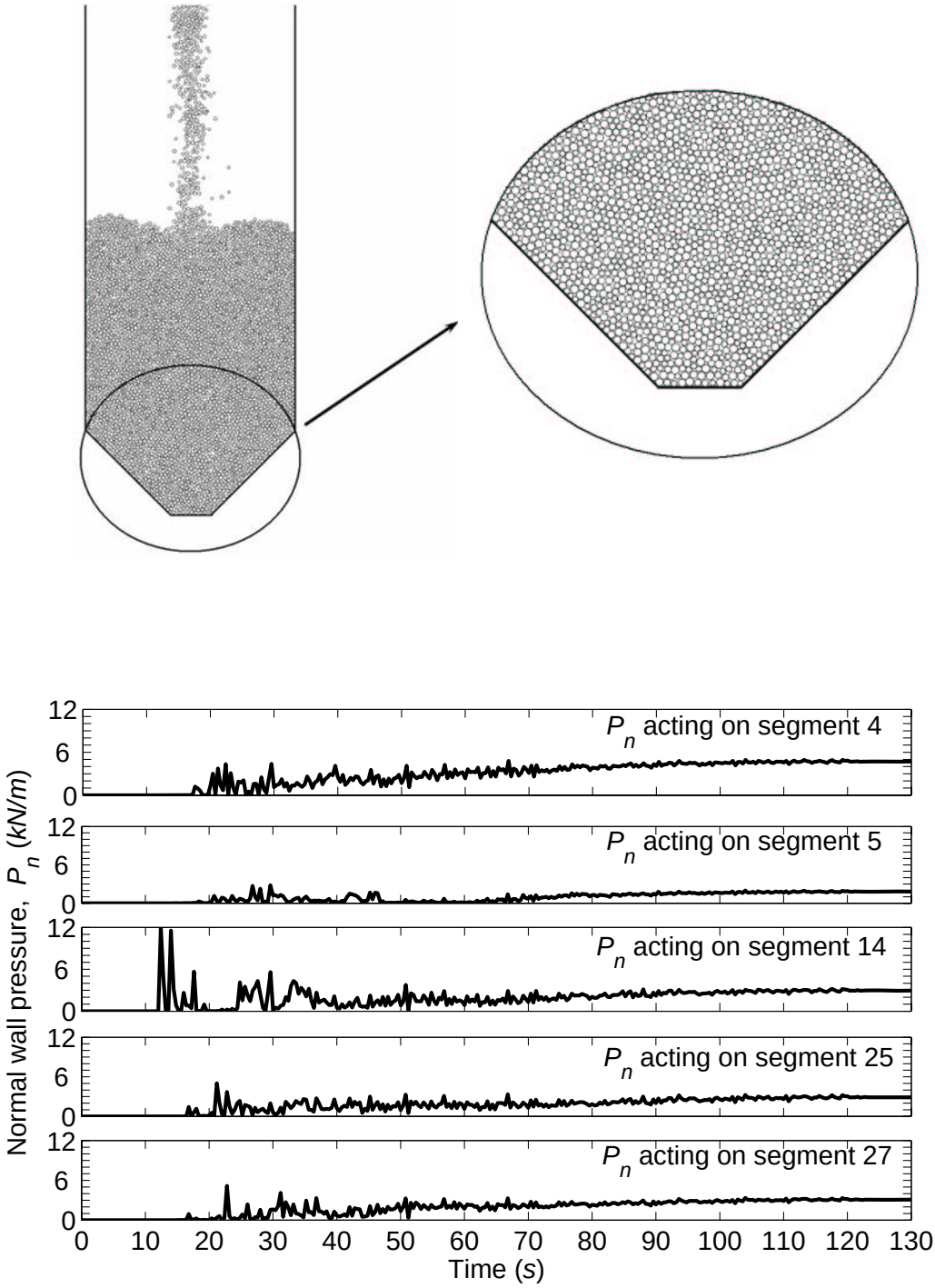

Figure 4.10: The variations of normal wall pressure with time along some hopper wall segments in the process of filling the silo with 45° bottom angle and 0.08 m outlet width.

Three different values of bottom angle have been used in computations

to investigate pressure distribution during filling process. We use the silo with the outlet width of $0.08\,m$ and three bottom angles of $15°, 45°$ and $60°$. Figure 4.9 shows the effect of bottom angle on the average normal pressure. The comparison indicates that the bottom angle has significant effect on the pressure distribution only on the base of the hopper. The model with bigger bottom angle give higher pressure on the base of the hopper.

4.3.2 Effect of a Varied Mass-Flow Silo and a Constant Mass-Flow Silo

In this section, we study the dynamic process of granular discharge from the silo. The silo system under consideration is shown in Figure 4.6(b). To simulate the discharging process, we used two models of silo including a varied mass-flow silo and a constant mass-flow silo. In the varied mass-flow silo, particles are allowed to flow out from the silo under gravitational force. In the constant mass-flow silo, particles that have discharged re-enter at the top of the silo and fall on to the top surface of particles.

At the initial time $t = 0\,s$, an assembly of $7,500$ particles rests on the base of the silo with outlet width of $0.006\,m$, the discharge process starts when the outlet of the silo is opened.

For a varied mass-flow model, particles are allowed to flow out from the silo under gravitational force. To determine the relative rate of discharge from movement of interfaces between shaded strata, particles are colored into many layers using two different colors, gray and green.

Four bottom angles of $15°$, $30°$, $45°$ and $60°$ have been used in computation to investigate their impact on the flow pattern, the deformation of the interfaces and the wall pressure. Figures 4.11, 4.12, 4.13 and 4.14 show the flow pattern of particle in silo with bottom angles of $15°$, $30°$, $45°$ and $60°$, respectively. The particle velocities near the side wall are smaller than those in the middle part of the silo. Figure 4.15 shows effect of bottom angle of the hopper on discharge pattern for four different bottom angles of $15°$, $30°$, $45°$ and $60°$. The comparison indicates that the movement of particles through a conical bottomed silo with a higher bottom angle is faster and its interface is clearly v-shapes.

A stable arch (bridge) may apparent over the hopper outlet of the silo. Here, it is found that the flow of the bulk solid is stopped at time $t = 19\,s$, once the arch is formed over the hopper outlet of the silo having 15° bottom angle and $0.04\,m$ outlet width as shown in Figure 4.16. It is recognized that using large outlet can prevent arching. Thus in the following investigations, we only use the silo having $0.06\,m$ outlet width.

Figure 4.17 shows that particles flow out from the silo with a zig-zag behavior at three executive times. There are three different flow zones: pipe zone, pipe feed zone and plug flow zone as shown in Figure 4.18. The variation of normal pressure with time on some segments of the hopper wall with 30° is shown in Figure 4.19. It is indicated that in the varied mass-flow silo, the pressure distribution reduces its fluctuation as the height of the bulk materials in the silo decreases.

Influence of bottom angle on the bottom wall pressure is investigated for the varied mass-flow silo. The computed average normal pressures for different bottom angle are compared in Figure 4.20. The comparison indicates that bottom angle of the hopper wall is one of the important factors dominating the pressure on the hopper wall. With the increase of the wall angle from 30° to 60°, the wall pressure decreases from $3.3\,N/m$ to $2.5\,N/m$.

For a constant mass-flow model, particles that have discharged out of the silo re-enter at the top of the silo and fall on to the top surface of particles. The discharging process starts when the outlet of the silo is opened. To see the flow pattern, we set layers of particles by coloring those particles in different layer with different color. Here, we use two colors, grey and green, to separate these layers.

Three bottom angles of 30°, 45° and 60° have been used in computation to investigate the pressure distribution along the silo wall and the flow pattern during discharging process. The particles flow out from the silo under gravity as shown in Figures 4.21, 4.22 and 4.23 for the bottom wall with angle of 30°, 45° and 60°, respectively. Figures 4.24 and 4.25 show the velocity field and rotation of particle in the process of discharging the constant mass-flow silo with

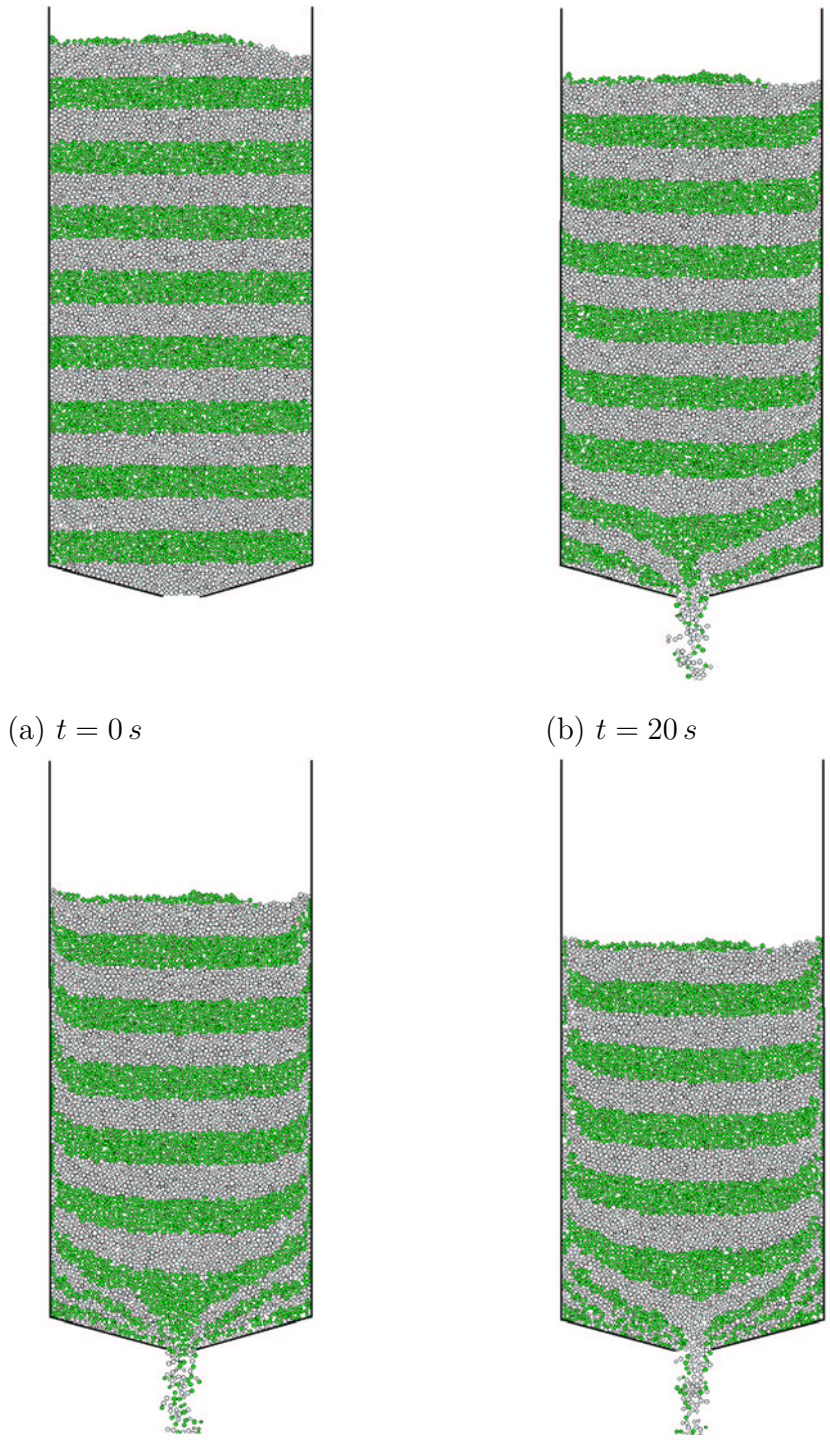

(a) $t = 0\,s$ (b) $t = 20\,s$

(c) $t = 60\,s$ (d) $t = 100\,s$

Figure 4.11: Flow pattern of particles in a silo with bottom angle of 15° during discharging process at four different times.

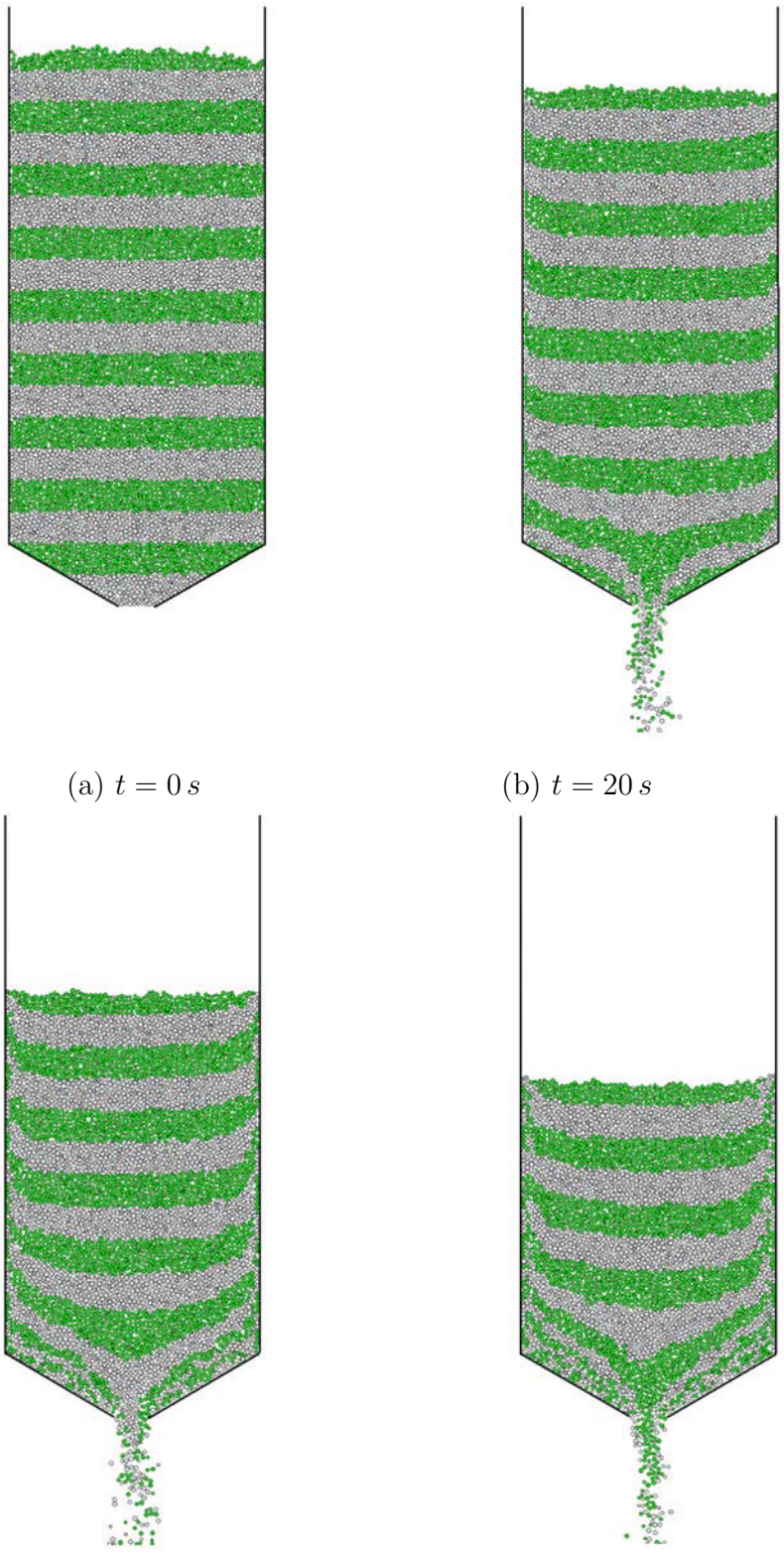

(a) $t = 0\,s$ (b) $t = 20\,s$

(c) $t = 60\,s$ (d) $t = 100\,s$

Figure 4.12: Flow pattern of particles in a silo with bottom angle of 30° during discharging process at four different times.

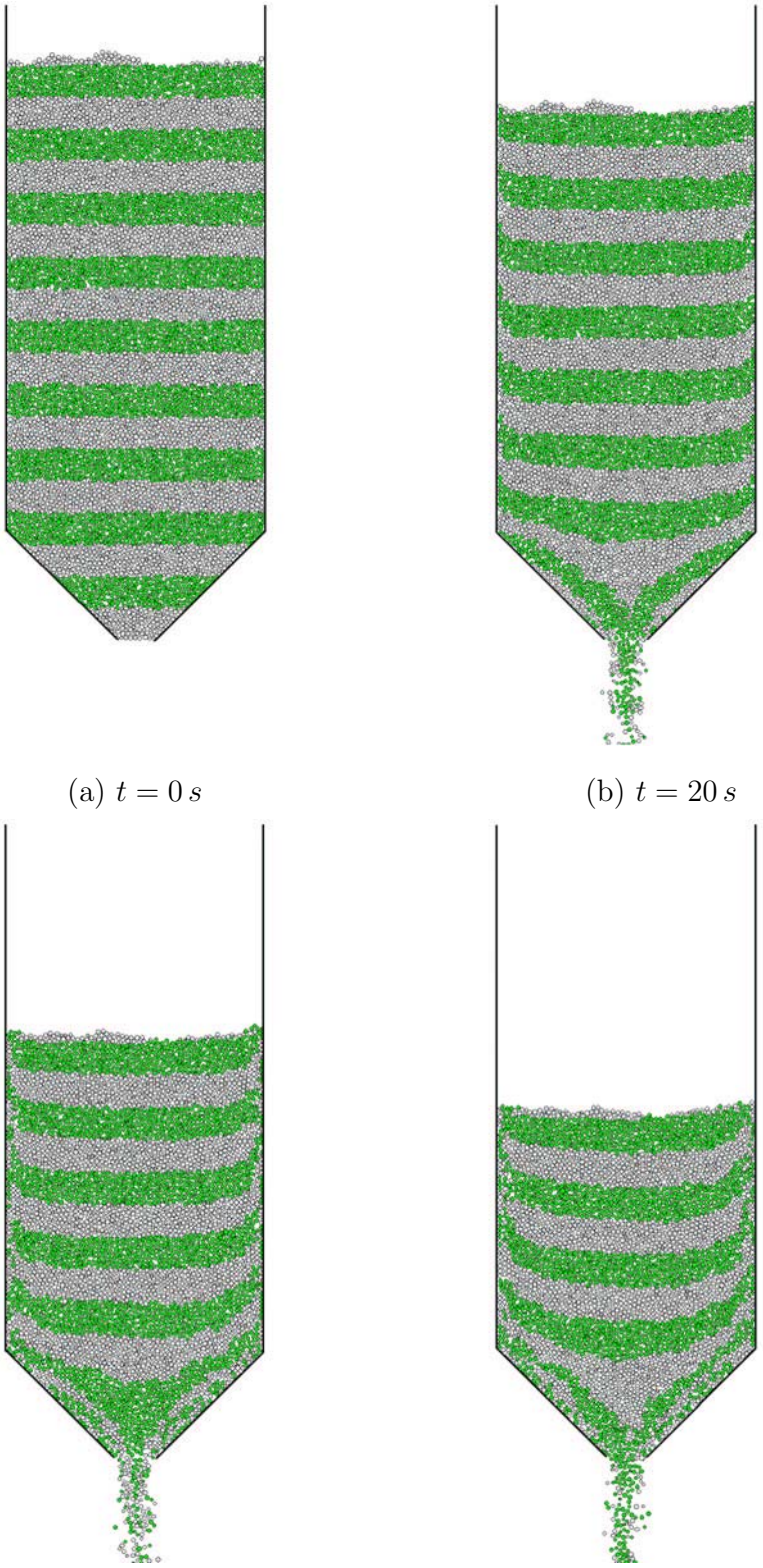

(a) $t = 0\,s$ (b) $t = 20\,s$

(c) $t = 60\,s$ (d) $t = 100\,s$

Figure 4.13: Flow pattern of particles in a silo with bottom angle of 45° during discharging process at four different times.

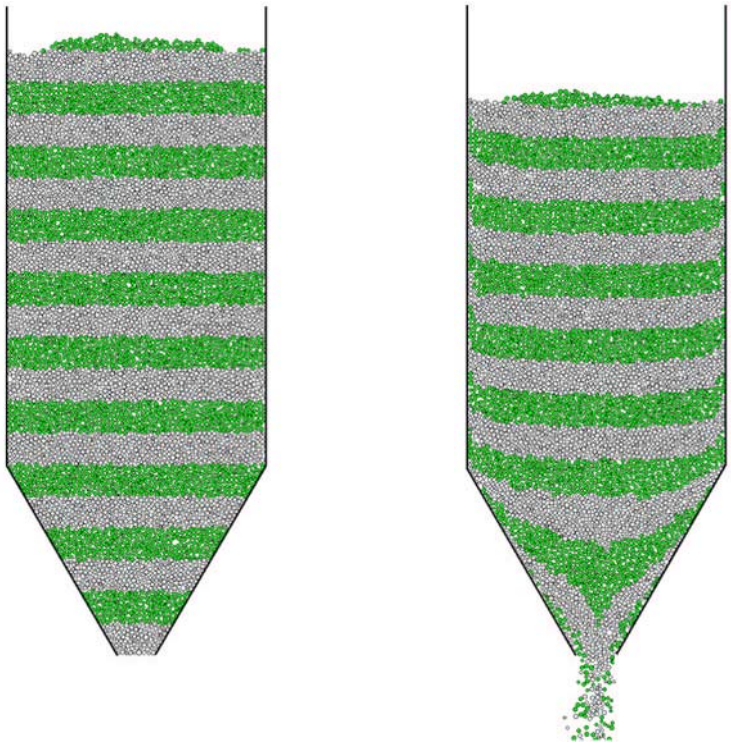

(a) $t = 0\,s$ (b) $t = 20\,s$

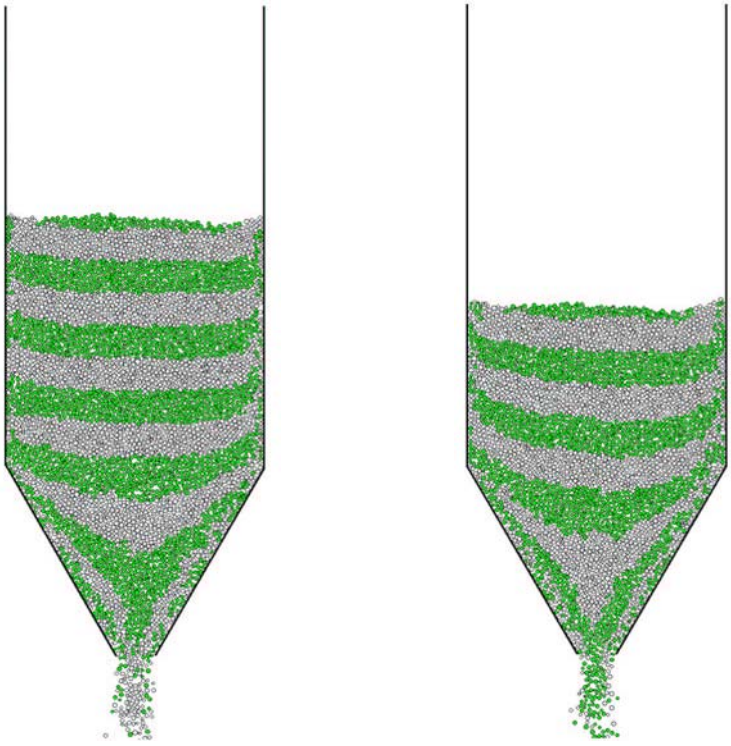

(c) $t = 60\,s$ (d) $t = 100\,s$

Figure 4.14: Flow pattern of particles in a silo with bottom angle of 60° during discharging process at four different times.

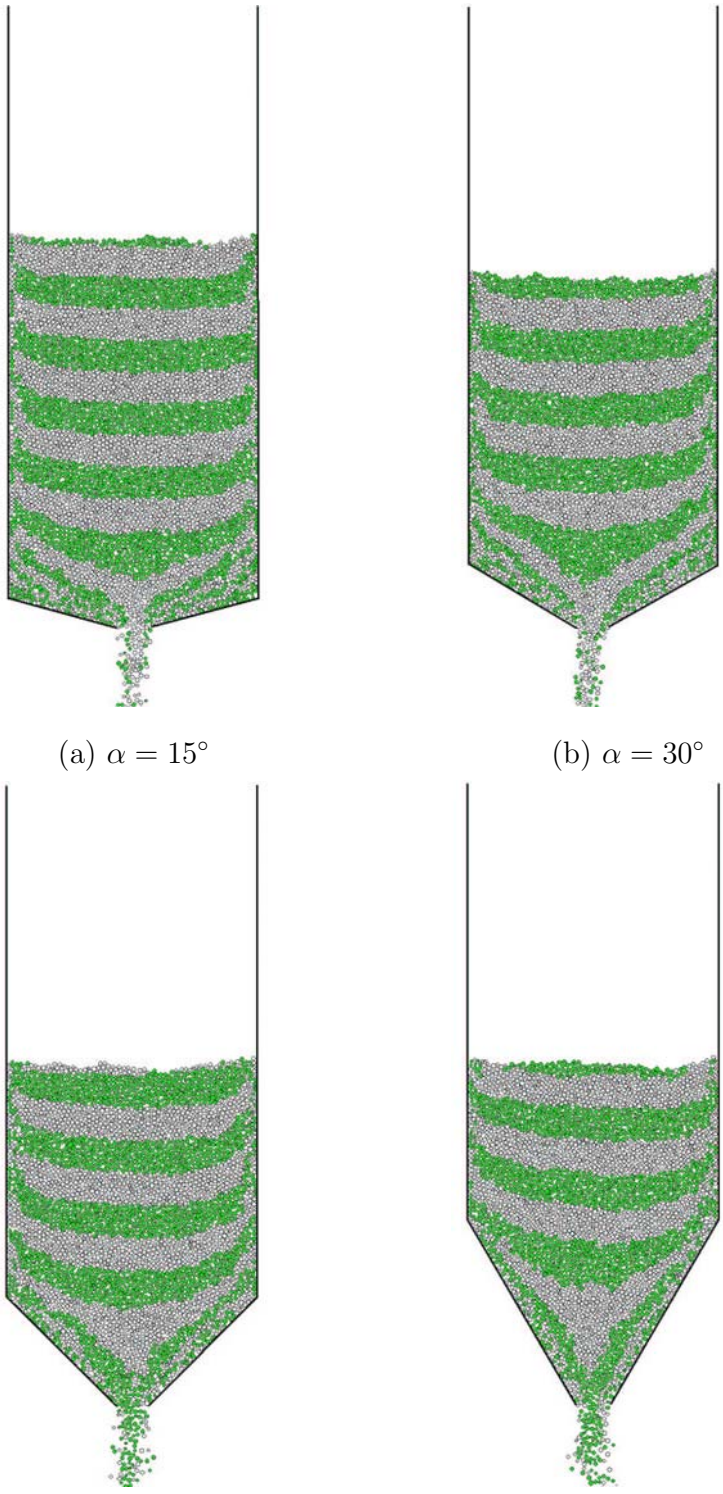

(a) $\alpha = 15°$ (b) $\alpha = 30°$

(c) $\alpha = 45°$ (d) $\alpha = 60°$

Figure 4.15: Discharge pattern of granular flow from a silo with four different bottom angles at $t = 100\,s$: (a) $\alpha = 15°$; (b) $\alpha = 30°$; (c) $\alpha = 45°$ and (d) $\alpha = 60°$.

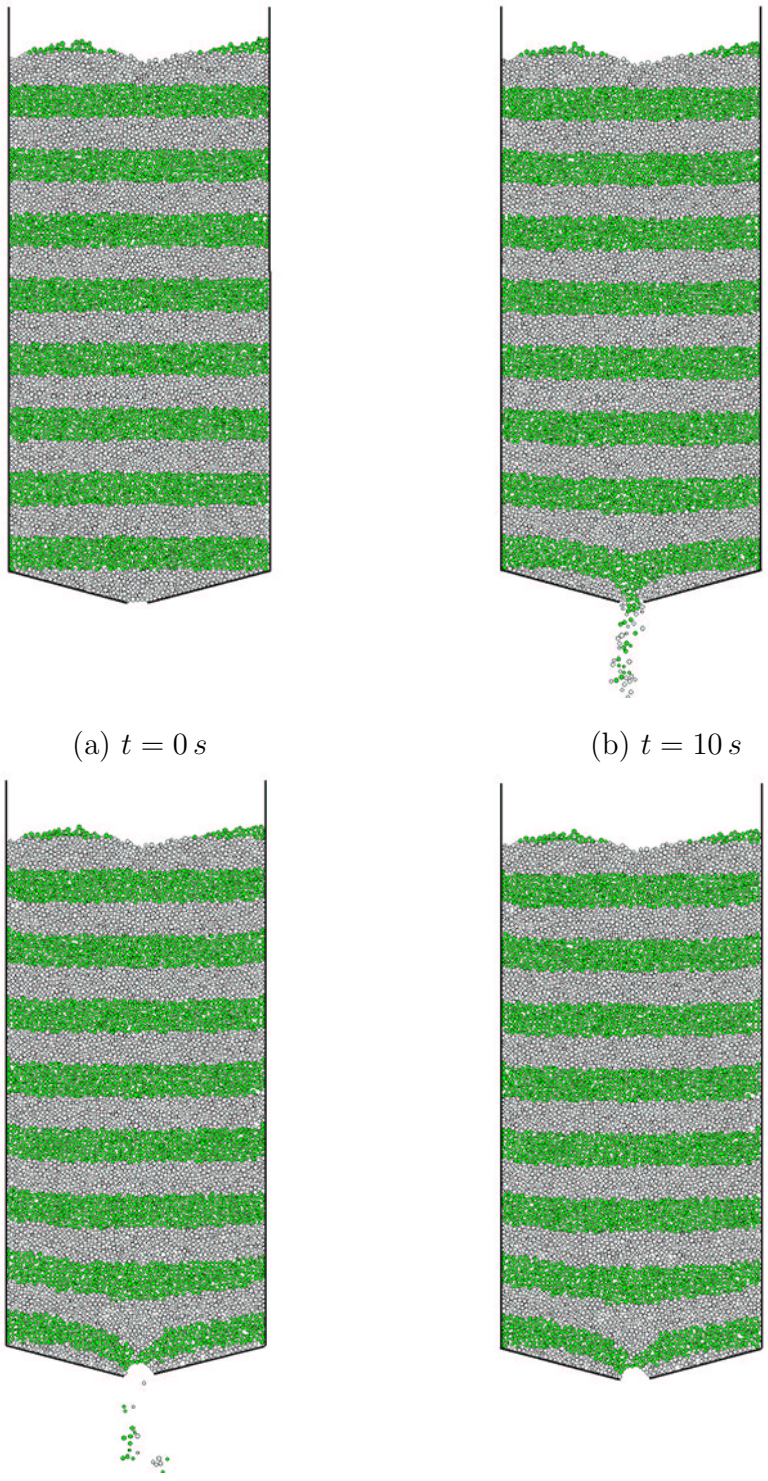

(a) $t = 0\,s$ (b) $t = 10\,s$

(c) $t = 19\,s$ (d) $t = 22\,s$

Figure 4.16: Formulation of arching above the outlet of the silo with 15° bottom angle and $0.04\,m$ outlet width at four different times.

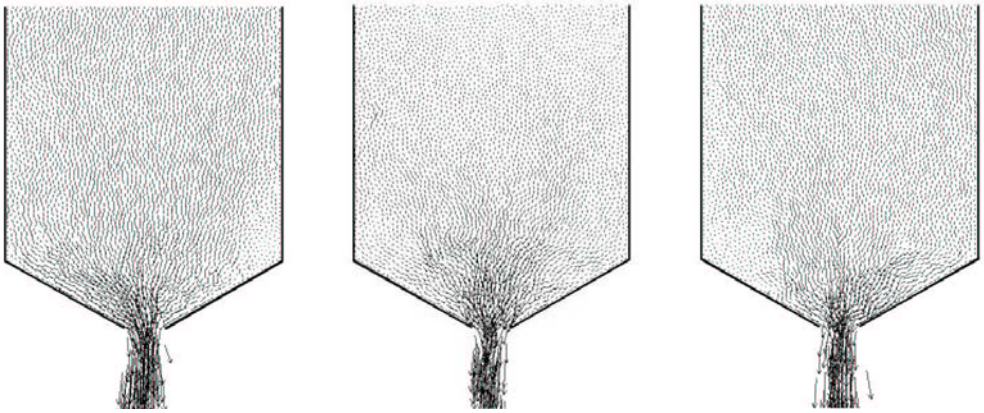

(a) $t = 42\,s$ (b) $t = 47\,s$ (c) $t = 52\,s$

Figure 4.17: Zig-Zag flow pattern during discharging soybean from the silo with 30° bottom angle at three different times: (a) $t = 42\,s$; (b) $t = 47\,s$ and (c) $t = 52\,s$.

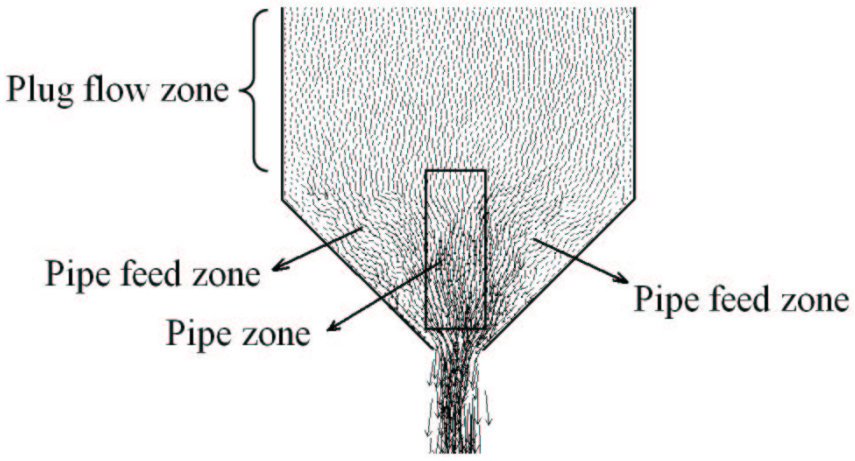

Figure 4.18: Flow zones.

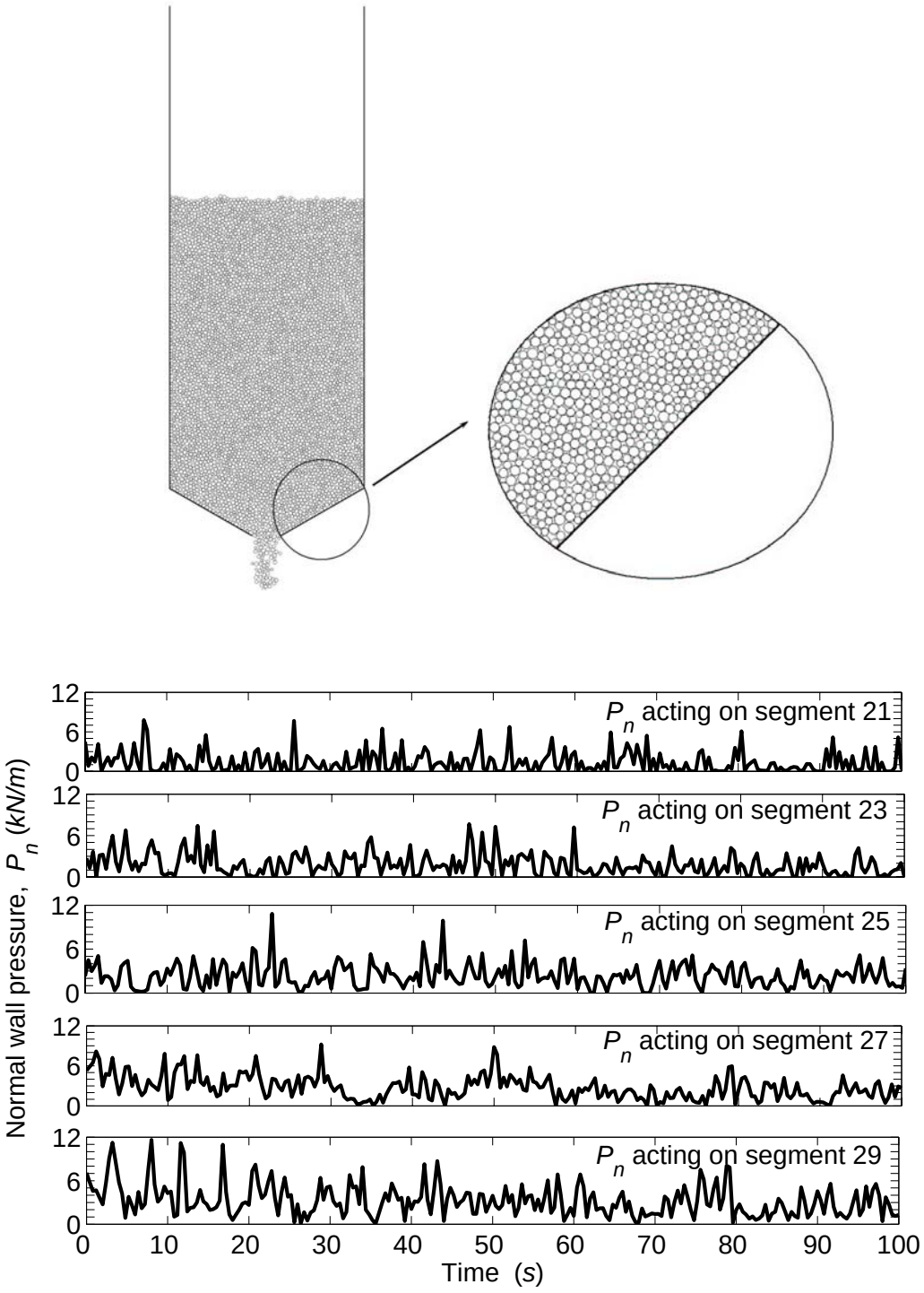

Figure 4.19: The variations of normal wall pressure with time along some hopper wall segments of the varied mass-flow silo with 30° bottom wall in the discharging process.

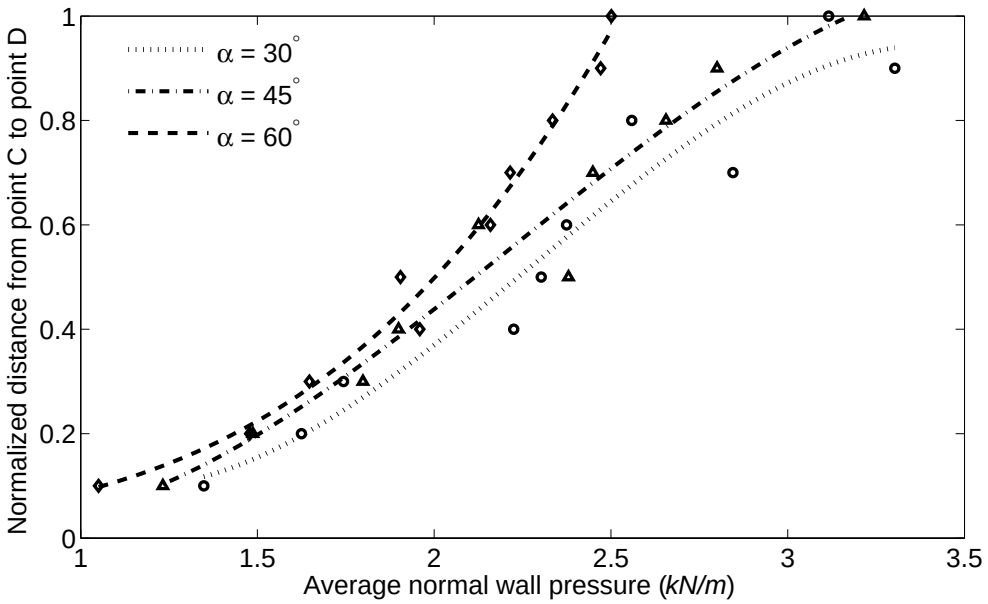

Figure 4.20: Average normal wall pressure along the normalized distance from point C to point D in the first 90 s of discharge process obtained from the varied mass-flow silo with various bottom wall of angles of 30° (dotted line), 45° (dashed-dotted line) and 60° (dashed line).

30° bottom angle, respectively. Figure 4.26 shows the variation of normal wall pressure with time on some segments of the hopper wall with 30° angle during discharging particles from the constant mass-flow silo. It indicates that the pressure distribution always fluctuates with time. The computed average normal wall pressure for different mass-flow silo is compared in Figure 4.27. It is indicated that the average wall pressure of the constant mass-flow silo is higher than the pressure of the varied mass-flow silo.

4.4 Concluding Remarks

An efficient discrete element method has been developed for solving the two-dimensional granular flow problem arising from the filling and discharge processes. A numerical investigation shows that the method developed is robust in capturing the characteristics of the the flow of granular material in silos. The results gained from the study indicates that the effect of bottom angle of the hopper wall have important effect on the pressure distribution on the hopper

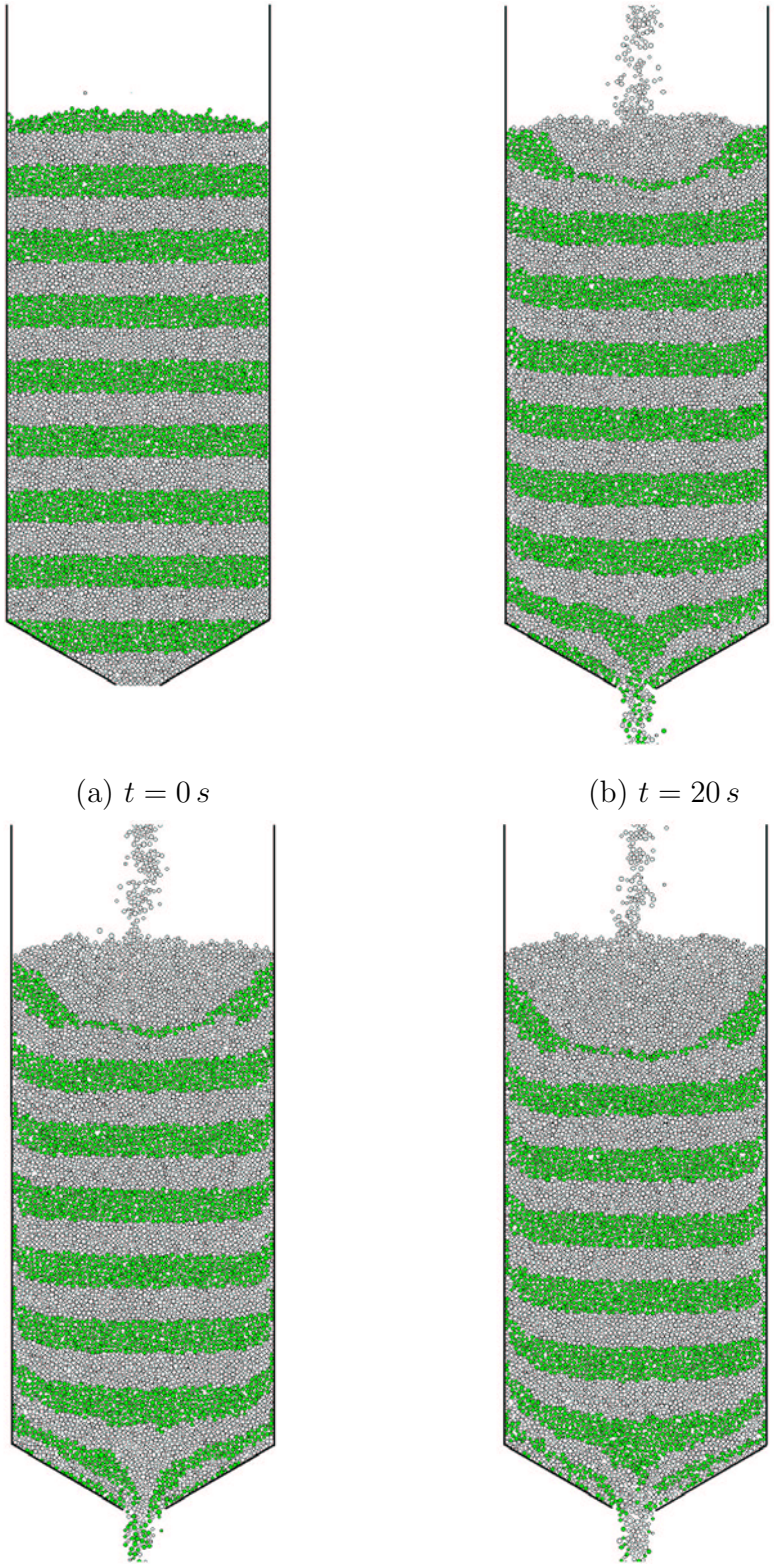

(a) $t = 0\,s$ (b) $t = 20\,s$

(c) $t = 30\,s$ (d) $t = 40\,s$

Figure 4.21: Flow pattern of particles in a constant mass-flow silo with bottom angle of 30° during discharging at four different times.

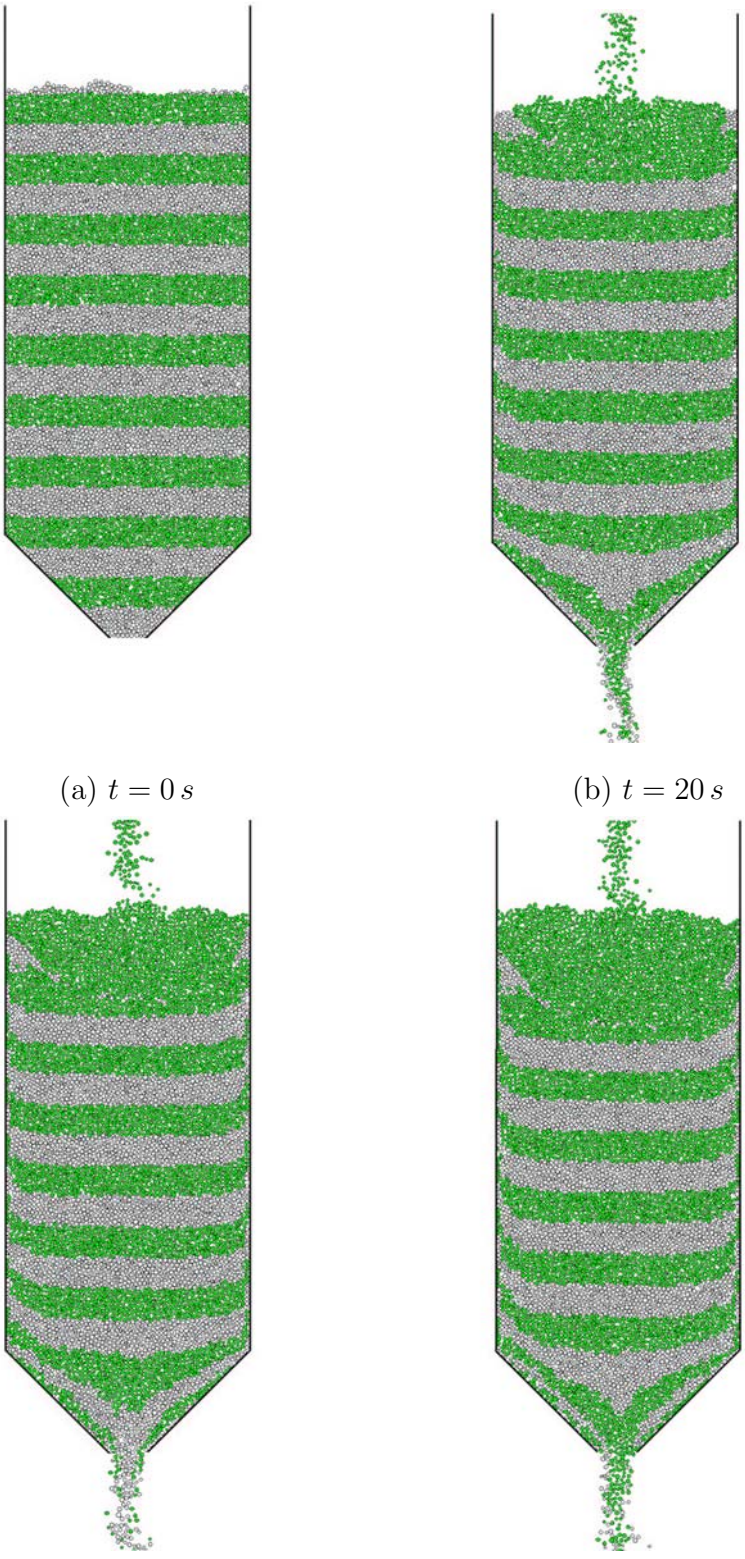

(a) $t = 0\,s$ (b) $t = 20\,s$

(c) $t = 30\,s$ (d) $t = 40\,s$

Figure 4.22: Flow pattern of particles in a constant mass-flow silo with bottom angle of 45° during discharging process at four different times.

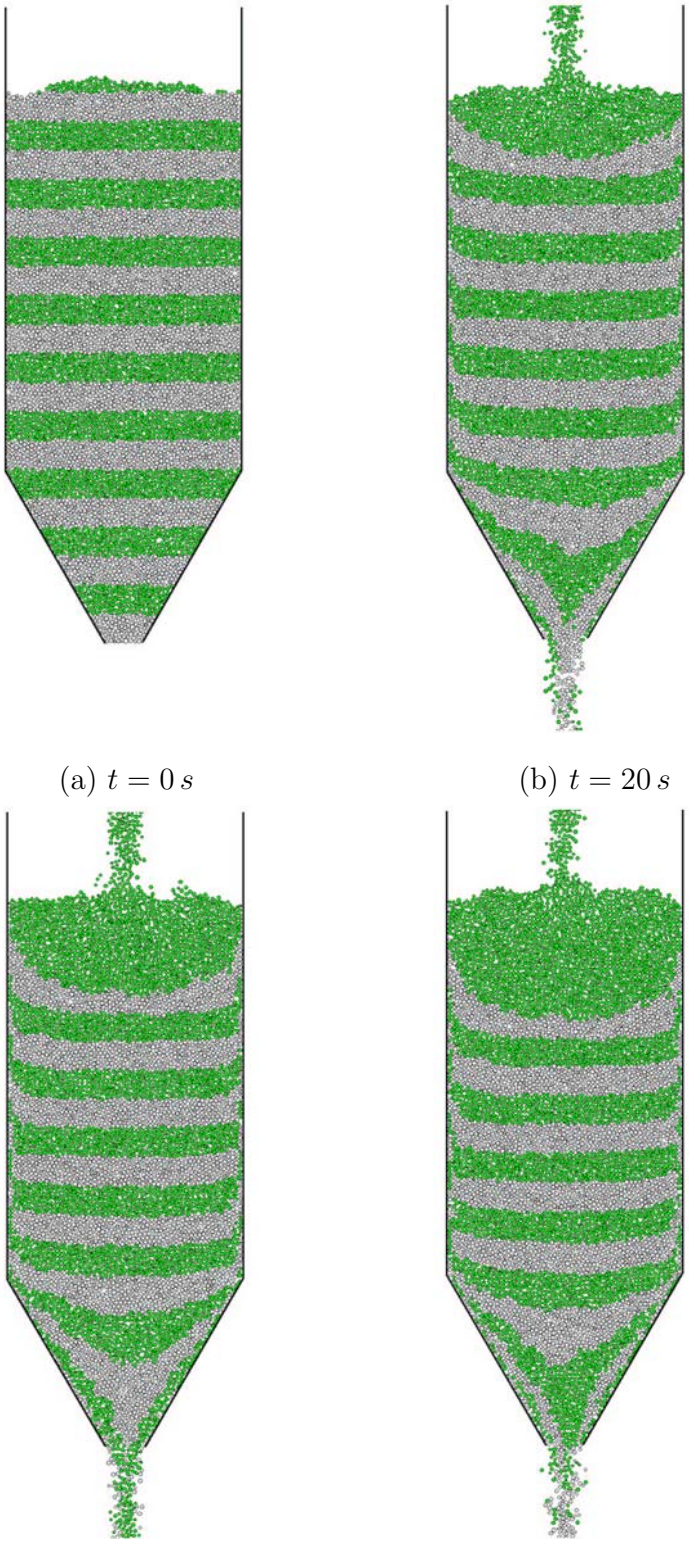

(a) $t = 0\,s$ (b) $t = 20\,s$

(c) $t = 30\,s$ (d) $t = 40\,s$

Figure 4.23: Flow pattern of particles in a a constant mass-flow silo with bottom angle of 60° during discharging process at four different times.

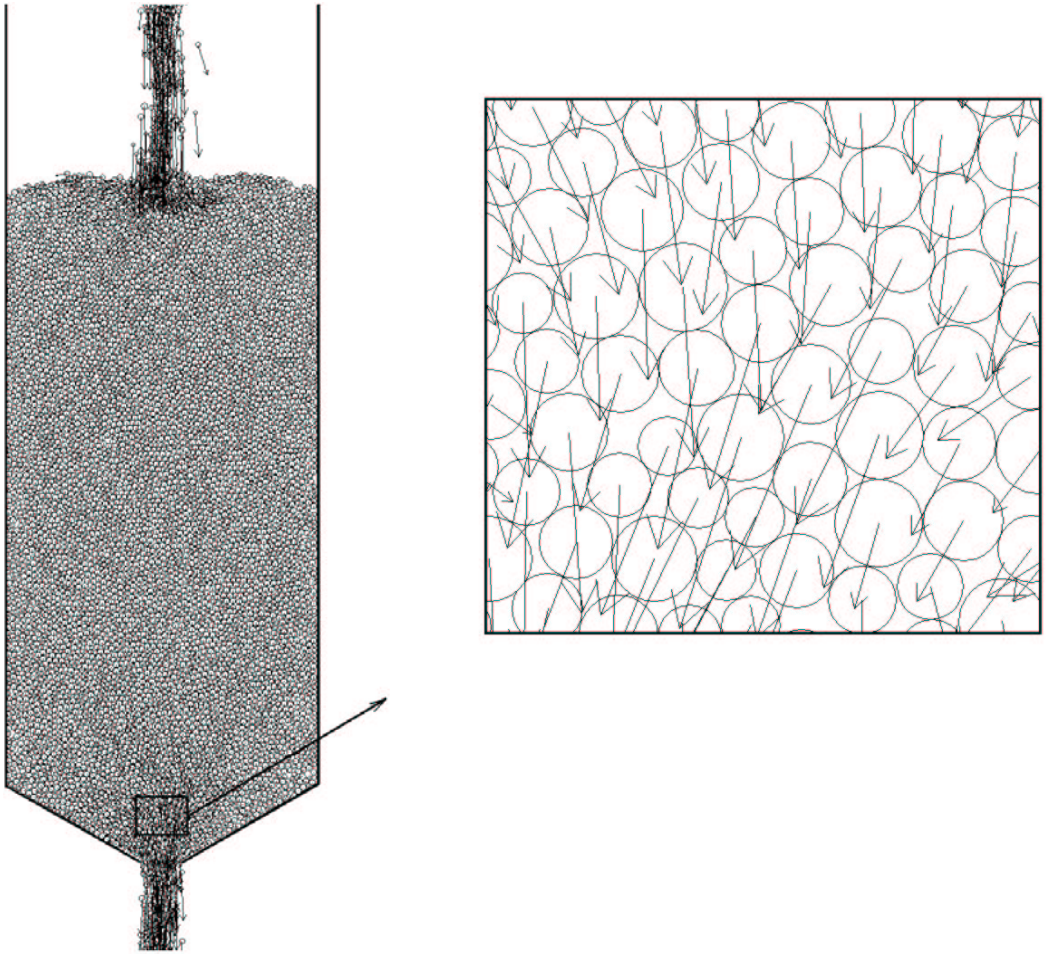

Figure 4.24: Velocity field of particles in a silo with 30° bottom angle.

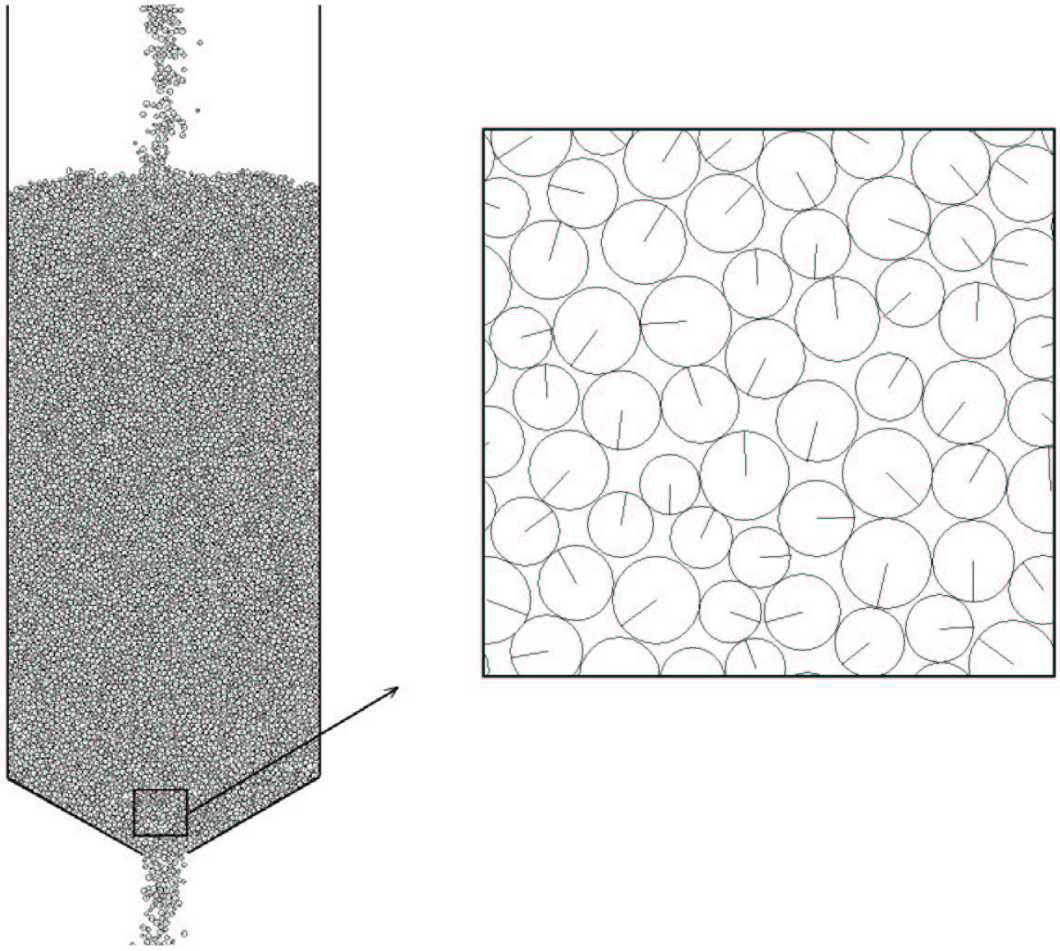

Figure 4.25: Rotation of particles in a silo with 30° bottom angle.

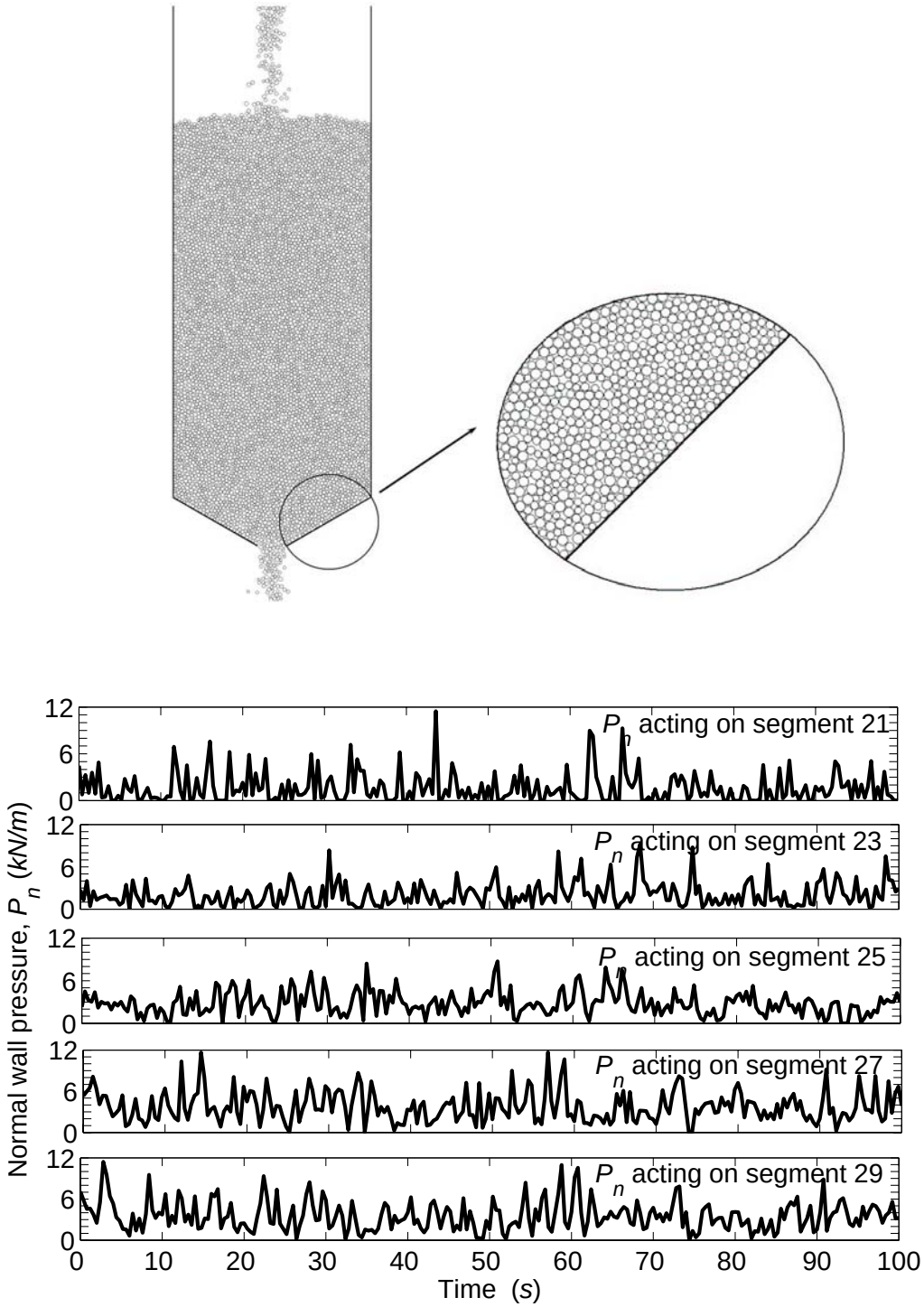

Figure 4.26: The variations of normal pressure with time along some hopper wall segments of the constant mass-flow silo with 30° bottom wall in the discharging process.

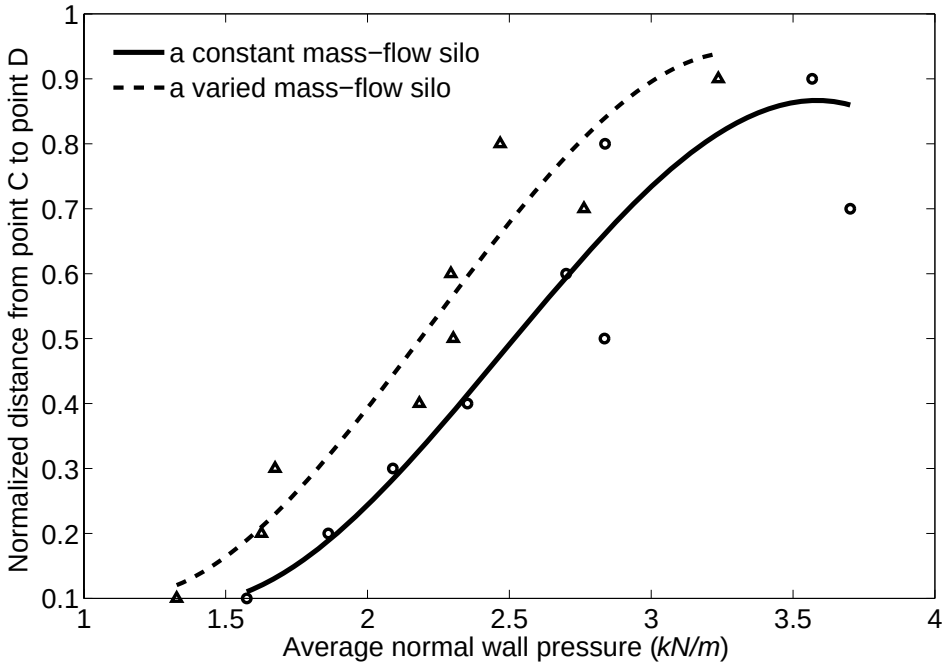

Figure 4.27: Average normal pressure acting on the hopper wall in the first 100 s (from point C to point D in Figure 4.5) obtained from the varied mass-flow silo (dashed line) and constant mass-flow silo (solid line) with bottom angles of 30°.

wall. By increasing the wall angle from 30° to 60°, the wall pressure decreases from from 3.3 N/m to 2.5 N/m. Thus, it is important to choose proper bottom angle in the design of silos.

The study shows that the dead zone of particles is found near the outlet. It has been known that the outlet width of the silo has significant influence on the pattern of the solid flow and the wall pressure. The study also clearly show that using large outlet width can prevent arching.

CHAPTER V

FINITE ELEMENT MODEL FOR AIR-PARTICLE FLOW

5.1 General Overview

This chapter presents a finite element model based on the Arbitrary Lagrangian Eulerian approach to study air-particle flow in a vertical-sided silo with conical hopper bottom. Nine particles are used to analyze the flow pattern in the silo and pressure distribution along the hopper wall. To fully understand and control the local flow behavior of air and particles in the silo, it is essential to develop a sophisticated model and computational technique for the flow analysis. Our model couples the interaction of air flow with the particle flow using the Arbitrary Lagrangian Eulerian (ALE) formulation. The ALE method is an intermediate between the Lagrangian and Eulerian methods. The governing equations for air flow are the continuity equation and the Navier-Stokes equations. For particle movement, Newton's law is applied. The complete model includes the governing equations for the air flow, the governing equations for the motion of fine particles, the interaction conditions between air and particle at the interfaces, and boundary conditions.

In the following three sections, we present the governing equations for air-particle flow, finite element formulations and numerical results and discussion, respectively.

5.2 Mathematical Model and Computational Domain

To study the motion of solid particles immersed in an air, we assume that the air-solid particle system occupies a bounded domain $\bar{\Omega}$ in $\mathbf{R}^2$. At a typical instant of time t, Q particles occupy Q closed connected subsets $\sum_{q=1}^{Q} \Omega_q \subset \mathbf{R}^2$ which is surrounded by a viscous homogeneous fluid filling the domain $\bar{\Omega} - \sum_{q=1}^{Q} \Omega_q$ called the flow-channel area.

In this study we use two coordinate systems: a reference system, Ω, where the model is drawn and the particle movement is solved, and a moving mesh system, Ω_{def}, corresponding to the deformed mesh of the flow channel, where we simulate the air flow. The time evolution of the domain Ω_{def} is determined by means of an Arbitrary Lagrangian-Eulerian (ALE) mapping $\mathbf{x} : \Omega \times \mathbf{R}^+ \mapsto \Omega_{def}$ which maps any point $(\mathbf{X}, t)$ to its image $\mathbf{x}(\mathbf{X}, t)$.

5.2.1 Transformation

In the flow-channel area, the two coordinate systems, $(X, Y) \in \Omega$ and $(x, y) \in \Omega_{def}$, are connected through a transformation T. At the initial state at $t = 0$, the two mesh systems are assumed to coincide. The transformation T maps the point initially located at (X, Y) to the point (x, y) at time t:

$$T \; : \; \begin{array}{rcl} x & = & x(X, Y, t) \\ y & = & y(X, Y, t). \end{array}$$

Suppose that the functions x and y are continuous differentiable with respect to X and Y. Then the infinitesimals dX and dY transform into dx and dy according to

$$\begin{array}{rcl} dx & = & x_{,X}dX + x_{,Y}dY, \\ dy & = & y_{,X}dX + y_{,Y}dY, \end{array} \tag{5.1}$$

where $(\cdot)_{,X}$ denotes differentiation with respect to X. System (5.1) can be written in matrix form as

$$\begin{bmatrix} dx \\ dy \end{bmatrix} = \begin{bmatrix} x_{,X} & x_{,Y} \\ y_{,X} & y_{,Y} \end{bmatrix} \begin{bmatrix} dX \\ dY \end{bmatrix}. \tag{5.2}$$

The 2×2 matrix of partial derivatives in (5.2) is called the Jacobian matrix of the transformation. Denote the matrix by $\mathbf{J}$, then

$$|\mathbf{J}| \; = \; x_{,X}y_{,Y} - x_{,Y}y_{,X}. \tag{5.3}$$

For $|\mathbf{J}| \neq 0$, the transformation is invertible and there exists an inverse transformation at time t, i.e.,

$$T^{-1} \; : \; \begin{array}{rcl} X & = & X(x, y) \\ Y & = & Y(x, y). \end{array}$$

As in (5.2), we have

$$\begin{bmatrix} dX \\ dY \end{bmatrix} = \begin{bmatrix} X_{,x} & X_{,y} \\ Y_{,x} & Y_{,y} \end{bmatrix} \begin{bmatrix} dx \\ dy \end{bmatrix}. \tag{5.4}$$

From (5.2), we also have

$$\begin{bmatrix} dX \\ dY \end{bmatrix} = \mathbf{J}^{-1} \begin{bmatrix} dx \\ dy \end{bmatrix}, \tag{5.5}$$

where

$$\mathbf{J}^{-1} = \begin{bmatrix} I_{Xx} & I_{Xy} \\ I_{Yx} & I_{Yy} \end{bmatrix} = \frac{1}{|\mathbf{J}|}\mathbf{M}, \tag{5.6}$$

$$\mathbf{M} = \begin{bmatrix} y_{,Y} & -x_{,Y} \\ -y_{,Y} & x_{,X} \end{bmatrix},$$

in which the I syntax is used to emphasize the computation of the Jacobian of the inverse transformation from the inverse of the original Jacobian.

Equating terms in (5.4) and (5.5), we obtain

$$\begin{aligned} X_{,x} &= \tfrac{1}{|\mathbf{J}|}(y_{,Y}), \\ X_{,y} &= \tfrac{1}{|\mathbf{J}|}(-x_{,Y}), \end{aligned} \tag{5.7}$$

$$\begin{aligned} Y_{,x} &= \tfrac{1}{|\mathbf{J}|}(-y_{,Y}), \\ Y_{,y} &= \tfrac{1}{|\mathbf{J}|}(x_{,X}). \end{aligned} \tag{5.8}$$

These relations are crucial in transforming the calculation results from Ω_{def} to Ω.

5.2.2 Motion of Air-Particle Flow in the Deformed Mesh System

To study the motion of particles in the silo, the particle movement is governed by Newton's second law:

$$\begin{aligned} m_q \tfrac{\partial \mathbf{V}_q}{\partial t} &= \mathbf{F}_v + \mathbf{F}_q + \mathbf{F}_g\ , \quad q = 1, 2, 3..., Q \\ \mathbf{V}_q|_{t=0} &= 0. \end{aligned} \tag{5.9}$$

The position $\mathbf{X}_q$ of the center of the qth particle can be determined by the equation:

$$\begin{aligned} \tfrac{d\mathbf{X}_q}{dt} &= \mathbf{V}_q\,, \qquad q = 1, 2, 3..., Q \\ \mathbf{X}_q|_{t=0} &= \mathbf{X}_q^0. \end{aligned} \tag{5.10}$$

In equation $(5.9)_1$, $\mathbf{V}_q$ and m_q denote the velocity vector and the mass of the qth particle. The three applied loads, drag force $\mathbf{F}_v$, collision force $\mathbf{F}_q$ and $\mathbf{F}_g$ the gravitational force are defined based on the following assumptions:

- All boundaries of particles experience drag force $\mathbf{F}_v$ from fluid,

$$\mathbf{F}_v = -\mathbf{n}_f \cdot (-p\,\mathbf{I} + \eta(\nabla\mathbf{v} + (\nabla\mathbf{v})^T)) \tag{5.11}$$

  which consists of the pressure and the viscous drag of the fluid.

- To prevent the collisions among the particles, and the particles and the boundary walls, the particle-particle interaction force $\mathbf{F}_{q,p}$ and the particle-wall interaction force $\mathbf{F}_{q,w}$ are applied when the distance between two particles, or between a particle and a wall, is within the order of the element size [21]

$$\mathbf{F}_q = \sum_{p=1, p\neq q}^{Q} \mathbf{F}_{q,p} + \sum_{w=1}^{4} \mathbf{F}_{q,w}, \tag{5.12}$$

  in which

$$\mathbf{F}_{q,p} = \begin{cases} 0, \text{ for } d_{q,p} > R_q + R_p + \alpha \\ \frac{1}{\varepsilon_q}(\mathbf{X}_q - \mathbf{X}_p)(R_q + R_p + \alpha - d_{q,p})^2, \\ \quad \text{for } d_{q,p} \leq R_q + R_p + \alpha \end{cases} \tag{5.13}$$

  and

$$\mathbf{F}_{q,w} = \begin{cases} 0, \text{ for } d_{q,w} > 2R_q + \alpha \\ \frac{1}{\varepsilon_w}(\mathbf{X}_q - \mathbf{X}_w)(2R_q + \alpha - d_{q,w})^2, \\ \quad \text{for } d_{q,w} \leq 2R_q + \alpha \end{cases} \tag{5.14}$$

  where $d_{q,p}$ denotes the distance between the centers of the qth and pth particles, $d_{q,w}$ denotes the distance between the centers of the qth particle and the imaginary particle on the other side of the wall, $\mathbf{X}_q$ and R_q are

center and radius of the qth particle, α is the force range, and ε_q and ε_w are small positive stiffness parameters.

To determine the drag force $\mathbf{F}_v$ in (5.11), air is assumed to be an isotropic, homogeneous incompressible fluid. The motion of the air is described by the continuity equation and the Navier-Stokes equations

$$\nabla \cdot \mathbf{v} = 0, \tag{5.15}$$

$$\rho_f \frac{\partial \mathbf{v}}{\partial t} + \rho_f(\mathbf{v} \cdot \nabla)\mathbf{v} - \nabla \cdot \sigma = \mathbf{F}, \tag{5.16}$$

for $\mathbf{x}$ in $\Omega_{def}(t)$ where ρ_f denotes the blood density, $\mathbf{v} = [u, v]^T$ represents the 2D velocity vector, and $\mathbf{F}$ is the volume force acting on the fluid. The quantity σ in equation (5.16) is the stress tensor given by

$$\sigma = -p\mathbf{I} + \eta(\nabla \mathbf{v} + (\nabla \mathbf{v})^T), \tag{5.17}$$

where η is the air viscosity and p is the air pressure.

On the wall, the no-slip condition is applied. On the inflow boundary Γ_{in}, the velocity is assumed to be constant, while on the outflow boundary Γ_{out}, the stress-free condition is used:

$$\begin{aligned} \mathbf{v} &= \mathbf{v}_0 \quad \text{on } \Gamma_{in} \\ \sigma \cdot \mathbf{n} &= 0 \quad \text{on } \Gamma_{out}. \end{aligned} \tag{5.18}$$

Due to the movement of the coordinate system, the mesh velocity $\mathbf{\Psi} = (\Psi_x, \Psi_y)$ is introduced in the deformed domain Ω_{def}. To guarantee a smoothly varying distribution of the nodes, we assume that the nodes on $\partial\Omega_q$ move with the particle (no slip) and that each component of the mesh velocity in the silo is governed by a Laplace equation:

$$\nabla^2 \mathbf{\Psi} = \mathbf{0}, \quad \forall \mathbf{x} \in \Omega_{def}. \tag{5.19}$$

The above equation is to smooth gradient of the mesh velocity over the domain so as to reduce mesh distortion. Once the mesh velocity components are determined, we can determine the smoothed deformed mesh for the flow channel at each

time instant by updating the coordinates of the nodes according to the following formulae

$$x = X + \int_0^t \Psi_x \, dt, \tag{5.20}$$

$$y = Y + \int_0^t \Psi_y \, dt, \tag{5.21}$$

Another condition that needs to be specified is that the air, particles and mesh move with the same velocity on the particle boundaries, i.e.,

$$\mathbf{\Psi} = \mathbf{v} = \mathbf{V}_q \quad \text{on } \partial\Omega_q. \tag{5.22}$$

We now have the strong coupled problem for the air-particle flow in the silo. These equations are solved to yield $\mathbf{V}_q$ in Ω and $\mathbf{v}, p, \mathbf{\Psi}$, in Ω_{def}.

5.3 Finite Element Formulations

The weak formulation of the air flow problem is to find $(\mathbf{v}, p, \mathbf{\Psi}) \in \Im \equiv [\mathrm{H}^1(\Omega_{def})]^2 \times \mathrm{H}^1(\Omega_{def}) \times [\mathrm{H}^1(\Omega_{def})]^2$ in the deformed mesh system at each time instant such that all the Dirichlet boundary conditions are satisfied and $\forall(\hat{\mathbf{v}}, \hat{p}, \hat{\mathbf{\Psi}}) \in \Im_0 \equiv \{(\hat{\mathbf{v}}, \hat{p}, \hat{\mathbf{\Psi}}) \in \Im |\ \hat{\mathbf{v}} = \mathbf{0}$ on $\partial\Omega_{def_\mathbf{v}}$, $\hat{p} = 0$ on $\partial\Omega_{def_p}$, and $\hat{\mathbf{\Psi}} = \mathbf{0}$ on $\partial\Omega_{def_\mathbf{\Psi}}\ \}$,

$$\int_{\Omega_{def}} \hat{p}\, (\nabla \cdot \mathbf{v})\, d\Omega = 0, \tag{5.23}$$

$$\int_{\Omega_{def}} \Big(\rho_f \hat{\mathbf{v}} \cdot \frac{\partial}{\partial t}\mathbf{v} + \eta \nabla\hat{\mathbf{v}} : \nabla\mathbf{v} + \rho_f \hat{\mathbf{v}} \cdot (\mathbf{v} \cdot \nabla)\mathbf{v} - p\nabla \cdot \hat{\mathbf{v}} \Big)\, d\Omega = \int_{\partial\Omega_{def}} \hat{\mathbf{v}} \cdot (\sigma \cdot \mathbf{n})\, ds \tag{5.24}$$

and

$$\int_{\Omega_{def}} \nabla\hat{\mathbf{\Psi}} : \nabla\mathbf{\Psi}\, d\Omega = 0, \tag{5.25}$$

where $\Omega_{def_\mathbf{v}}$, Ω_{def_p}, and $\Omega_{def_\mathbf{\Psi}}$ are the parts of boundary where the velocity, the pressure, the magnetic potential and the mesh velocity are specified. It should also be addressed that various surface integral terms, arising in the formulation, vanish as the test functions involved in the terms are zero on the boundary.

Since the computations are conducted in the reference coordinates, Ω, we need to transform equations (5.23) - (5.25) in the deformed coordinates to

those equations in the reference coordinates. Through this and using $(5.18)_2$, we obtain

$$\int_{\Omega} \hat{p}\ (\nabla \cdot \mathbf{v})\ |\mathbf{J}|\ d\Omega\ =\ 0, \tag{5.26}$$

$$\int_{\Omega} \Big(\rho_f \hat{\mathbf{v}} \cdot \frac{\partial}{\partial t}\mathbf{v}\ +\ \eta \nabla \hat{\mathbf{v}} : \nabla \mathbf{v}\ +\ \rho_f \hat{\mathbf{v}} \cdot (\mathbf{v} \cdot \nabla)\mathbf{v} - p \nabla \cdot \hat{\mathbf{v}} \Big)\ |\mathbf{J}|\ d\Omega\ =\ 0, \tag{5.27}$$

and

$$\int_{\Omega} \nabla \hat{\mathbf{\Psi}} : \nabla \mathbf{\Psi}\ |\mathbf{J}|\ d\Omega\ =\ 0, \tag{5.28}$$

where the derivatives of the unknown functions Ψ_i $(i = x, y)$ are determined by the following expressions:

$$\begin{aligned} \Psi_{i,x} &= \Psi_{i,X} I_{X,x} + \Psi_{i,Y} I_{Yx}, \\ \Psi_{i,y} &= \Psi_{i,X} I_{X,y} + \Psi_{i,Y} I_{Yy}, \end{aligned} \tag{5.29}$$

and for the test functions:

$$\begin{aligned} \hat{\Psi}_{i,x} &= \hat{\Psi}_{i,X} I_{X,x} + \hat{\Psi}_{i,Y} I_{Y,x}, \\ \hat{\Psi}_{i,y} &= \hat{\Psi}_{i,X} I_{X,y} + \hat{\Psi}_{i,Y} I_{Y,y}, \end{aligned} \tag{5.30}$$

The derivatives of other unknown functions u, v and w are defined in the same way as those of the Ψ_i functions.

5.4 Numerical Results and Discussion

To understand the air-particle flow in a silo, a 2D domain with nine particles are used. The computation domain is a silo with height of 1.2 m and width of 0.4 m. The particles are circular with diameter of 0.01 m. In room temperature, the density and viscosity of air are respectively 1.184 kg/m^3 and $1.965 \times 10^{-5} Pa \cdot s$, and air flow into the silo with speed 0.1092 m/s from the top to the bottom. All particles are assumed to be solid with the density of 1033 $kg \cdot m^{-3}$.

The Arbitrary Lagrangian Eulerian approach is used to handle the dynamics of deforming geometry and the moving boundaries. New mesh coordinates on the channel area are calculated based on the movement of the particles. The Navier-Stokes equations are formulated in the moving coordinate system.

Particle interactions, particle collisions are neglected and the volume force acting on the air is set to zero. Via the simulations of the model we can describe the flow pattern and pressure distribution in the particle-air system.

Figure 5.1 shows the 2D geometry of the silo and the finite element mesh. The computation domain consists of 2970 elements with 1509 notes. Figure 5.2 shows the velocity distributions for the models with nine particles.

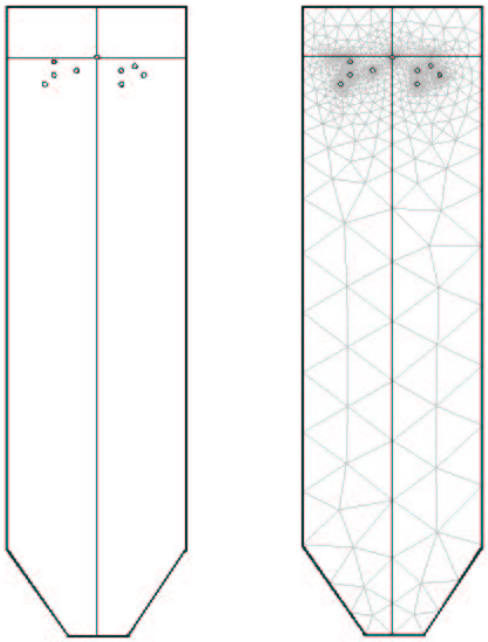

Figure 5.1: The 2D geometry of the silo and its finite element mesh

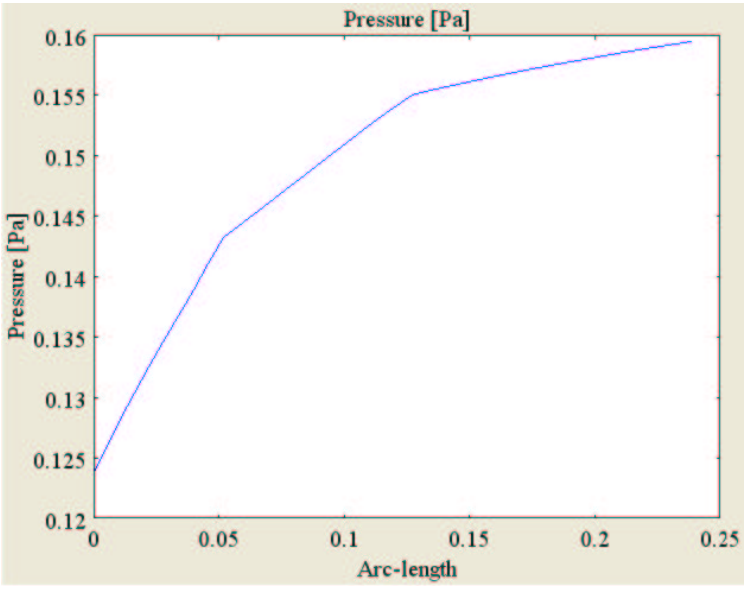

Figure 5.3: Pressure distribution along the hopper wall

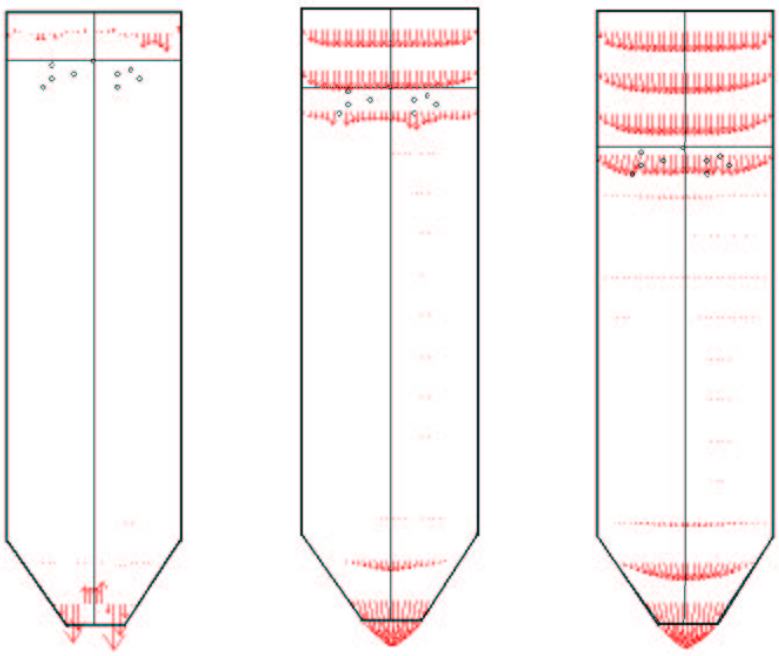

(a) $t = 0\,s$ (b) $t = 1\,s$ (c) $t = 2.24\,s$

Figure 5.2: Velocity profiles of air at various instants of time

Figures 5.3 and 5.4 show pressure distribution along the hopper wall and pressure distribution along the flow path in the silo, respectively. The results show that the model can capture the behavior of air-particle flow in the silo.

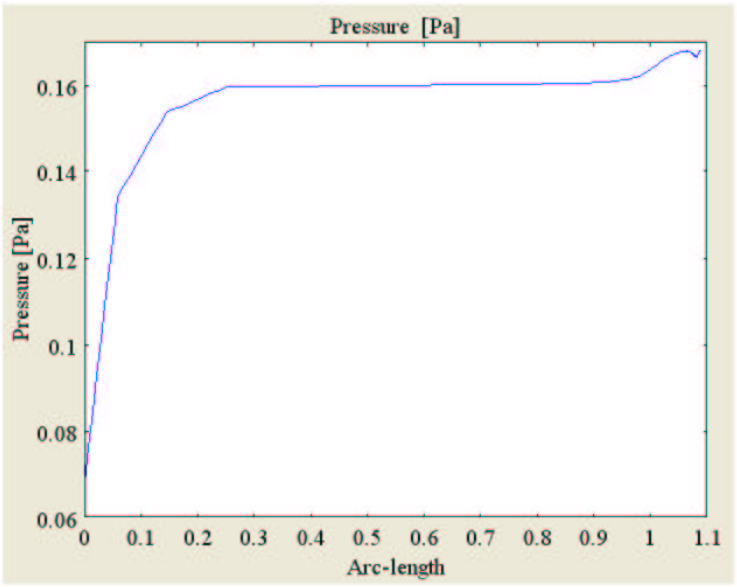

Figure 5.4: Pressure distribution along the flow path in the silo

5.5 Concluding Remarks

The finite element method has been used by many researchers for simulating the granular flow in the silo. However, most existing models do not take into account of the interaction between air flow and particles. In the present study, the finite element method based on the Arbitrary Lagrangian Eulerian approach has been developed for modelling the air-particle flow in a vertical-sided silo with conical hopper bottom. A numerical study has been undertaken to study the flow pattern and pressure distributions along the flow direction.

CHAPTER VI

CONCLUSIONS AND DISCUSSION

6.1 A Brief Summary

The project focuses on the development of mathematical models based on the discrete element method and the finite element method for the study of granular flow during filling of granular materials into the silo and discharging of granular materials from the silo. The results and conclusions gained from this study are summarized as follows:

(1) A two-dimensional discrete element model for simulating granular flows in silos has been constructed. A numerical investigation of the static and dynamic processes of granular flow during filling and discharging processes has been carried out to study the effect of inlet flow rate and bottom angles on wall pressure and flow patterns. The investigation shows that

   (i) For the static process of granular filling in the silo, it can be concluded that the higher inlet flow rate and bigger bottom angle gave higher pressure on the base of the hopper wall. The influence of bottom angle on the bottom wall pressure throughout the static process of material filling into the silo has also been investigated. The investigation showed that the pressure variation is large at the early stage of the filling process and it then becomes smaller as the height of the bulk material increases. It is noted that the bottom angle has significant effect on the pressure distribution only on the base of the hopper. The model with higher inlet flow rate and bigger bottom angle gave higher pressure on the base of the hopper wall.

   (ii) For the dynamic process of granular discharging from the silo. From the results obtained, it can be concluded that the movement of particle

through a conical bottomed silo with a higher bottom angle is faster and its interface is clearly v-shape in the varied mass-flow model. In our simulation, the blockage of particles are found at the outlet. The arch is formed over the hopper outlet of the silo having 15° bottom angle and $0.004\,m$ outlet width. The computed average normal pressures for different bottom angle are compared. The comparison indicates that bottom angle of the hopper wall is one of the important factors dominating the pressure on the hopper wall. With the increase of the wall angle from 30° to 60°, the wall pressure decreases from $3.3\,kN/m^2$ to $2.5\,kN/m^2$.

(iii) Both models of the mass-flow silo and the constant mass-flow silo are used to study the granular flow in the silo. It is found that both models are capable of investigating the influence of the bottom angle of the hopper wall on the pressure distribution. Results obtained from both models are compared and it has been found that the average wall pressure of the constant mass-flow silo is higher than the wall pressure of the varied mass-flow silo.

(2) A finite element model based on the Arbitrary Lagrangian Eulerian approach has been developed to study the air-particle flow. The model with nine particles is used in the simulation to study the flow pattern in the silo and the pressure distributions along the hopper wall. The results show that the model can capture the flow pattern of the air-particle flow in the silo.

(3) The silo configuration and the properties of the stored granular solid are important factors for the pressure acting inside a silo during filling and discharging processes. Mathematical modelling and numerical simulation enable one to obtain a better understanding of the complex phenomenon of the flow behavior of materials in silos. From the simulation results obtained form the discrete element method and the finite element method, we can conclude that these methods have a number of advantages over the experimental method. In this dissertation, we focus on effects of the inlet flow

rate and the bottom angle of the hopper wall on the pressure distribution. The results demonstrate that the bottom angle of the hopper wall is one of the important factors dominating the pressure on the hopper wall. Thus, it is necessary to consider the bottom angle when we design a silo.

(4) This research provides information for improving the design of the silo and increasing the quality and productivity of products. The research outcomes also provide useful information for potential development of computer software.

6.2 Future Research

In the present research, we concentrated on the development of mathematical models to study granular flow and air-particle flows in the silo during filling and discharging process. In this work, 2-D simulations of granular flow in the silo with 7,500 particles and air-particle flow in the silo with 9 particles are presented. Further research work could be carried out to use large number of multi-scale particles ($>$ 7,500 particles) and many types of silos including asymmetric conical, pyramid and cylindrical flat-bottomed slot in 3-D simulation.

REFERENCES

[1] Aoki R, Tsunakawa H. The pressure in a granular material at the wall of bins and hoppers. Journal of Chemical Engineering of Japan 1969;2:126-129.

[2] Banton J, Villard P, Jongmans D, Scavia C. Two-dimensional discrete element models of debris avalanches: Parameterization and the reproducibility of experimental results. JournalL of Geophysical Research 2009;114:doi:10.1029/2008JF001161.

[3] Brown CJ, Lahlouh EH, Rotter JM. Experiments on a square planform steel silo. Chemical Engineers Science 2000;55:4399-4413.

[4] Bui HH, Fukagawa R, Kobayashi T, Tamoi K. DEM Simulation of Three-Dimensional Soil Failure with Cutting Blade. Proceeding of 7^{th} APISTVS Conference Changchun, China 2004;September 14 to 16:113-121.

[5] Butterfield R, Harkness RM. The kinematics of Mohe-Coulomb Materials in Stress-Strain Behaviour of Solis. Proc. of the Roscoe Memorial Symposium 1972;220-233.

[6] Campbell CS, Gong A. The stress tensor in two-dimensional granular flow shear flow. Journal of Fluid Mechanics 1986;164:107-125.

[7] Campbell CS, Gong A. Granular material flows - An overview. Powder Technology 2006;162:208-229.

[8] Chen JF, Rotter JM, Ooi JY, Zhong Z. Correlation between the flow pattern and wall pressures in a full scale experimental silo. Engineering Structures 2007;2308-2320.

[9] Cleary PW. Large scale industrial DEM modeling. Engineering Computations 2004;21(2/3/4):169-204.

[10] Cleary PW. Industrial particle flow modeling using discrete element method. Engineeriing Computations: International Journal for Computer-Aided Engineering and Software 2009;26(6):698-743.

[11] Cleary PW. DEM prediction of industrial and geophysical particle flows. Particuology 2009;doi:10.1016/j.partic.2009.05.006.

[12] Cleary PW. The effect of paricle shape on hopper discharge. Second International Conference on CFD in the Minerals and Process Industries CSIRO, Melbourne, Australia 6-8 December 1999;71-76.

[13] Cleary PW, Sawley ML. Three-dimensional modelling of industrial granular flows. Second International Conference on CFD in the Minerals and Process Industries CSIRO, Melbourne, Australia 6-8 December 1999;95-100.

[14] Cleary PW, Sawley ML. DEM modelling of industrial granular flows: 3D case studies and the effect of particle shape on hopper discharge. Applied Mathematical Modelling 2002;26:89-111.

[15] Collinson R. Mathematicla Models and Numerical Techniques for Plasticity Flows of Granular Materials. Curtin University of Technology Ph.D. afhandling 1998.

[16] Cundall PA, Strack ODL. Discrete numerical model for granular assembiles. Geotechnique 1979;29(1):47-65.

[17] Dong KJ, Yu AB, Brake I. DEM simulation of particle flow on a multi-deck banana screen. Minerals Engineering 2009;22:910-920.

[18] Fraige FY, Langston PA, Matchett AJ, Dodds J. Vibration induced flow in hoppers: DEM 2D polygon model. Particuology 2008;6:455-466.

[19] Goda TJ, Ebert F. Three-dimensional discrete element simulations in hoppers and silos. Powder Technology 2005;158(1-3):58-68.

[20] Goodey RJ, Brown CJ, Rotter JM. Verification of a 3-dimensional model for filling pressures in square thin-walled silos. Engineering Structures 2003;25:1773-1783.

[21] Goodey RJ, Brown CJ, Rotter JM. Predicted patterns of filling procedures in thin-walled square sios. Engineering Structures 2006;28:109-119.

[22] Granular Vocano Group. A Review of Plastic-Frictional Theory Part. 1 Introduction, Mohr-Coulomb, and Von Mises Stresses. Avaiable from $http://www.granular\_volcano\_group.org/frictional\_theory.html$

[23] Guaita M, Couto A, Ayuga F. Numerical simulation of wall pressure during discharge of granular material from cylindrical silos with eccentric hoppers. Biosystems Engineering 2003;85:101-109.

[24] Harris D. Constitutive equations for planar deformations of rigid-plastic materials. Journal of Mechanics and Physics of Solids 1993; 41(9):1515-1531.

[25] Hasatani M, Itaya Y, Miura K. Drying of granular materials in an inclined vibrated fludized bed by combined radiative and onvective heating. Drying Technology: An International Journal 1991;9(2):349-366.

[26] Hill JM, Wu YH. Some axially symmetric flows of Mohr-Coulomb compressible granular materials. Proc. of the Royal Society of London A 1992;438:67-93.

[27] Hill JM, Wu YH. Plastic flows of granular materials of shear index n: Part II plane and axially symmetric problems for $n = 2$. Journal of Mech. and Physics of Solids 1993;41:95-115.

[28] Hill JM, Wu YH. The punch problem for shear index granular materials. Quarterly Journal of Mechanics and Applied Mathematics 1996; 49:81-105.

[29] Hill KM, Gilchrist JF, Ottino JM. Mixing of granualr materials: A test-bed dynamical system for pattern formation. International Jouranl of Bifurcation and Chaos 1999;9(8):1467-1484.

[30] Hirshfeld D, Rapaport DC. Granular flow from s silo: Discrete-particle simulations in three dimensions. The European Physical Journal E 2001;4:193-199.

[31] Hopkins MA, Louge MY. Inelastic microstructure in rapid granular flows of smooth disks. Phys. Fluids. A 1991;3(1):47-57.

[32] Hopkins MA, Shen HH. Constitutive Relations for a Plannar, Simple Flow of Rough Disks. International Journal of Engineering Science 1986; 24(11):1717-1730.

[33] Hsiau SS, Hsu CC, Smid J. The discharge of fine silica sands in a silo. Physics of Fluids 2010;22:1-9.

[34] Janssen HA. Test on grain pressure in silos. Zeitschrift des Vereines Deutscher Ingenieure 1895;39(35):243-254.

[35] Jenike AW. Storage and flow of solids. Bul. 123, Utah Engineering Expt. Sta. Univ. of Utah, November 1964.

[36] Jenike AW, Johanson JR. Bin loads. Journal of Struct. Div., ASCE 94, St4 1969:April:1011-1041.

[37] Jenike AW, Gravity flow of bulk silids. Salk Lake City, UT 1961;Bulletin 108.

[38] Jofriet JC, Negi SC, Lu Z. A numerical model for flow of granular materials in silos. part 3: Parametric study. J. Agric Engng Res. 1997;68:237-246.

[39] Karlsson T, Klisinski M, Runesson K. Finite element simulation of granualr material flow in plane silos with complicated geometry. Powder Technology 1998;99:29-39.

[40] Katayama T, Aoyoma E, Yamamoto K, Sakaue S. Evaluation of two-component powder mixing by vertical vibration investigation of powder behavior and mixed state by internal pressure fluctuation. Journal of Materials Processing Technology 2004;155-156: 1571-1576.

[41] Ketterhagen WR, Curtis JS, Wassgren CR. Stress results from two-dimensional granular shear flow simulations using various collision models. Phys Rev E 2005;71:1-11.

[42] Ketterhagen WR, Curtis JS, Wassgren CR, Hancock BC. Predicting the flow mode from hoppers using the discrete element method. Powder Technology 2009;195:1-10.

[43] Kim YM. A granular motion simulation by discrete element method. Journal of Mechanical Science and Technology 2008;22:812-818.

[44] Lade PV. Elasto-plastic stress -strain theory for cohesionless soil with curved yield durface. Int. Journal of Solids and Structures 1977;13: 1019-1035.

[45] Langston PA, Tüzün U, Heyes DM. Continuous potential discrete particle simulations of stress and velocity-fields in hoppers transition from fluid to granular flow. Chemical Engineering Science 1994;49: 1259-1275.

[46] Langston PA, Heyes DM, Tüzün U. Discrete element simulation of granular solid flow in hoppers: discharge rate and wall stress predictions in 2&3 dimensions. Chemical Engineering Science 1995;50:967-980.

[47] Langston PA, Tüzün U, Heyes DM. Discrete element simulation of granular flow in 2D and 3D hoppers: dependence of discharge rate and wall stress on particle interactions. Chemical Engineering Science 1995;50(6):967-987.

[48] Langston PA, Tüzün U, Heyes DM. Discrete element simulationvof internal -stress and flow-fields in funnel flow hoppers. Powder Technology 1995;85:153-169.

[49] Li J, Webb C, Pandiella SS, Campbell GM. A numberical simulation of separation of crop seeds by screening-effect of particle bed depth. Institution of Chemical Engineers 2002;80:109-117.

[50] Li J, Webb C, Pandiella SS, Campbell GM. Discrete particle motion on sieves- a numerical study using the DEM simulation. Powder Technology 2003;133:190-202.

[51] Li J, Langston PA, Webb C, Dyakowski T. Flow of sphero-disc particles

in rectangular hoppers a DEM and experimental comparision in 3D. Chemical Engineering Science 2004;59:5917-5929.

[52] Li Y, Xu Y, Jiang S. DEM simulations and experiments of pebble flow with monosized spheres. Powder Technology 2009;193:312-318.

[53] Lu Z, Negi SC, Jofriet JC. A numerical model for flow of granular materials in silos. part 1: Model development. J. agric Engng Res. 1997; 68:223-229.

[54] Makino H, Hirata M. Computer simulation and optimization of sand filling using the distinct element method. Simulation and Rapid Prototyping 2003;5:1-16.

[55] Markauskas D. Discrete element modelling of complex axisymmetrical particle flow. Mechanika 2006;6:32-38.

[56] Masson S, Martinez J. Effect of particle mechanical properties on silo flow and stresses from distinct element simulations. Powder Technology 2000;109:164-178.

[57] Masson S, Martinez J. Effect of particle properties and silo geometry on stresses predicted by discrete simulations of bulk materials. 15^{th} ASCE Engineering Mechanics Conference 2002;June 2-5:1-8.

[58] McCoy BJ, Madras G. Cluster kinetics of granular mixing. American Instituteof Chemical Engineers 2005;51(2):406-414.

[59] Naon B, Saix C, Bdrthomieu G, Benet JC. Modelling convective drying of granular materials: Application to natural rubber. Drying Technolgy: An International Journal 1995;13:571-583.

[60] Negi SC, Lu Z, Jofriet JC. A numerical model for flow of granular materials in silos. part 2: Model validation. J. agric. Engng Res. 1997; 68:231-236.

[61] Nielsen J. Pressures from flowing granular solids in silos. Philosophical 2004;59:5917-5929.

[62] Nguyen TV, Brennen C, Sabersky RH. Gravity flow of granular materials in conical hoppers. Journal of Appiled Mechanics 1979;46:529-535.

[63] Ooi JY, Chen JF, Lohnes RA, Rottor JM. Prediction of static wall pressures in coal silos. Construction and Building Materials 1996;10(2): 109-116.

[64] Ooi JY, Rotter JM. Wall pressures in square steel silos form finite element analysis. Computers & Structures 1990;37(4):361-374.

[65] Ooi JY, Rotter JM. Elastic predictions of pressures in conical silo hoppers. Engineering Structure 1991;13:2-12.

[66] Portillo PM, Muzzio FJ, Ierapetritou MG. Characterizing powder mixing processes utilizing compartment models. International Journal of Pharmaceulics 2006;320:14-22.

[67] Rombach G, Eibl J. Granular flow of materials in silos. International Journal of Bulk Solid Handling 1995;15(1):65-70.

[68] Rombach GA, Neumann F. 3-D finite element modelling of granular flow in silos. 17^{th} ASCE Engineering Mechanics Conferenc University of Delawark, Newaek, DE 2004;June:13-16.

[69] Rong GH, Negi SC, Jofriet JC. Simulation of flow behaviour of bulk solids in bins. part 2: Shear bands, flow corrective inserts and velocity. Journal of Agricultural Engineering Research 1995;62(4):257-269.

[70] Roscoe KH, Schofield AN, Wroth CP. On the yielding of soils. Geotechnique 1958;9:71-83.

[71] Rotter JM, Brown CJ, Lahlouh EH. Patterns of wall pressure on filling a square planform steel silo. Engineering Structures 2002;24: 135-150.

[72] Rotter JM, Holst JMFG, Ooi JY, Sanad AM. Silo pressure perdictions using discrete-element and finite-element analyses. Phil. Trans. R. Soc. Lond. A 1998;356:2685-2712.

[73] Santomaso A, Olivi M, Canu P. Mechanisms of mixing of granular materials in drum mixers under rolling regime. Chemical Engineering Science 2004;59:3269-3280.

[74] Schmidt LC, Wu YH. Prediction of dynamic wall pressures on silos. Internaltionl Journal of Bulk Solid Handling 1989;9:333-338.

[75] Sitharam TG. Numerical simulation of particulate materials using discrete element modelling. Current Science 2000;78:876-886.

[76] Spencer AJM. A theory of the kinematics of ideal soils under plane strain conditions. J. of the Mechanics and Physics of solids 1964;12: 337-351.

[77] Spencer AJM, Kingston MR. Plane mechanics and kinematics of compressible ideal granular materials. Rheologica Acta 1973;12: 194-199.

[78] Walker DM. An approximate theory of pressure and arching in hoppers. Chem. Engrg. Sci. 1966;21:975-997.

[79] Walker DM, Blanchard MH. Pressures in experimental coal hoppers. Chem. Engrg. Sci. 1967;22:1713-1745.

[80] Walton OR, Braun RL. Viscosity, granular-temperature, and stree calculations for shearing assemblies of inelastic, frictional disks. Journal of Rheology 1986;949-980.

[81] Wu J, Binbo J, Chen J, Yang Y. Multi-scale study of particle flow in silos. Advanced Power Technology 2009;20:62-73.

[82] Wu YH, Conllinson R. Determination of velocity and stress discontinuities in quasi-static granular flows. ANZIAM J. 2000;42(E):C1558-C1579.

[83] Wu YH, Hill JM, Yu A. A finite element method for granular flow through a frictional boundary. Communications in Nolinear Science and Numerical Simulation 2007;12:486-495.

[84] Wu YH, Schmidt LC. A boundary element method for prediction of silo pressure. International Journal of Computers and Structures 1992;45:315-323.

[85] Xiang J, Munjiza A, Latham JP, Guises R. On the validation of DEM and FEM/DEM models in 2D and 3D. Engineering Computations: International Journal for Computer-Aided Engineering and Software 2009;673-687.

[86] Yang SC, Hsiau SS. The simulation and experimental study of granualar materials discharged from a silo with the placement of inserts. Powder Technology 2001;120:244-255.

[87] Zhao D, Nezami EN, Hashash YMA, Ghaboussi J. Three-dimensional discrete element simulation for granular materials. Engineering Computations: International Journal for Computer-Aided Engineering and Software 2006;23:749-770.

[88] Zhong Z, Ooi JY, Rotter JM. The sensitivity of silo flow and wall stresses to filling method. Engineering Structures 2001;23:756-767.

[89] Zhou YC, Wright BD, Yang RY, Xu BH, Yu AB. Rolling friction in the dynamic simulation of sandpile formation. Physica A 1999; 269:536-553.

[90] Zhu HP, Yu AB. Micromechanic modeling and analysis of unsteady-state granual flow in a cylindrical hopper. Journal of Engineering Mathematics 2005;52:307-320.

[91] Zhu HP, Wu YH, Yu AB. Discrete and continuum modeling of granular flow. China Particuology 2005;3:354-363.

[92] Zuo SC, Xu Y, Yang QW. Discrete element simulation of the behavior of bulk granular material during truck braking. Engineering Computations: International Journal for Computer-Aided Engineering and Software 2006;23:4-15.

APPENDIX

Folder: Granular flow during filling and discharging of a silo

Folder of granular flow during filling and discharging of a silo contains 2 subfolders "Initial Process " and "Main Process"

(1) **Initial Process**

Source file: test_init.c

Input file: input_init.in

Source codes are in directory C:\granular\init_process

To run the program, we use the following commands:

- C:\granular\init_process\test_init init_input.in a.out This command gives "DEsim2D.IC" which is used for generate an input file for main simulation.
- C:\granular\init_process\copy\ DEsim2D.IC main_input.in
  In a file named "main_input.in", data information is changed as follows:
  - line 2: start time = 0.0
  - line 3: end time = 50.0
  - lime 8: number of walls = 8

(2) **Main Process**

Source file: test.c

Input file: main_input.in

Source codes are in directory C:\granular\main_process

Java application is in the directory C:\granular\javamovie

To run the program, we use the following commands:

- C:\granular\main_process\test main_input.in a.out f.out
  To see the results using Java program. We use the following command:
  - C:\granular\javamovie\java -mx1000m Movie2D ..\main_process\a.out 0 1000 0

Input file

number of environment data: 10

start time: 0.0, end time: 50.0

number of samples per unit time: 5.0, simulation time step: 5.2711e-6

gravity in x-direction: 0.0, gravity in y-direction: -1.0361

movie bounding box: 0.0, movie bounding box: 45.0

movie bounding box: 0.0, movie bounding box: 505.0

Number of particle species: 2, Particle species[i].N: 3,500, 4,000

Number of wall species: 1, Wall species[i].N: 9

$k_n[i][j]$ $nun[i][j]$ $k_s[i][j]$ $\mu[i][j]$

Particle Species[i].dbar .ddev .rho

wall[i].L .m .I .periodicbndry

.x0 .y0 .theta .xdot .ydot .thetadot

Example of Input data

10

0.0 50.0

5.0 5.2711e-6

0.0 -1.0361

0.0 45.0

0.0 505.0

2 3500 4000

1 9

2.8322e+4 1.3048e+2 2.2570e+4 3.3000e-1

2.8322e+4 1.3048e+2 2.2570e+4 3.3000e-1

5.6645e+4 1.3962e+2 4.5314e+4 3.5000e-1

2.8322e+4 1.3048e+2 2.2570e+4 3.3000e-1
2.8322e+4 1.3048e+2 2.2570e+4 3.3000e-1
5.6645e+4 1.3962e+2 4.5314e+4 3.5000e-1

5.6645e+4 1.3962e+2 4.5314e+4 3.5000e-1
5.6645e+4 1.3962e+2 4.5314e+4 3.5000e-1
5.6645e+4 1.3962e+2 4.5314e+4 3.5000e-1

6.0000e-1 1.0000e-1 1.0330e+0
7.5000e-1 1.0000e-1 1.0330e+0

40.0 0.0 0.0 -1
0.0 0.0 4.71238898 0.0 0.0 0.0
40.0 0.0 0.0 -1
0.0 700.0 4.71238898 0.0 0.0 0.0
600.0 0.0 0.0 -1
0.0 100.0 0.0 0.0 0.0 0.0
600.0 0.0 0.0 -1
40.0 100.0 0.0 0.0 0.0 0.0
100.0 0.0 0.0 -1
0.0 0.0 0.0 0.0 0.0 0.0
100.0 0.0 0.0 -1
40.0 0.0 0.0 0.0 0.0 0.0
22.6274 0.0 0.0 -1
16.0 100.0 0.785398 0.0 0.0 0.0
22.6274 0.0 0.0 -1
24.0 100.0 5.497787 0.0 0.0 0.0
8.0 0.0 0.0 -1
16.0 100.0 4.71238898 0.0 0.0 0.0

MATLAB programs

Some MATLAB programs used for calculation the normal wall pressure along the bottom wall of the silo.

(a) Matlab program is used to calculate the normal wall pressure along some hopper wall segments in the process of filling process.

```
clear;
B=load('f7.out');
A7=B(1:1601,:);
%at time = 80 sections
t=A7(:,1) [m n]=size(A7);
L7=16.5644/10;
endsec7=16.5644;
nsec7=L7:L7:endsec7;


sec1=A7(:,2);
sec2=A7(:,3);
sec3=A7(:,4);
sec4=A7(:,5);
sec5=A7(:,6);
sec6=A7(:,7);
sec7=A7(:,8);
sec8=A7(:,9);
sec9=A7(:,10);
sec10=A7(:,11);


aveps1=sum(sec1)/m;
aveps2=sum(sec2)/m;
aveps3=sum(sec3)/m;
aveps4=sum(sec4)/m;
aveps5=sum(sec5)/m;
```

```
aveps6=sum(sec6)/m;
aveps7=sum(sec7)/m;
aveps8=sum(sec8)/m;
aveps9=sum(sec9)/m;
aveps10=sum(sec10)/m;

% converse length each section centimeter to meter
Lsec7=1.65644/100;
avef7=[aveps1 aveps2 aveps3 aveps4 aveps5 aveps6 aveps7 aveps8 aveps9
aveps10]/Lsec7 ;

C= load('f9.out');
A9 = C(1:1601,:);
t=A9(:,1) [p q]=size(A9) L9=8/10;
endsec9=8;
nsec9=L9:L9:endsec9;
sec1=A9(:,2);
sec2=A9(:,3);
sec3=A9(:,4);
sec4=A9(:,5);
sec5=A9(:,6);
sec6=A9(:,7);
sec7=A9(:,8);
sec8=A9(:,9);
sec9=A9(:,10);
sec10=A9(:,11);

aveps1=sum(sec1)/p;
aveps2=sum(sec2)/p;
aveps3=sum(sec3)/p;
aveps4=sum(sec4)/p;
```

```
aveps5=sum(sec5)/p;
aveps6=sum(sec6)/p;
aveps7=sum(sec7)/p;
aveps8=sum(sec8)/p;
aveps9=sum(sec9)/p;
aveps10=sum(sec10)/p;

Lsec9= 0.8/100;
avef9=[aveps1 aveps2 aveps3 aveps4 aveps5 aveps6 aveps7 aveps8 aveps9
aveps10]/Lsec9;

D= load('f8.out');
A8 = D(1:1601,:);
t=A8(:,1) [s t]=size(A8) L8=16.5644/10;
endsec8=16.5644;
nsec8=L8:L8:endsec8;
sec1=A8(:,2); sec2=A8(:,3);
sec3=A8(:,4); sec4=A8(:,5);
sec5=A8(:,6); sec6=A8(:,7);
sec7=A8(:,8); sec8=A8(:,9);
sec9=A8(:,10); sec10=A8(:,11);

aveps1=sum(sec1)/s;
aveps2=sum(sec2)/s;
aveps3=sum(sec3)/s;
aveps4=sum(sec4)/s;
aveps5=sum(sec5)/s;
aveps6=sum(sec6)/s;
aveps7=sum(sec7)/s;
aveps8=sum(sec8)/s;
aveps9=sum(sec9)/s;
```

```
aveps10=sum(sec10)/s;


Lsec8= 1.65644/100;
avef8=[aveps10 aveps9 aveps8 aveps7 aveps6 aveps5 aveps4 aveps3 aveps2
aveps1]/Lsec8;


newsec1=nsec7;
newsec2=(16.5644+0.8):0.8:(16.5644+8);
newsec3=(16.5644+8+1.65644):1.65644:16.5644+8+16.5644;


distance=[newsec1 newsec2 newsec3]/41.1288;
pressure=[avef7,avef9,avef8];
hold on


set(0,'DefaultAxesColorOrder',[0 0 0],'DefaultAxesFontSize',20);
plot(distance, pressure,'-','MarkerSize',5,'LineWidth',2.5);
xlabel('Normalized distance from point A to point D (m)'); ylabel(' Average
normal wall pressure (kN/m)');
```

(b) Matlab program is used to calculate the normal wall pressure along some hopper wall segments in the process of discharging process.

```
clear;
B=load('f7.out');
A7=B(1:8:2001,:);
t=B(1:8:2001,1) [m n]=size(A7);
Lsec7=1.96299/100;
sec1=A7(:,2)/Lsec7;
sec2=A7(:,3)/Lsec7;
sec3=A7(:,4)/Lsec7;
sec4=A7(:,5)/Lsec7;
sec5=A7(:,6)/Lsec7;
```

```
sec6=A7(:,7)/Lsec7;
sec7=A7(:,8)/Lsec7;
sec8=A7(:,9)/Lsec7;
sec9=A7(:,10)/Lsec7;
sec10=A7(:,11)/Lsec7;

figure
set(0,'DefaultAxesColorOrder',[0 0 0],'DefaultAxesFontSize',18);

subplot(511);
plot(t,sec1,'-','MarkerSize',5,'LineWidth',2);
axis([0 100 0 12000]);
set(gca,'ytick',0:1000:12000);
set(gca,'XTick',0:10:100);
set(gca,'XTickLabel',' ',' ',' ',' ',' ',' ',' ',' ',' ',' ',' ',' ');
set(gca,'YTickLabel','0',' ',' ',' ','4',' ',' ',' ','8',' ',' ',' ', '12');

subplot(512);
plot(t,sec3,'-','MarkerSize',5,'LineWidth',2);
axis([0 100 0 12000]);
set(gca,'ytick',0:1000:12000);
set(gca,'XTick',0:10:100);
set(gca,'XTickLabel',' ',' ',' ',' ',' ',' ',' ',' ',' ',' ',' ',' ');
set(gca,'YTickLabel','0',' ',' ',' ','4',' ',' ',' ','8',' ',' ',' ', '12');

subplot(513);
plot(t,sec5,'-','MarkerSize',5,'LineWidth',2);
axis([0 100 0 12000]);
set(gca,'ytick',0:1000:12000);
set(gca,'XTick',0:10:100);
```

```
set(gca,'XTickLabel',' ',' ',' ',' ',' ',' ',' ',' ',' ',' ',' ',' ',' ');
set(gca,'YTickLabel','0',' ',' ',' ','4',' ',' ',' ',' ','8',' ',' ',' ',' ', '12');
ylabel('Normal wall pressure, P_n(kN/m)','Fontsize',20);


subplot(514);
plot(t,sec7,'-','MarkerSize',5,'LineWidth',2);
axis([0 100 0 12000]);
set(gca,'ytick',0:1000:12000);
set(gca,'XTick',0:10:100);
set(gca,'XTickLabel',' ',' ',' ',' ',' ',' ',' ',' ',' ',' ',' ',' ',' ');
set(gca,'YTickLabel','0',' ',' ',' ','4',' ',' ',' ',' ','8',' ',' ',' ',' ', '12');


subplot(515);
plot(t,sec9,'-','MarkerSize',5,'LineWidth',2);
axis([0 100 0 12000]);
set(gca,'ytick',0:1000:12000);
set(gca,'XTick',0:10:100);
set(gca,'XTickLabel','0 ','10 ','20 ','30 ','40 ','50 ','60 ','70 ','80 ','90','100');
set(gca,'YTickLabel','0',' ',' ',' ','4',' ',' ',' ',' ','8',' ',' ',' ',' ', '12');
xlabel('Time (s)','Fontsize',20);
```

(c) Matlab program is used to calculate an average normal wall pressure along the bottom wall in the first 100 s of discharging process to investigate effect of two different mass-flow silos: varied mass-flow and constant mass-flow silo.

```
clear;
B=load('f7-30con.out');
A30con=B(1:2001,:);
t=B(1:2001,1);
[m n]=size(A30con);
```

```
L30con=19.6299/10;
endsec30con=19.6299;
nsec30con=L30con:L30con:endsec30con;
sec1=A30con(:,2);
sec2=A30con(:,3);
sec3=A30con(:,4);
sec4=A30con(:,5);
sec5=A30con(:,6);
sec6=A30con(:,7);
sec7=A30con(:,8);
sec8=A30con(:,9);
sec9=A30con(:,10);
sec10=A30con(:,11);

aveps1=sum(sec1)/m;
aveps2=sum(sec2)/m;
aveps3=sum(sec3)/m;
aveps4=sum(sec4)/m;
aveps5=sum(sec5)/m;
aveps6=sum(sec6)/m;
aveps7=sum(sec7)/m;
aveps8=sum(sec8)/m;
aveps9=sum(sec9)/m;
aveps10=sum(sec10)/m;

% converse length each section centimeter to meter
Lsec30con =1.96299/100;
averf30con=[aveps1 aveps2 aveps3 aveps4 aveps5 aveps6 aveps7 aveps8 aveps9
aveps10]/Lsec30con;
```

```
normaldis30con=nsec30con/19.6299;


C=load('f7-30varied.out');
A30var=C(1:2001,:);
t=C(1:2001,1) [m n]=size(A30var);
L30var=19.6299/10;
endsec30var=19.6299;
nsec30var=L30var:L30var:endsec30var;
sec1=A30var(:,2);
sec2=A30var(:,3);
sec3=A30var(:,4);
sec4=A30var(:,5);
sec5=A30var(:,6);
sec6=A30var(:,7);
sec7=A30var(:,8);
sec8=A30var(:,9);
sec9=A30var(:,10);
sec10=A30var(:,11);


aveps1=sum(sec1)/m;
aveps2=sum(sec2)/m;
aveps3=sum(sec3)/m;
aveps4=sum(sec4)/m;
aveps5=sum(sec5)/m;
aveps6=sum(sec6)/m;
aveps7=sum(sec7)/m;
aveps8=sum(sec8)/m;
aveps9=sum(sec9)/m;
aveps10=sum(sec10)/m;


Lsec30var =1.96299/100;
```

```
averf30var=[aveps1 aveps2 aveps3 aveps4 aveps5 aveps6 aveps7 aveps8 aveps9
aveps10]/Lsec30var ;
normaldis30var=nsec30var/19.6299;
[xs30con ys30con]=Poly_Fit(averf30con,normaldis30con);
[xs30var ys30var]=Poly_Fit(averf30var,normaldis30var);
set(0,'DefaultAxesColorOrder',[0 0 0],'DefaultAxesFontSize',20);
hold on
plot(xs30con,ys30con,'-','MarkerSize',5,'LineWidth',3);
plot(xs30var,ys30var,'–','MarkerSize',5,'LineWidth',2.5);
h = legend('a constant mass-flow silo','a varied mass-flow silo',2);
set(h,'Interpreter','none') h = legend('a constant mass-flow silo','a varied
mass-flow silo',2);
xlabel('Average normal wall pressure (kN/m) ');
ylabel('Normalized distance from point C to point D (m)');
plot(averf30con,normaldis30con,'o','MarkerSize',5,'LineWidth',2)
plot(averf30var,normaldis30var,'′','MarkerSize',5,'LineWidth',2)


% Poly_Fit.m
function [xs ys]=Poly_Fit(x,y) n=input('Enter a degree of polynomial:');
k=polyfit(x,y,n);
for j=1:n+1
fprintf('The coefficient k( %1.0f)= %10.5f\n',j,k(j)) end


x_incr=(max(x)-min(x))/100; xs=min(x):x_incr:max(x);
ys=polyval(k,xs);
```

BIOGRAPHY

NAME	Ms. Wariam Chuayjan
DATE OF BIRTH	May 4, 1977
PLACE OF BIRTH	Nakhon Si Thammarat, Thailand
INSTITUTIONS ATTENDED	Thammasat University, 1996–2000
	Bachelor of Science (Applied Mathematics)
	King Mongkut's University of Technology
	North Bangkok
	Master's Degree (Applied Mathematics)
	Mahidol University, 2002–2005
	Doctor of Philosophy (Mathematics)
SCHOLARSHIP	Staff Development Project of the Commission
	on higher Education,
	Thailand, 2005–2008
HOME ADDRESS	97 Moo 7
	Amphur Pakphanang
	Nakhon Si Thammarat 80140 Thailand
E-MAIL	wariam_chuayjan@hotmail.com